Corso di Dottorato in SCIENZE, TECNOLOGIE E BIOTECNOLOGIE PER LA SOSTENIBILITA'

Natural products for cancer therapy: bio-molecular perspectives on anti-tumour properties of climacostol and its analogues.

Dept. Innovation in Biological, Agro-food and Forest systems,

University of Tuscia

Viterbo, Italy

Tutor
Prof. Davide Cervia

Co-tutor
Prof. Simona Picchietti

PhD student
Francesca Proietti Serafini

TABLE OF CONTENTS

ABSTRACT

Several modern drugs, including those for cancer therapy, are natural products or their semisynthetic derivatives. Some of them have gone on to become current drug candidates, others are in clinical trials. The success of natural products in drug discovery is related to their inherently structural diversity, and to the new technologies in use, such as automated separation techniques, highthroughput screening and combinatorial chemistry, to exploit their feature. Natural compounds may act either as chemo-preventive agents or as factors that increase therapeutic efficacy of existing drugs, thus counteracting cancer cell drug resistance. Marine environment, due to its physical and chemical conditions, has proven to be a novel source for structural entities with biological activity. Despite of exploration of the marine environment has led to the isolation of thousands of bioactive marine molecules, the therapeutic application of these molecules remains poorly investigated. Herein we describe the biological activities in mammalian cells of Climacostol, a compound produced by the ciliated protozoan *Climacostomum virens*, focusing on its anti-tumour action and its possible therapeutic activity. Climacostol displayed cytotoxic properties *in vitro*, thus causing a reduction of viability/proliferation of different tumour and non-tumour cell lines. Importantly, climacostol toxicity was more selective against tumour than non tumour cells. We then focused on the B16-F10 mouse melanoma cells. Climacostol mode of action has been linked to its ability to interact with the DNA double helix, causing DNA damage, and subsequently inducing the intrinsic apoptotic pathway in B16-F10 mouse melanoma cells. Of interest, we found that the apoptotic mechanism of climacostol based on the up-regulation of p53 and its pro-apoptotic targets, such as Noxa and Puma. In addition, *in vivo* melanoma progression was studied using a B16-F10 allograft transplantation tumour model. When melanomas were treated with intra-tumoural injections of climacostol, it significantly improved the survival of transplanted mice, decreased tumour growth rate and tumour weight, induced a notable reduction of viable cells inside the tumour, activated apoptosis and up-regulated the p53 signalling network. Autophagy is a self-eating process by which aged or damaged intracellular organelles and proteins are degraded into lysosomes via autophagosomes, which occurs at a basal level in all eukaryotic cells and may support cell survival or activate death pathways. It has been shown that autophagy can have a binary function, acting as a tumor suppressor in the early stages of cancer and tumor enhancer in established tumours. Thus, we investigated how climacostol regulates autophagy as well as the involvement of p53-dependent mechanisms and their impact on cell death/survival. Using both *in vitro* and *in vivo* approaches, we

showed that climacostol potently and selectively impairs autophagy in B16-F10 mouse melanoma cells, which were committed to die by apoptosis. In particular, we monitored autophagy over time and we observed that climacostol exerts a marked and sustained buildup of autophagosomes as the result of dysfunctional autophagosomal degradation. Hence, our data indicated that the pro-apoptotic function of climacostol could be attributed to the block of autophagosome turnover. The mechanistic insights we obtained disclosed a two-edged role played by climacostol in either promoting autophagy, independently on p53 levels, or suppressing autophagosome turnover via the up-regulation of p53, thus more autophagic vacuoles may be accumulated in melanoma cells, further contributing to cell death. The p53-dependent regulation of AMPK activity is the major responsible of climacostol-induced autophagy disruption, although the mTOR pathway unrelated to p53 levels also plays a role. Since the up-regulation of the p53 system is at the molecular crossroad regulating both the anti autophagic action of climacostol and its role in the apoptosis induction, it might be important to explore the dual targeting of autophagy and apoptosis with agents acting on p53 for the selective killing of tumours.

Key words: apoptosis, autophagy, p53, tumour cells, natural products and derivatives

Natural products for cancer therapy: bio-molecular perspectives on anti-tumour properties of climacostol and its analogues.

Dept. Innovation in Biological, Agro-food and Forest systems, University of Tuscia, Viterbo, Italy

Tutor: Prof. Davide Cervia

This PhD thesis dealt with the assessment of the bioactivity of selected natural compounds and their potential in pharmacology studies. In particular, using well-established mouse models of melanoma, the anti-tumour properties of these novel molecules, such as the toxin climacostol and its synthetised derivatives, was investigated both *in vitro* and *in vivo*.

Key words: apoptosis; autophagy; p53, tumour cells; ciliates, natural products and derivatives

1. Introduction

This PhD thesis is focused on the biological activities of climacostol, a natural toxin produced by the freshwater ciliated protozoan *Climacostomum virens* and this oral communication reports the main results of the following three activities directed to:

A1) determine the cytotoxic, anti-proliferative and pro-apoptotic effects of climacostol;

A2) establish climacostol's role on autophagic machine;

A3) assess the anti-tumoural efficacy of climacostol analogues.

2. Natural compounds Applications

Natural compounds are extensively researched for cancer therapy and several modern drugs have been isolated from natural sources. The achieve success of natural products in drug discovery is due to their biochemical characteristics. The continuing contribution of natural products to the expansion of the chemotherapeutic armamentarium is increasingly evident, in fact about 80% of anticancer drugs approved by the Food and Drug Administration (FDA) belongs to natural sources and they are characterised by various mechanisms of action, including mainly cell death via apoptosis and/or necrosis, autophagy, interaction with microtubules, inhibition of topoisomerases I

or II, alkylation of DNA, and interference with tumour signal transduction (Catalani *et al*., 2016; Newman and Cragg, 2016). Natural compounds may act as chemo-preventive agents and as factors that rise therapeutic effectiveness of existing drugs, thus overcoming cancer cell drug resistance that is the principal factor determining the failure in conventional chemotherapy.

3. Experimental Procedure

Climacostol has been extensively studied for its anti-proliferative and pro-apoptotic abilities on B16-F10 mouse melanoma cells. In addition, the anti-cancer activity of climacostol *in vivo* was recently described in a melanoma allograft model, injecting B16-F10 cells subcutaneously in mice (Catalani *et al*., 2016; Perrotta *et al*., 2016). The experimental procedure consisted in intra-tumour injections of climacostol or vehicle every 3-4 days for ca. 3 week. Using the same protocol, we determined the autophagic status both in B16-F10 mouse melanoma cells after treatment with climacostol and in mouse melanomas locally treated with climacostol. Thanks to the collaboration with the group of Prof. Enrico Marcantoni (University of Camerino), new climacostol derivatives were synthetised in order to improve the bioactivity and stability of the native molecule. These innovative analogues were tested on different cell lines in order to assess their effects as potential new chemotherapeutic drugs.

4. Materials and Methods

Climacostol and its analogues Chemically-synthesized climacostol and its two analogues AN1 and AN2 were dissolved in ethanol (1 mg/ml) and stored in the dark at –20°C. The solutions were diluted with the appropriate medium at the time of the experiment.

Cell cultures. Murine melanoma B16-F10, murine glioma GL261, human glioblastoma U87MG, human melanoma A375 and SK-MEL-5 (obtained by the American Type Culture Collection) cell lines were cultured in Iscove's supplemented with 10% heat inactivated foetal bovine serum, glutamine (200 mM), penicillin/streptavidin (100 U/ml), 1% Hepes 1 M (Euroclone), pH 7.4, and grown at 37°C in a humidified atmosphere containing 5% CO2 (logarithmic growth phase, routine passages every 3 days).

Animals. Female C57BL/6 mice (8-10 weeks old) were purchased from Charles River Laboratories (Calco, Italy), housed in a regulated environment (23 ± 1°C, 50 ± 5% humidity) with a 12 h light/dark cycle (lights on at 08.00 a.m.), and provided with food and water ad libitum.

MTT assay. Cell viability of tumoural and-non tumoural cells was evaluated by MTT analysis after climacostol and/or analogues treatments.

Microscopy analysis. At least 24h prior to cell treatment, B16-F10 cells were plated at an appropriate cell density on glass coverslips in 6 well plates. After 24h of treatment with climacostol, cells were washed once in PBS and fixed in 4% paraformaldehyde for 15 min at room temperature and washed three times in PBS (Cell Signaling Tecnology, Danvers, MA, USA). For fluorescence detection, cells were also stained with the appropriate Alexa Fluor secondary antibodies (Life Technologies, Monza, Italy). Coverslips were mounted with ProLong Gold with DAPI (Life Technologies, Monza, Italy) and fluorescein phalloidin and analysed using a DMI4000 B automated inverted microscope equipped with a DCF310 digital camera (Leica Microsystems, Wetzlar, Germany).

Western blotting. B16-F10 cells and *in vivo* resected B16-F10 tumours were homogenized in RIPA lysis buffer, supplemented with a mix of protease and phosphatese inhibitors (cOmplete and PhosSTOP; Roche Diagnostic, Milano, Italia). Equal amounts of proteins were separated by 4-20% SDS-polyacrylamide gel electrophoresis (Criterion TGX Stain-free precast gels and Criterion Cell System and transferred onto nitrocellulose membrane using a Bio-Rad Trans-Blot Turbo System. The membranes were probed using mouse monoclonal anti-p53, the rabbit anti-LC3 and anti-p62/SQSTM1, anti-cleaved-caspase 3, anti-phospho-Akt (Ser473), anti-phospho-S6 (Ser240/244), and anti-phospho-AMPKα (Thr172) and mouse anti-p53 (Cell Signaling Technology, Danvers, MA, USA) primary antibodies. After the incubation with the appropriate horseradish-peroxidase-conjugated secondary antibody, bands were visualised using the Clarity Western ECL substrate with ChemiDoc MP imaging system (Bio-Rad, Hercules, CA, USA). Then, bands were quantified for densitometry using the Bio-Rad Image Lab software.

Real-time PCR. Briefly, total RNA from *in vitro* B16-F10 cells and *in vivo* resected B16-F10 tumours was extracted with the High Pure RNA Isolation Kit and the High Pure RNA Tissue Kit, respectively (Roche Applied Science, Mannheim, Germany), according to the manufacturer's protocol. First-strand cDNA was generated from 1 μg of total RNA using iScript Reverse Transcription Supermix (Bio-Rad, Hercules, CA, USA). A set of primer pairs was designed to hybridize to unique regions of the appropriate gene sequence (Supplementary Table S1). PCR was

performed using SsoAdvanced Universal SYBR Green Supermix and the CFX96 Touch Real-Time PCR Detection System (Bio-Rad). The fold change was determined relative to the control after normalizing to Rpl32 (internal standard) through the use of the formula $2^{-\Delta\Delta CT}$.

mRFP-GFP-LC3 assay. B16F10 cells were plated on 14 mm coverslips coated with poly-D-lysine and then cultured for 24 hours. These cells were transiently transfected with mRFP-GFP-LC3 plasmid, a generous gift from Dr. Pura Muñoz-Cánoves (Pompeu Fabra University, Barcelona, Spain), using Lipofectamine LTX and Plus Reagent (Life technologies, Monza, Italia). Three hours following transfection at 37°C, two-thirds of the media is replenished with fresh media. Subsequently, B16F10 cells were treated with Climacostol or vehicle for an additional 24 hours. After drug treatment, cells were washed once in PBS and fixed with 4% paraformaldehyde (in PBS) for 15 min at room temperature. After washing, coverslips were mounted on glass slides with ProLong Gold with DAPI (Life Technologies, Monza, Italy) and analysed using a Carl-Zeiss LSM 710 inverted confocal microscope.

Electron transmission microscopy. For EM, B16-F10 cells were fixed in 2% paraformaldehyde and 2% glutaraldehyde in cacodylate buffer (0,1 M pH 7.2) over night at 4°C. The cells were then processed and analyzed at Centro Interdipartimentale di Microscopia Elettronica (CIME), Università degli Studi della Tuscia, Viterbo.

Statistical analysis. Statistical significance of raw data between the groups in each experiment was evaluated using unpaired Student's t-test (single comparisons) or one-way ANOVA followed by the Newman-Keuls post-test (multiple comparisons). EC50 (the concentration producing half the maximum effect) and Emax concentration (producing the maximum effect) were determined by non-linear regression curve analysis of the concentration-effect responses. Potency values among concentration-response curves were compared with the F test. Kaplan-Meyer data were analysed with the multiple comparison survival curve method using the Log-rank (Mantel-Cox) test. Tumour growth was analysed using two-way ANOVA, followed by the Bonferroni post-test. Data belonging from different experiments were represented and averaged in the same graph. The GraphPad Prism software package (GraphPad Software, San Diego, CA, USA) was used. The results were expressed as means ± SEM of the indicated n values.

5. Results and Discussion

5.1 Cytotoxic, anti-proliferative and pro-apoptotic effects of climacostol

Climacostol has been shown to reduce the growth of different human tumour cells line while being devoid of effects on endothelial cells. In particular, we examined the cytotoxic properties of climacostol on the highly tumourigenic B16 mouse melanoma cells. In line with results obtained in other tumour cells, Climacostol inhibits also viability and proliferation of melanoma cells. Moreover, confocal immunostaining experiments for phospho-histone H2A.X, a marker of DNA damage, indicate that climacostol is a compound that quickly forms adducts with DNA, thus leading to DNA damage and cell death. Flow cytometry analysis revealed that climacostol treatment for 24 and 48h induced apoptosis in melanoma cells, instead, apoptosis in vehicle-treated cells was undetectable. Consequently, we showed even that B16F10 cells expressed high levels of active Caspase 3 at 24 hours after climacostol treatment, while no specific staining was observed in the control cells. Of interest, here we demonstrated that climacostol treatment caused the dissipation of mitochondrial membrane potential through the formation of permeability transition pore, the translocation of Bax to the mitochondria and Cytochrome C release from the mitochondria. The latter, in turn, activates Caspase 9-dependent apoptotic disassembly and Caspase 9-dependent proteolytic cleavage of Caspase 3. As shown Fig. 1a, exposure of B16-F10 cells for 24 h to climacostol resulted in a significant increase of p53 protein levels when compared to control cells. Thus, to determine whether the pro-apoptotic effect of climacostol involved p53 signalling, B16-F10 cells were transiently transfected for 48h with a p53-specific or a non-targeting siRNA, followed by climacostol treatment for 24 h. As shown in Fig. 2a, climacostol increased p53 levels in cells transfected with non-targeting siRNA while its effect was fully inhibited after p53 siRNA transfection. The analysis of apoptotic cells revealed that p53 silencing abolished the apoptotic effects of climacostol, thus indicating that the mechanism by which climacostol induces apoptosis in B16-F10 melanomas is mainly dependent on p53 activity (Fig. 1b). The efficacy of climacostol was also tested *in vivo*; to this end B16-F10 cells were injected subcutaneously in mice, when the syngeneic implantation was established, mice were intra-tumour injected with vehicle (control) or climacostol every 3–4 days for 3 weeks. Local administration of climacostol decreased tumour volumes throughout the entire study period; in particular, tumour growth rate increased steadily for vehicle-treated animals (control) while we observed a significant and persistent inhibition of tumour load in climacostol-treated animals. In addition, immunostaining experiments of the cleaved Caspase 3 revealed an high amount of clustered apoptotic cells in tumours treated with climacostol, while the stain for the cleaved Caspase 3 was poor in control tumours. These results were also confirmed by Western blot experiments, also the expression of p53 was enhanced in melanomas treated with climacostol. Accordingly, we also found a significant increase of p53, Noxa and Puma mRNAs in the climacostol-treated group, while mRNA expression of p21 was not affected.

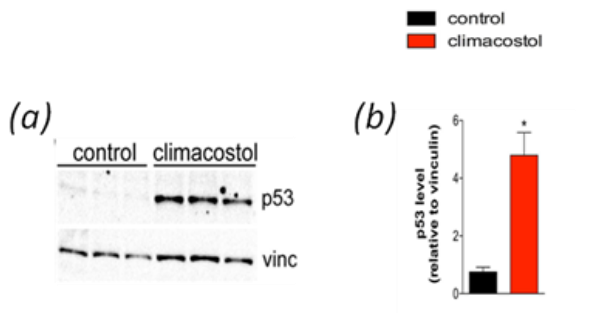

Figure 1 *(a) Western blot analysis of p53 expression. Vinculin was used as the internal standard; (b) Densitometry analysis of p53 expression (n = 3) * p < 0.001 vs control.*

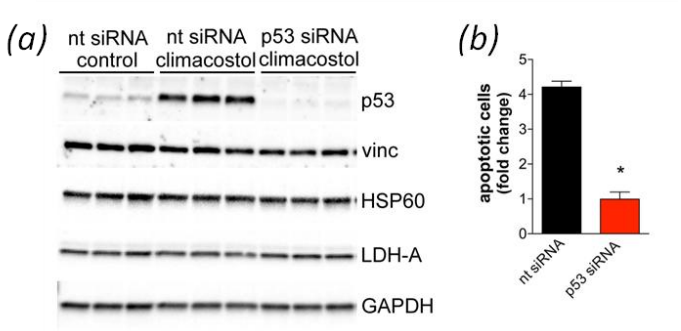

Figure 2 *(a) Western blot analysis of p53 expression. Vinculin, HSP60, LDH-A, and GAPDH were used as internal standards and to test possible off-target effects of siRNA transfection (n = 3). (b) Evaluation by flow cytometry of Annexin V/PI.*

5.2 Climacostol's role on autophagic machine

Climacostol potently and selectively impairs autophagy in multiple cancer cell lines, *i.e.* human melanoma and murine/human glial tumour cells. Indeed, the transcripts encoding LC3b, p62, beclin 1, bnip 3, bnip 3L, atg3, atg4, and atg5 autophagy genes were significantly enhanced in climacostol-treated group suggesting an important perturbation of autophagic machinery. These data were also confirmed by fluorescence microscopy and western blot analysis. In fact, we detected an increase of LC3 puncta staining in melanoma tumours from climacostol-treated mice by fluorescence microscopy, while in control group was visualized a diffuse LC3 staining (Fig. 3a). The increase and clustering of LC3 may be the consequence of induction or suppression of autophagic process, so we measured the autophagosomal cargo protein p62 to understand the state of autophagic flux (Mizushima *et al.*, 2010; Klionsky *et al.*, 2016). The treatment of B16-F10 allografts with climacostol increased p62 immunofluorescence in melanoma cells, leading to accumulation of p62-positive aggregates when compared to control. These results were confirmed by western blot experiments detecting a significant rise of p62 protein band in climacostol-treated tumours (Fig. 3c,d). The effect of climacostol was then evaluated by treating cells with chloroquine, a well-known lysosomotropic compound, which accumulates preferentially in the lysosomes of cells and prevents the fusion of autophagosome with lysosome and lysosomal protein degradation (Qiu *et al.*, 2014;

Vakifahmetoglu-Norberg *et al*., 2015). Of notice, the inhibition of the autophagic flux exerted by climacostol was not modified in the presence of chloroquine.

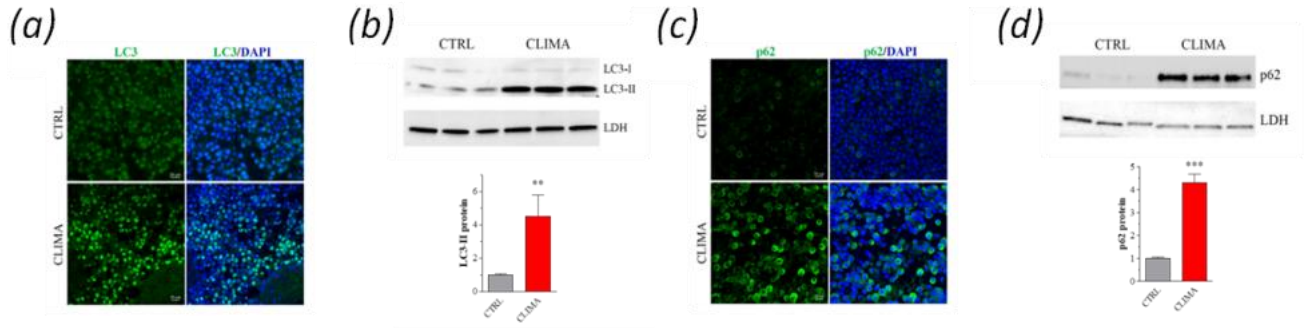

Figure 3 *(a) Representative immunofluorescence imaging of LC3. DAPI (blue) was used for nuclei detection.(b) Western blot analysis of LC3. LDH-A was used as internal standards. (c) immunofluorescence imaging of p62. DAPI (blue) was used for nuclei detection. (d) Western blot analysis of p62. LDH-A was used as internal standards.*

The autophagic response of melanoma cells was also analysed using TEM (Fig 4). B16-F10 cells treated with climacostol for 6 h showed accumulation of autophagosomes in the cytosol. Climacostol-treated cells showed disorganized structures, swollen cristae in mitochondria and accumulation of melanosomes in the cytoplasm. By contrast, control cells showed a few autophagosomes, also called initial autophagic vacuoles (AVi), featured as a double-membraned structure with undigested cytoplasmic contents, late or degradative autophagic vacuoles (AVd), characterized by a single limiting membrane with cytoplasmic materials at various stages of degradation and finally melanosomes (Mizushima *et al*., 2010; Klionsky *et al*., 2016). Autophagy is also a dynamic process, therefore we employed B16-F10 cells transiently expressing mRFP-GFP-LC3 as a dual-fluorescence pH sensor to assay overtime the acidification of autophagic vacuoles (autophagosome-lysosome fusion) in the live cells after climacostol treatment (Kimura *et al*., 2007). The expression of this tandem fluorescent-tagged LC3 reporter is useful to monitor autophagosomes (pH neutral) and autophagosome-lysosome fusion (pH acid) (Kimura *et al*., 2007; Mizushima *et al*., 2010; Klionsky *et al*., 2016). Autophagosomes appear yellow as results of both green and red fluorescence, while autolysosomes appears as only red vacuoles, since the low lysosomal pH quenches GFP more quickly than mRFP. After treatment of the cells with climacostol for increasing times, yellow punctate fluorescence significantly increased while only-red puncta significantly decreased, indicating a time-dependent blockade of autophagosome-lysosome fusion/autophagosome maturation. Similar results were observed with CQ. The kinetics of climacostol as inhibitor of autophagic flux in melanoma cells was further confirmed by immunoblot experiments. All together, these data provide compelling evidence that climacostol is an efficient

agent acting fast to impair the autophagic flux due to distal autophagy blockade, resulting in autophagosome accumulation in the cytosol.

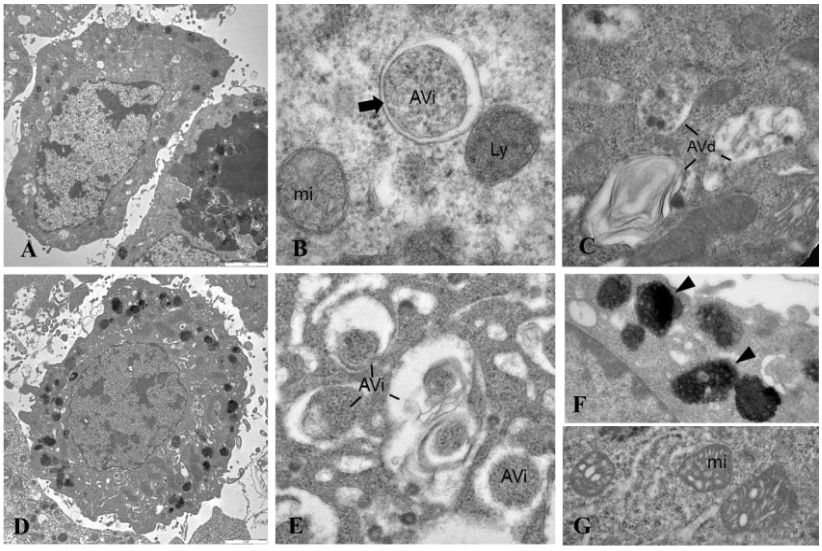

Figure 4 *(a,b,c) Control cells showed a few autophagosomes (AVi), late or degradative autophagic vacuoles (AVd) and melanosomes. (d,e,f,g) Climacostol-treated cells showed disorganized structures, swollen cristae in mitochondria, accumulation of autophagosomes and melanosomes in the cytoplasm.*

To gain more mechanistic insights on climacostol effects, we evaluated different autophagy signalling molecules and we demonstrated that climacostol compromises autophagosome turnover via the up-regulation of p53-AMPK axis, although the mTOR pathway unrelated to p53 levels also plays a role. The p53-dependent regulation of AMPK activity is the major responsible of autophagy disruption but has not a key regulating cell death, thus indicating that climacostol effects on autophagy and apoptosis are two separate events, which may act independently on life/death decision of the cell. To test whether autophagy has a key role regulating cell fate in our system, we measured the cytotoxic effect of climacostol by exclusion dye staining with trypan blue in B16-F10 cells transfected with an AMPKα-specific or a non-targeting siRNA. As expected, cell viability of AMPKα siRNA cells remained high. Of notice, climacostol (24 h, 30 μg/ml) displayed a similar high toxicity both in the presence of AMPKα or when its expression was successfully knocked-down. Finally, cultured B16-F10 cells were treated with climacostol (24 h, 30 μg/ml) both in the absence and in the presence of the pan-caspase inhibitor Z-VAD-(OMe)-FMK at 100 μM. As expected, the activation of caspase 3 induced by climacostol was indeed blunted, at least in part, by Z-VAD-(OMe)-FMK, on the contrary, caspase inhibition did not affect the accumulation of LC3-II and p62 obtained after climacostol treatment. Of interest, Z-VAD-(OMe)-FMK administration was

unable to rescue climacostol-induced loss of cell viability, as assessed by MTT analysis. These data argue that climacostol is able to induce a caspase-independent cell death in melanoma cells.

5.3 Climacostol analogues

In order to identify the structural traits of the native molecule that could be modified to increase its bioactivity and/or stability, Buonanno *et al*. (2018) have synthetised two synthetic new analogues of climacostol, *i.e*. the 1,3-dihydroxy-2-methyl-5-[(Z)-non-2'-enyl]benzene (AN1) and the 1,3-dihydroxy-2-methyl-5-[(Z)-non-2'-enyl]benzene (AN2), carrying an additional OH- group and an CH3- group, respectively, in the aromatic ring. We examined the *in vitro* cytotoxic activities of these novel climacostol analogues on different cells of both tumour (B16-F10, GL261, SK-N-BE, and CT26 cells) and non-tumour (C2C12 cells) origin, by MTT assay. Cell treatment with AN1, AN2 and climacostol (24 h) caused a concentration-dependent reduction of MTT absorbance with an E_{max} concentration value of ca. 30 μg/ml. At the E_{max} concentration compounds decreased cell viability between 90% and 100%. Data also indicated that the viability of cells is negatively affected by AN1 and AN2 with a comparable potency, i.e. EC_{50} ranging from ca. 18 to 40 μg/ml. Noteworthy is that both AN1 and AN2 displayed similar or even lower potencies when compared to climacostol. In agreement with our previous results, immunostaining experiments with a fluorescently antibody that binds specifically to cleaved (active) caspase 3 revealed that B16-F10 melanoma cells expressed active caspase 3 at 9 h after 30 μg/ml AN1, AN2 and climacostol treatment, while no specific stain was observed in vehicle-treated (control) cells.

6. Conclusions and Future Perspectives

In this PhD thesis we demonstrate that local treatment of climacostol in melanoma transplanted mice inhibited tumour growth, tumour weight and viable cells inside the tumour, thus inducing apoptosis of cancer cells and a significant amelioration of animal survival. In addition, intra-tumoural injections of climacostol in melanoma transplanted mice impaired autophagy in melanoma cells and they were committed to die by apoptosis. Taken together these data indicated that climacostol effects on apoptosis and autophagy are two separate events, although both reflecting the upstream activation of p53 system. Since the activation of p53 system is at the molecular crossroad regulating both the anti-autophagic action of climacostol and its role in the apoptosis induction, it might be important to explore the dual targeting of autophagy and apoptosis with agents acting on p53 for the selective killing of tumours. These findings suggest the efficacy of ciliate bioactive molecules to identify novel lead compounds in drug discovery and development.

8. References

Catalani E, Proietti Serafini F, Zecchini S, Picchietti S, Fausto AM, Marcantoni E, Buonanno F, Ortenzi C, Perrotta C, Cervia D (2016) Natural products from aquatic eukaryotic microorganisms for cancer therapy: Perspectives on anti-tumour properties of ciliate bioactive molecoles. *Pharmacological Research* **113**: 409–420.

Kimura S1, Noda T, Yoshimori T (2007) Dissection of the autophagosome maturation process by a novel reporter protein, tandem fluorescent-tagged LC3. *Autophagy* **5**: 452-460.

Klionsky DJ (2016) Guidelines for the use and interpretation of assays for monitoring autophagy (3rd edition) *Autophagy* **1**: 1-222

Mizushima N, Yoshimori T, Levine B (2010) Methods in mammalian autophagy research. *Cell.* **3**: 313-326.

Newman DJ, Cragg GM (2016) Natural Products as Sources of New Drugs from 1981 to 2014. *J Nat Prod.* **3**: 629-661.

Perrotta C, Buonanno F, Zecchini S, Giavazzi A, Proietti Serafini F, Catalani E, Guerra L, Belardinelli MC, Picchietti S, Fausto AM,

Giorgi S, Marcantoni E, Clementi E, Ortenzi C, Cervia D (2016) Climacostol reduces tumour progression in a mouse model of melanoma via the p53-dependent intrinsic apoptotic programme. *Sci Rep*. **6**: 27281.

Qiu WH, Zhou BS, Chu PG, Luh F and Yen Y (2007) The induction of growth arrest DNA damage-inducible gene 45 beta in human hepatoma cell lines by S-adenosylmethionine. *Am J Pathol* **171**: 287–296.

Vakifahmetoglu-Norberg H, Xia H, Yuan J (2015) Pharmacologic agents targeting autophagy. *J Clin Invest* **1**: 5–13.

1. Introduction

1.1 Natural product for human therapy

Natural products from natural sources including plants, animals, marine organism or micro-organisms have played a critical role in treating and preventing human diseases since the ancient time (Khazir *et al*., 2014). To date, about half of the currently drugs used in clinic are naturally derived or are related to them, and many more are under clinical trials (Harvey *et al*., 2015; Newman *et al*., 2012). The success of natural products in drug discovery is due to their enormous structural diversity, shaped by millions of years of evolution and natural selection, and to the recent advances in technology and instrumentation for their rapid identification (Baker *et al*., 2007). For drug discovery, two different strategies can be used: classical pharmacology or phenotypic drug discovery, and reverse pharmacology or target-based drug discovery (Lee *et al*., 2012). In classical pharmacology, compounds are evaluated in different cell lines for quantitative measurement of cellular parameters in order to find those that alter their phenotype, the mechanism will be evaluate later (Horman, 2016). On the contrary, in reverse pharmacology, compounds are screened to find an high-affinity binding to target protein involved in the disease and only active compounds will be check in tissues or whole organisms (Horman, 2016). Notably, in recent years, there has been a renewal of interest in the use of phenotypic screening approaches to identify drug leads and clinical candidates with distinct and therapeutically relevant molecular mechanisms of action (MMOAs) (Sumner *et al*., 2015; Luo *et a*l., 2014; Moffat *et al*., 2014). To date, over 50% of all available drugs on the market belongs to natural sources, of which over 80% of anticancer agents approved by the Food and Drug Administration (FDA) are derived from natural sources (Trendowski 2015; Javed *et al*., 2011; Chinembiri *et al*., 2014; Newman and Cragg, 2014; Sithranga Boopathy and Kathiresan, 2010; Nobili, et al., 2009). These drugs are characterised by different mechanisms of action, including primarily cell death via apoptosis, necrosis and/or autophagy, interaction with microtubules, inhibition of topoisomerases I or II, alkylation of DNA, and interference with tumour signal transduction (Ranjan *et al*., 2015; Safdari et al., 2015; Beesoo *et al*., 2014; Khazir *et al*., 2014; Nobili *et al*., 2009). Natural compounds may act both as chemo-preventive agents that block the progression to invasive cancer and as factors that increase therapeutic efficacy of existing drugs. Therefore, natural products can overcome cancer cell drug resistance, which is the main factor determining the failure in traditional cytotoxic chemotherapy (Trendowski, 2015; Beesoo *et al*., 2014; Khazir et al., 2014; Sithranga Boopathy and

Kathiresan, 2010; Nobili *et al*., 2009; Baharuddin et al., 2016; Zambelli *et al*., 2016; Magne Nde *et al*., 2015; Wang *et al*., 2015; Khalife, et al., 2014; Schnekenburger *et al*. 2014; Thakur *et al*., 2014; Wang *et al*., 2014; Uzoigwe and Sauter, 2012). Recent exploitation is now focused on the bioactive substances of water environment, with a very promising outcome in special using marine microorganisms from high competitive environments. Thus, acquatic microorganisms have evolved biochemical and physiological mechanisms that include the production of unique peptides and metabolites belonging to different chemical classes, such as terpenoids, alkaloids, polyketides, shikimic acid derivatives, sugars, steroids and a multitude of mixed biogenesis metabolites, with high bioactivity (Catalani *et al*., 2016; Javed *et al*., 2011; Penesyan *et al*., 2010; Molinski *et al*., 2009; Zhang *et al*., 2005; Haefner, 2003). The first marine-derived anticancer agent to be developed for clinical use was cytarabine, isolated from the Caribbean sponge *Cryptotheca crypta* in 1969. Since then, several new anticancer agents derived from marine sources have entered preclinical and clinical trials, thanks to improvements in the technology of deep-sea collection, extraction, and large-scale production through aquaculture and synthesis (Li *et al*., 2015).

1.2 Mechanisms of cell death/survival

Cells can sense and integrate signals from the environment in order to respond to it. In the presence of an environmental stimulus, which can be nutrients or a stress, intracellular pathways are activated, and their interaction determines the cell fate. In this chapter, we will discuss mostly about apoptosis and autophagy, that are very frequently affected in cancer cells allowing them to survive and proliferate.

1.2.1 Apoptosis

The term “apoptosis” derives from the Greek words “απο“ and “πτωσιζ“ meaning “dropping off” and refers to the falling of leaves from trees in autumn (Wong, 2011). Although the morphologic features of apoptotic cell death were noted as early as 1885 by Fleming (Fleming, 1885), the expression apoptosis was first used by Kerr, Wyllie and Currie in 1972 to describe a distinct morphological aspect of cell deletion (Kerr *et al*., 1972; Kerr, 2002). Apoptotic cell death is characterized by reduction of cell volume (known as pyknosis), chromatin condensation and fragmentation, initially into large and subsequently into small fragments, dynamic membrane blebbing and loss of adhesion to neighbours or to extracellular matrix (Kroemer *et al*., 2009). The dying cell degrades into apoptotic bodies than it is removed by resident phagocytes, thanks to the phosphatidylserine (PS) externalization on the outer cell membrane. This biochemical change is required for effective

phagocytosis of apoptotic cells by macrophages (Kroemer *et al*., 2009; Ouyang *et al*., 2012; Jayakiran, 2015). Our understanding of the apoptotic process in mammalian cells was gained by the main model systems of developmental biology, including the nematode *Caenorhabditis elegans*, the fruitfly *Drosophila melanogaster* and the mouse *Mus musculus* (Lettre, 2006). Apoptosis contributes to development and health of multicellular organisms, it also plays an important role to maintain homeostasis, especially in the immune system (Sun, 2001; Elmore, 2007). Apoptotic responses also occurs when cells get damaged by disease or DNA damaging agents (Norbury and Hickson, 2001). Recent evidence indicates that deregulation or defects along apoptotic signaling pathway are associated with uncontrolled proliferation, cancer development and progression and also tumour resistance to drug therapies.

1.2.1.1 Apoptotic pathways

The apoptosis cascade is highly complex and sophisticated, involving two main apoptotic pathways: the extrinsic pathway, so called death receptor pathway (Dickens *et al*., 2012), and the intrinsic or mitochondrial pathway (Tait and Green, 2010) (see Fig. 1).

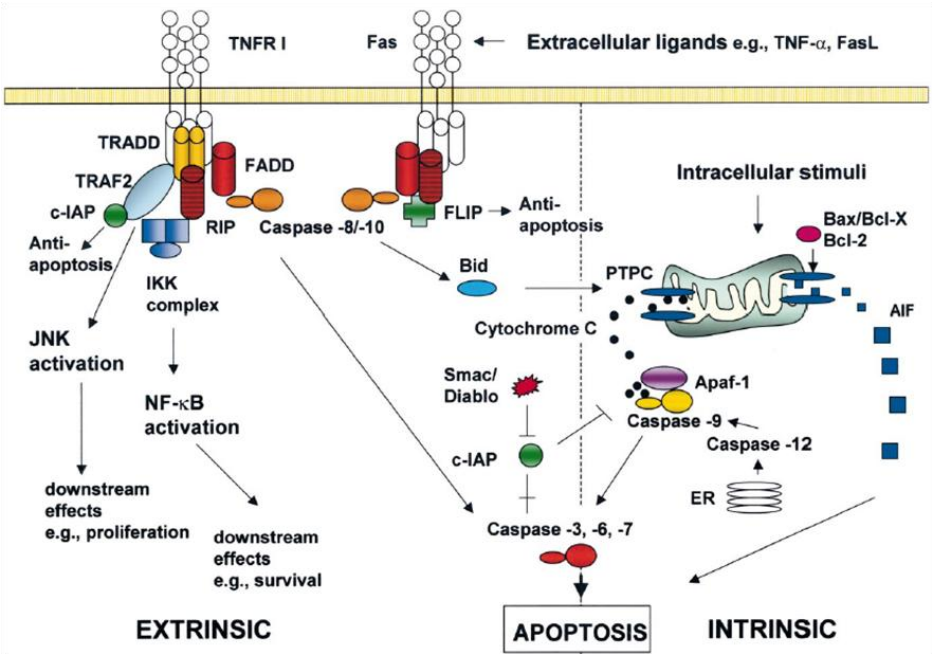

Fig.1 Scheme of Apoptotic Pathways

Each pathway activates its own initiator caspase, which will converge on the same final execution pathway that entails the cleavage and activation of caspase-3. Caspase is a family of cystein proteases, that are in turn controlled positively and/or negatively by B-cell lymphoma protein-2 (Bcl-2) family members (described later) (Elmore, 2007; Galluzzi *et al*., 2018). Melanoma, one of the most aggressive cancers, is characterized by a high resistance to programmed cell death. Therefore, the most promising approach to eliminate tumour cells should be to involve apoptosis as a therapeutic target.

1.2.1.2 Extrinsic pathway – death receptor orchestrated apoptosis

The extrinsic pathway mediates apoptosis in response to extracellular signals that involves ligands, related to the tumor necrosis factor (TNF) family proteins, and death receptors, belonging to the superfamily of TNF receptor (Ashkenazi *et al*., 1998; Flusberg *et al*., 2015; Gibert *et al*., 2015; Strasser *et al*., 2009). The death receptors are structurally defined by similar cysteine-rich extracellular domain, which defines their ligand specificity, and an intracellular protein-protein interaction domain, called death domain (DD), that is essential for transducing the apoptotic signal. To date, the well-known ligand and corresponding death receptors include: Fas ligand (FasL)/Fas cell surface death receptor (FasR) and Tumor necrosis factor alpha (TNFα)/TNF receptor superfamily member 1A (TNFR1) (Wajant, 2002; Aggarwal *et al*., 2012; Fleten *et al*., 2016; von Karstedt *et al*., 2017). In the case of FAS, its ligand causes a conformational change at the intracellular tails of the preassembled receptor that allows the adaptor molecule Fas-associated death domain (FADD) to bind the death domain of Fas through its own death domain. In contrast, signaling downstream of TNFR1 requires the TNFR1-associated death domain protein (TRADD). TRADD is characterised by distinct functional domains including an N-terminal domain that binds TNF receptor associated factor 2 (TRAF2) and promotes NFκB activation, and a C-terminal death domain that binds DD-containing proteins, such as FADD. FADD contains a protein-protein interaction domain, termed death effector domain (DED), that mediates the recruitment of procaspase-8, thereby forming a death-inducing signaling complex (DISC). The formation of the DISC signaling platform leads to homodimerization and activation by autoproteolytic cleavage of caspase-8 molecules (Kallenberger *et al*., 2014; Fu *et al*., 2016). The signal downstream of DISC formation leads to the activation of the effector caspases, these proteases cleave cellular death substrates, resulting in morphological changes observed in apoptotic cells (Scaffidi *et al*., 1998; Barnhart *et al*., 2003).

1.2.1.3 Intrinsic pathway - mitochondrial-dependent apoptosis

The intrinsic pathway can be activated by a plethora of stimuli that may act in either a positive or negative manner. Negative signals involve the absence of some growth factors, hormones and cytokines that can lead to failure of suppression of apoptotic programs and subsequent trigger of apoptosis. Other stimuli, including radiation, toxins, hypoxia, hyperthermia, viral infections and free radicals can act in a positive manner. The critical step for intrinsic pathway is the integrity of mitochondrial structure and function, which is controlled by pro-apoptotic and anti-apoptotic members of B-cell lymphoma 2 (BCL2) family. These family of proteins regulates cell death mainly by dynamic interactions that regulate mitochondrial outer membrane permeabilization (MOMP), leading to the irreversible release of intermembrane space proteins into the cytosol, subsequent caspase activation and apoptosis (Kale *et al*., 2018). Under physiological condition, anti-apoptotic proteins such as Bcl-2, inhibit MOMP by binding to pro-apoptotic pore-formers Bcl-2 proteins, such as BCL-2 Associated X (Bax) and BCL2 Antagonist/Killer 1 (Bak), maintaining them in an inactive conformation. Bax and Bak are comprised of nine alpha-helices, however inactive monomers of BAX and BAK are slightly different. The carboxyl-terminal transmembrane helix (α9) of Bax is sequestered to the protein core within the hydrophobic BH3 domain-binding groove, therefore Bax is mostly located between the mitochondrial outer membrane (MOM) and the cytosol (Edlich *et al*., 2011; Schellenberg *et al*., 2013). In contrast, the α9 of Bak is constitutively resides at the MOM, where is associates with Voltage-Dependent Anion Channel 2 (VDAC2) (Cheng *et al*., 2003; Ma *et al*., 2014). In presence of apoptotic stimuli, p53-upregulated modulator of apoptosis (PUMA) engages Bcl-xL and release p53 allowing it to activate Bax, which can promote MOMP. Following MOMP, pro-apoptogenic factors, notably cytochrome c, are released from the mitochondrial intermembrane space into the cytosol (Tait and Green, 2010). Once in the cytosol, cytochrome c binds and activates the adaptor molecule apoptotic peptidase activating factor 1 (Apaf-1), in the presence of ATP or dATP, causing its oligomerisation and leads to apoptosome formation. Caspase-9 forms homodimers and heterodimers/multimers with Apaf-1 upon association of their caspase recruitments domains (CARDs) (Riedl *et al*., 2007; Hu *et al*., 2014; Wu *et al*., 2016; Li *et al*., 2017). Activated caspase-9 cleaves and activates caspase-3 and -7 and subsequent exposure of PS to the extracellular side of the cell membrane. Finally, executioner caspases cleave cellular death substrates, culminating in DNA fragmentation and cell membrane disruption/blebbing. Besides cytocrome c, mitochondria also release Apoptosis-Inducing Factor (AIF) and endonuclease G that translocate to the nucleus, thus mediating large-scale DNA degradation independently of caspase (stage I condensation) (Susin *et al*., 2000; Li *et al*., 2001). In addition, caspase-3 favors DNA fragmentation and more pronounced and advanced chromatin condensation by inactivating Inhibitor of Caspase-Activated DNase (ICAD), which releases active caspase-activated DNase (CAD) (stage II

condensation) (Enari *et al*., 1998; Sakahira *et al*., 1998; Susin *et al*., 2000; Kawane *et al*., 2003). In this respect, cancer is characterised by an imbalance towards too little apoptosis, or too much cell proliferation and survival. Recently, several small molecules have been designed to activate pro-apoptotic proteins as well as to block anti-apoptotic proteins and are currently under clinical evaluation for cancer treatment.

1.2.2 Autophagy

The term autophagy, from the Greek autòs "himself" and phagéin "to eat", was introduced for the first time in 1963 by Christian De Duve (Deter and De Duve, 1967) and refers to the degradation of the cytoplasmic components of the cell through the lysosomal machinery (Levine and Kroemer, 2008; Mizushima *et al*., 2008; Rubinsztein, 2006). Autophagy can be divided into three types (Mizushima *et al*., 2011). The first type is microautophagy: cytoplasmic material is trapped by means of direct invagination or protrusion of the lysosomal/vacuolar membrane and digestion occurs inside the lysosome; the second form is chaperone-mediated autophagy (Chaperone-Mediated Autophagy, CMA) target proteins are selectively targeted to lysosomes through the coordinated action of cytoplasmic chaperones; and the last form of autophagy is macroautophagy (hereafter denoted simply as autophagy), cytoplasmic contents and damaged organelles are degraded by lysosomal enzymes via the formation of double-membraned vescicles called as autophagosomes (Antonioli *et al*., 2017; Galluzzi *et al*., 2017; Klionsky *et al*., 2016; Klionsky *et al*., 2016; Abada and Elazar, 2014). Autophagy is active in all cells and it is involved in the maintenance of cellular metabolism and homeostasis and its basic machinery is conserved throughout eukaryotes. In addition, autophagy functions as an inducible response to cellular stress caused by exposure to chemical and physical agents, such as xenobiotics, oxidants, infectious agents and pro-inflammatory states, hypoxia, and chemicals that induce an autophagy response by inactivation of Mammalian Target of Rapamycin (mTOR) (Kroemer *et al*., 2010). In particular, mTOR associates with a multi-protein complex that includes the regulatory-associated protein of mTOR (Raptor), G-protein β-subunit like protein (GβL) and proline-rich Akt/PKB substrate 40 kDa (PRAS40) (Vander Haar *et al*., 2008). Autophagy is also negatively regulated through the Class I phosphatidylinositol-3-kinase (PI3K/AKT) pathway. AKT induces mTOR by inactivating its upstream inhibitor, the tuberous sclerosis complex-2 protein (TSC2) (Jung *et al*., 2010). Autophagy is now known to play a role in many diverse disease processes including cancer, it seems that cancer cells built-in this mechanism to protect themself against a variety of intrinsic and extrinsic stress signals.

1.2.2.1 The basic autophagy machinery

Autophagy can be divided into seven discrete steps, including induction, nucleation, vesicle expansion, completion, fusion, degradation and export of metabolic building blocks (Kundu and Thompson, 2008). All steps are carried out by proteins encoded by a set of evolutionarily conserved autophagy related genes (ATGs) and they are subdivided based on their respective function into six functional categories: (1) the ULK1–ATG13–FIP200–ATG101 protein kinase complex; (2) the PtdIns3K class III complex containing the core proteins VPS34, VPS15 and Beclin 1; (3) the PtdIns3P-binding WIPI/ATG18–ATG2 complex; (4) the multi-spanning transmembrane protein ATG9A; (5) the ubiquitin-like ATG5/ATG12 system and the ubiquitin-like ATG8/LC3 conjugation system; (6) the components involved in lysosomal degradation and macromolecular efflux (Noda *et al*., 2009; Popelka and Klionsky, 2015) (Fig. 2).

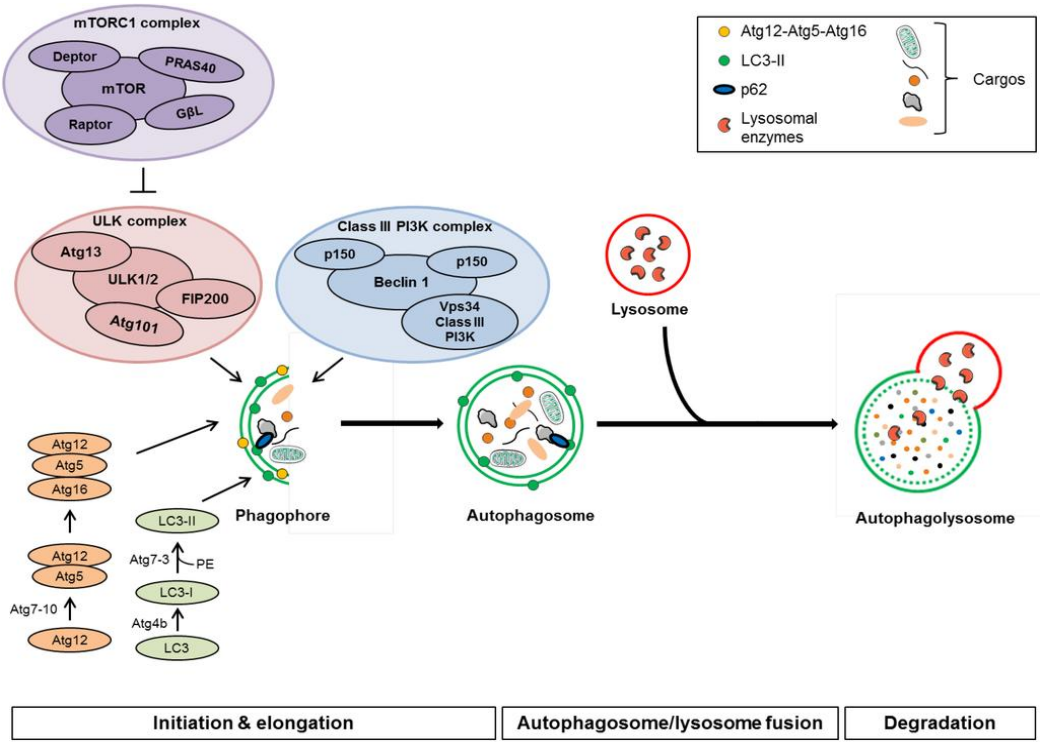

Fig.2 Schematic Representation of Autophagy Pathway

During amino acid deprivation, mTORC1 is inactivated and both ULK1 and ATG1/13 are rapidly dephosphorylated, resulting in autophagy induction. This step is mediated by ULK1 kinase complex that engages Atg9 to extract lipids from diverse sources like endosomes, the nucleus, Golgi bodies and ER to initiate the nucleation of the phagophore (Rosenfeldt and Ryan, 2009; Hosokawa *et al*., 2009). Once induced, the initial nucleation and assembly of the phagophore requires specific autophagy proteins, including ATG17, which recruits ATG13 and the multi-spanning transmembrane protein ATG9. ATG9 has been found on the autophagosomal membrane and it also traffics the plasma membrane, trans-Golgi network and endosomes (Puri *et al*., 2013; Orsi *et al*., 2012). Hence, it plays an important role in coordinating membranes transport from donor sources to the phagophore and its activity is dependent on the interactions with ULK1 and PtdIns3K kinases. The class III PtdIns3K complex consists of homologs of Vps34 (PIK3C3), Vps15 (PIK3R4) and Vps30 (BECN1) and leads to membrane modification involving the conversion of PtdIns to phosphatidylinositol 3-phosphate (PtdIns3P). The BATS domain (Barkor/Atg14(L) autophagosomes targeting sequence) of Atg14 is capable of sensing the nascent curvature of the isolation membrane incorporated with PI3P and recruits Vps34 at the omegasomes (PI3P-rich-shaped structure formed at the periphery of ER). The further extension and elongation of the phagophore is dependent on two ubiquitin-like conjugation systems: the ATG12 conjugation system and the LC3 (microtubule-associated protein 1 light chain 3, the mammalian Atg8 homologue) conjugation system. In particular, ATG12 is covalently linked to ATG5 via the concerted action of an E1-like enzyme (ATG7) and the E2-like enzymes (ATG10). Then, the Atg12−Atg5 conjugate interacts with ATG16L to form a multimeric ATG16L1 complex that associates with the outer membrane of the extending phagophore. The second ubiquitin-like conjugation system involved in autophagosome formation causes the processing of LC3. In most cells, LC3 is initially synthesized as full–length cytosolic protein (pro-LC3) with a C-terminal arginine residue that is cleaved off by Atg4, a cysteine protease, to expose a glycine residue at the C terminus, thus forming LC3-I. During autophagy, LC3-I is then activated by ATG7, transferred to ATG3 and conjugated to PE to produce a membrane-bound activated form of LC3, also known as LC3-II (Tanida *et al*., 2001; Mizushima *et al*., 2003; Ariosa and Klionsky, 2016). The transfer reaction of LC3 from ATG3 to PE is stimulated by the ATG16L1 complex, which may also induces a curvature into the growing phagophore through asymmetric recruitment of processed LC3-II. Finally, the isolation membrane closes to form the autophagosomes. After the closure of the autophagosome ATG16L1 complex dissociates from the autophagosomes, whereas LC3B–II remains both the inner and the outer surfaces of the autophagosomes, where it plays a role in selecting cargo for degradation as well as in the fusion of the autophagosome with the lysosome (see below). In fact, LC3-II has been proposed to act as a receptor for selective substrate, p62/SQSTM1, which is

involved in trafficking proteins to the proteasome and serves to facilitate the autophagic degradation of ubiquitinated protein aggregates. In particular, p62 protein is a ubiquitin-binding scaffold protein that is able to polymerize via an N-terminal PB1 domain and can interact with ubiquitinated proteins via the C-terminal ubiquitin-associated (UBA) domain. p62/SQSTM1 also binds directly to LC3 and GABARAP family proteins via a specific sequence motif, thus targeting ubiquitinated proteins to nascent autophagosomes (Shaid *et al*., 2013). When autophagosome formation is completed, its outer membrane fuses with the lysosome to form the autolysosome, LC3-II is delipidated by ATG4 to recycle LC3-I for further autophagosome formation. Then, the completed autophagosomes docks and fuses with the endosomes, multivesicular bodies, and finally lysosomes (Eskelinen, 2005). Following autolysosome formation, the lysosomal hydrolases degrade the intra-autophagosomal contents, as well as the degrataion of LC3-II on the luminal face of autophagosomes. After digestion of intra-autophagosomal contents, increased mTOR activity attenuates autophagy and generates proto-lysosome tubules and vesicles that extrude from the autolysosome. Finally, autolysosome matures into functional lysosome by accumulating of lysosomal hydrolases (Li *et al*., 2006). The final step in autophagy is the export of leucine and other amino acids resulting from autophagic degradation, and it is mediated by ATG22 together with other vacuolar effluxers, such as Avt3 and Avt4 and the release of autophagic amino acids allows the maintenance of protein synthesis and cellular functions under starvation/stress conditions (Harvey and Leinwand, 2011; Yang *et al*., 2006). In healthy cells, autophagy is constitutively active and works as a key quality-control mechanism to preserve the integrity of organelles and the proteome (Green *et al*., 2011; Green *et al*., 2011; Mizushima *et al*., 2008). However, autophagy can be rapidly stimulated during starvation, growth factor withdrawal or high bioenergetic demand, and also in response to a variety of cellular insults including oxidative and proteotoxic stress, metabolic and organellar stress (Kroemer *et al*., 2010). Stress-induced activation of autophagy proceed until nutrient availability is restored, while at the same time, removes damaged macromolecules and organelle, thus favoring repair and viability. Several studies have indeed confirmed that clearance of mitochondria, through mitophagy, and clearance of protein aggregates are examples of selective autophagy. Therefore, it is not surprising that autophagy defects underlie various disorders including neurodegeneration, metabolic disease, infectious diseases, and cancer (Ariosa and Klionsky, 2016).

1.2.2.2 The dual role of autophagy in cancer

Tumourigenesis is a multistage evolutionary process through which cancer cells gain abilities to survive in severely unfavorable environmental conditions, thus overcoming physiological barriers restraining growth. Autophagy can act as a '*Janus-faced*' player in cancer progression. In the early

steps of cancer development it plays a protective role, preventing the accumulation of damaged proteins and organelles, such as damaged mitochondria, which are known to be the major source of ROS, thereby limiting tumor-promoting effect of ROS. In contrast, in the late steps of cancer development (promotion, progression and metastasis) autophagy promotes tumour growth by helping cancer cells to overcome the adverse conditions of cancer microenvironment (Yang *et al*., 2015).

1.2.2.3 Autophagy as a tumour suppressor mechanism

Several studies have linked defects in the autophagic machinery with the acquisition of malignant features by healthy cells (Galluzzi *et al*., 2015). The first hint supporting an oncosuppressive role for autophagy during carcinogenesis has been demonstrated through genetic studies on mouse models. In particular, allelic loss of Beclin 1 in mice (Beclin $1^{-/-}$ animals are not viable) is associated with spontaneous development of hepatocellular carcinomas, lung adenocarcinomas, lymphomas and leukemia (Galluzzi *et al*., 2015). Similarly, the generation of knockout mice for different key autophagy genes that interact with Beclin-1, such as AMBRA1 (activating molecule in Beclin 1 regulated autophagy protein-1) (Fimia *et al*., 2007), BIF-1(Bax interacting factor-1) (Harrison *et al*., 2008) and UVRAG (Liang *et al*., 2006) has shown that these defects are associated with the development of spontaneous tumours, and for this reason they are classified as a new haploinsufficient tumour suppressor genes. Further, Beclin-1 autophagy gene is monoallelically deleted in 40-75% of cases of human sporadic human breast, ovarian and prostate cancers (Qu *et al*., 2003). Taken together these results suggests that Beclin-1 functions as a haploinsufficient tumor suppressor gene (Yue *et al*., 2003; Qu *et al*., 2003). However, some more recent findings about Beclin-1 has decreased the certainty of its role as tumor suppressor gene. In fact, Beclin1 is next to the tumour suppressor gene breast cancer 1 (BRCA1) on chromosome 17q21, and it is often co-deleted with its neighboring gene BRCA1, that thus represent the primary driver mutation in hereditary and sporadic breast cancers (Laddha *et al*., 2014). The mechanisms involved in the regulation of autophagy largely overlap with signaling pathways implicated in the control of cancer, in fact many oncogenes and tumour suppressors participate in the regulation of autophagy. Notably, tumor suppressor genes that negatively regulate mTOR, such as p53, phosphatase with tensin homologue (PTEN), alternative reading frame (ARF) stimulate autophagy while, conversely, oncogenes that activate mTOR, such as class I phosphoinositide 3-kinase (PI3K-I), Ras, Ras homolog enriched in brain (RHEB), and AKT inhibit autophagy. All together, these evidence supports the assumption that autophagy may play an important role in tumour suppression at early stages.

1.2.2.4 Autophagy as a tumour promoter mechanism

In established tumours, autophagy is emerging as a built-in mechanism that tumoural cells exploit to adapt to poorly oxygenated environment of tumour and to maintain their energy balance, by recycling intracellular components into biosynthetic pathways or ATP synthesis and regulating secretion of pro-tumourigenic factors. Interestingly, in advanced and aggressive tumours such as pancreatic cancer, as well known to be a hypovascular tumor, autophagy is drived by oncogenes to support energy metabolism and thus allow growth under nutrient deficit conditions (Harris, 2002). Furthermore, using a mouse model of non-small cell lung cancer (NSCLC), it was shown that inhibition of autophagy by Atg7 deletion leads to accumulate dysfunctional mitochondria, decreases in cell proliferation, resulting into reduced tumor burden. In this context, inhibition of autophagy reduces malignancy, resulting in a shift of Ras-induced adenomas and adenocarcinomas to benign oncocytomas, thus suggesting a pro-tumourigenic role of autophagy (Guo *et al*., 2013). Another aspect that connect autophagy to tumour progression, is the capability of advanced cancer cells to exploit autophagy as a trafficking and export mechanism of pro-inflammatory/pro-angiogenic cytokines and chemotactic/pro-invasive molecules, such as extracelluar ATP (Galluzzi, 2015; White *et al*., 2015; Maes *et al*., 2013). Therefore, autophagy promote tumor cell survival by increasing stress tolerance and providing a pathway that satisfy the enhanced bioenergetic and biosynthetic needs of these cells. In melanoma it has been shown that blocking autophagy may aggravate or induce cell apoptosis (Marino *et al*., 2010; Del Bello *et al*., 2013; Cervia *et al*., 2016; Rouaud *et al*., 2016; Hambright and Ghosh, 2017; Ryabaya *et* al., 2017; Ranieri *et al*., 2018; Zheng *et al*., 2018), likely due to excessive accumulation of autophagic vacuoles containing deleterious undegraded material which has the potential to turn autophagy into a destructive process. The role of autophagy and its regulation in cancers continue to emerge, and many studies aim to define new strategies to modulate autophagy for improving chemotherapy success (Yang *et al*., 2011).

1.2.2.5 Autophagy modulation for cancer therapy

Currently, several Food and Drug Administration (FDA)-approved drugs have been proposed as inducers (for example, rapamycin, fluspirilene,trifluoperazine, pimozide, niguldipine, nicardipine andamiodarone, loperamide) or inhibitors of autophagy (for example, chloroquine, hydroxychloroquine, verteporfin) (Zhang *et al*., 2007; Donohue *et al*., 2011). Nevertheless, several studies have been reported that inhibition of autophagy sensitizes cancer cells to DNA damaging anticancer agents. Pharmacological inhibitors of autophagy can be subdivided as early-stage inhibitors , including 3-methyladenine (Class-III-PI3K inhibitors), wortmannin, and LY294002, or late-stage inhibitors of the pathway, including chloroquine (CQ), hydroxychloroquine (HCQ) and bafilomycin A1. The natural compound bafilomycin A1 has been recently shown to activate early

stage of autophagy by down-regulating mTOR pathway, and inhibit later stages of autophagy by inducing caspase-independent cell death in hepatocellular carcinoma. In addition, another natural product, tetrandrine, which blocks autophagic flux and induces apoptosis in cancer cells, has been shown to induce a significant phosphorylation of AMPK. However, of these autophagy inhibitors, only CQ and HCQ have been evaluated in humans, because they are generally used as antimalarial drugs and in autoimmune disorders. CQ or HCQ are lysosomotropic agents that prevent the acidification of lysosomes, thereby impairing autophagosome degradation. Currently, there are more than 30 clinical trials registered in the National Cancer Institute and nearly all use CQ or HCQ for the treatment of refractory malignancies. Most of these trials are ongoing with promising results (Amaravadi *et al*., 2011; Carmeliet and Jain, 2011; Maes *et al*., 2014; Manic *et al*., 2014; Huang *et al*., 2013) and most of them used HCQ in combination with other anti-cancer treatments. A recent studies showed that chloroquine-induced autophagy cell death may be p53-dependent in Myc-driven lymphoma (Amaravadi *et al*., 2011) or p53-independent in glioma cells (Geng *et al*., 2010). Furthermore, it was observed that combination treatment with CQ and NVP-BEZ235, a double PI3K / mTOR inhibitor, may improve the antitumor effects induced by the blockage of autophagy in glioblastoma cells and in non-small cell lung cancer (Xu *et al*., 2011 Cerniglia *et al*., 2012). Nowadays, many Phase I / II trials are ongoing to evaluate the modulation of autophagy by CQ/HCQ in combination with standard treatment in patients with lymphomas, colorectal, kidney, lung, pancreas, prostate and ovary cancer. However, these drugs have different off-target effects and modulate other cellular activities, such as endocytosis, intracellular trafficking, biogenesis and lysosomal function (Baek *et al*., 2012). In any case, being able to pharmacologically modulate the cell fate with compounds that promote the activation of the apoptotic pathway in combination with inhibitors of the autophagic pathway could be a promising therapeutic strategy to enhance cancer treatment, including melanoma treatment. However, much work remains to be done to determine the specific impact of these modulators on tumor initiation, promotion, progression and therapeutic response for further clinical uses.

1.3 Crosstalk between apoptosis and autophagy

The connection between apoptosis and autophagy is a growing area of research and they could be directly linked in two different ways. First, the process of autophagy could control apoptosis either by making it more or less probable. Second, the process of apoptosis could control autophagy, increasing or decreasing it. More recently, the interplay between apoptosis and autophagy machinery has been described, leading to the idea that they can be triggered by common upstream signals and share common regulators, such as p53, the PI3K/Akt axis and the interaction between Bcl-2 and

Beclin-1 (Eum and Lee, 2011). Interestingly, Beclin 1, an important initiating factor of autophagy, was originally isolated as a Bcl-2- interacting protein (Liang *et al*., 1998). Beclin contains a BH3 domain, that is important for binding to antiapoptotic Bcl-2 homologs, such as Bcl-2 and Bcl-XL, and required for Bcl-2-mediated inhibition of autophagy (Maiuri *et al*., 2007; Koff *et al*., 2015). Reciprocally, members of the autophagy system can also affect the intrinsic apoptotic pathway. For instance, Autophagy-related gene 5 (ATG5), that is known as the "core" of autophagy, is also found to be involved in the regulation of apoptosis. It has been revealed that the over-expression of ATG5 can enhance the susceptibility of cells to activate the intrinsic cell death pathway. DNA damage induces calpain-mediated ATG5 cleavage, generating the ATG5 fragment (24-kDa) which translocates to the mitochondria, where binds to Bcl-XL, promoting the cytochrome c release and caspase activation, (Yousefi *et al*., 2006; Koff *et al*., 2015). The signaling adaptor p62, which shuttles ubiquitinated proteins to the lysosome, regulates the activity of the apoptotic initiator caspase-8 (Villar *et al*., 2017), but caspase-8 also cleaves p62 in response to death receptor activation (Jin *et al*., 2009; Norman *et al*., 2010). The proteins involved in the crosstalk between these pathways may have particularly important roles in cancer disease and hence detailed molecular information about the mechanisms of crosstalk is crucial for the development of anticancer therapeutics.

1.3.1 p53 a master regulator of autophagy and apoptosis

p53 is traditionally considered a “guardian of the genome”, being one of the major suppressors of tumorigenesis that can kill cancer cells or inhibit their growth. Loss or gain of p53 function results in the aberrant growth of cells, hence its cellular expression and its activity are tightly regulated. Upon irreparable DNA damage, the stress-responsive transcription factor p53 activates pro-apoptotic proteins, including PUMA, Noxa, Fas, Bax and pro-apoptotic members of the Bcl-2 family, thus promoting apoptosis. Moreover, p53 was also shown to increase genomic stability via suppression of retrotransposons, whose over expression leads to mutagenesis and hence reduces the risk of tumorigenesis, as it promotes either the repair or elimination of cells with damaged DNA (Harris *et al*., 2009). However, the exact mechanisms by which p53 mediates tumour suppression are not entirely understood. Whereas p53-dependent modulation of cell cycle arrest and apoptosis mechanisms appear crucial for p53-mediated tumour suppression in some studies, in other ones their involvement in p53 effects may be dispensable (Bykov *et al*., 2018). In recent years, p53 has also been reported to possess some novel “non-canonical” functions, including the regulation of autophagy via the AMPK/TSC2-mTOR signaling pathway (Mrakovcic and Fröhlich, 2018). In particular, p53 can act as either an activator or an inhibitor of autophagy depending on its subcellular localization. On the one hand, p53 functions as a nuclear transcription factor and transactivates

proapoptotic, cell cycle-arresting and proautophagic genes. On the other hand, cytoplasmic p53 can operate at mitochondria to promote cell death and can repress autophagy via poorly characterized mechanisms. In addition, cytoplasmic p53 was demonstrated to interact with Beclin-1 in embryonal carcinoma cells, which promotes its ubiquitination and degradation and thereby suppressing autophagy (Tripathi *et al*., 2014). Beclin-1-induced autophagy mediated by up- or down-regulated BCL2-family members can be furthermore blocked by caspase-mediated cleavage of Beclin-1, triggering apoptosis via cytochrome c release from the mitochondria (Yousefi *et al*., 2006). This mechanism represent another possibility of bidirectional interplay between apoptosis and autophagy. Although the extent to which autophagy regulation determines cell death/survival by p53 is unclear, it may underlie key aspects on the biology and treatments of cancer (Levine and Abrams, 2008; Sui *et al*., 2011; Tang *et al*., 2015; White, 2016; Simabuco *et al*., 2018).

1.4 A snapshot on melanoma

Melanoma is one of the most aggressive forms of cutaneous tumour characterised by abnormal proliferation of melanocytes and it is responsible for the 60-80% of skin cancer-related deaths worldwide, which is widely due to its disposition to spread to other tissue and organs (Gonzalez *et al*., 2013; Abildgaard *et al*., 2015). Recent epidemiologic evidence has demonstrated an increase in incidence in the white population over the past two decades (Ferlay *et al*., 2012). The main environmental risk factors for melanoma development is the exposure to ultraviolet light radiation (UV), which can trigger DNA damage through UV-induced ROS production, that in turn directly causing genetic alterations (Bertolotto, 2013). In particular, UVB induces the formation of cyclobutane pyrimidine dimers (CPDs) and 6–4 photoproducts, a specific link between two pyrimidine rings (Mouret *et al*., 2010), while UVA contributes through the formation of free radicals. Formation of dimers interferes with base pairing during DNA replication and thereby leads to mutations. Free radicals, single-strand breaks and double-strand breaks lead to immediate DNA damage upon replication.

Men are more susceptible to developing melanoma than women (relative risk (RR) 1.74), with men developing melanoma most commonly on the trunk and women on the extremities. Other risk factors include age (RR 1.02 per year increase), family history (RR 2.19 for positive family history), number of naevi (RR 3.08), hair color (RR 0.60 for black hair, RR 1.21 for blonde and 2.05 for red hair) and history of sunburns (RR 2.36 for >10 severe sunburns).

Of all melanomas, 5-12% are estimated to be hereditary. The most common driver gene is cyclin-dependent kinase inhibitor 2A (CDKN2A), which codes for proteins acting as tumor suppressors in

the cell cycle. Autosomal dominant inheritance of germline CDKN2A mutations has been implicated in approximately 20-40% of familial melanoma; the mutation frequency varies between different geographical regions.

Mutations affecting the mitogen-activated protein kinase (MAPK) pathway are present in the large majority of cutaneous melanomas, predominantly affecting the NRAS (approximately 20%) (Demunter *et al*., 2001) or BRAF (approximately 40–50%) proteins (Davies *et al.*, 2002). Whereas early-stage melanoma can be effectively treated with surgery, metastatic melanoma is still a therapeutic challenge despite the large number of chemotherapeutic regimens so far devoleped (Tsao *et al*., 2004; Gogas *et al*., 2007; Nikolaou *et al*., 2012; Finn *et al*., 2012; Megahed *et al*., 2014). Traditionally, melanoma was treated with different antineoplastic agents including dacarbazine, temozolomide, paclitaxel with or without carboplatin. In particular, chemotherapy with the alkylating agent decarbazine (DTIC) as monotherapy remains the standard of care in patients with inoperable metastatic melanoma. However, the response rate of melanoma to DTIC have been reported between 10-20% and it has not been demonstraed to improve overall survival. Melanoma has also a close relationship with the immune system, with tumour infiltration by immune cells often indicating their attempt to eliminate the tumour. Indeed, immunotherapy remains a critical component of treatment of melanoma, for istance Ipilimumab, which works to activate T cells, shrinks tumours and improve overall survival in patients with metastatic melanoma. Noteworthy, melanoma is a disease characterised by cutaneous, subcutaneous and nodal metastases, which has led to study various intra-lesion therapies. Indeed, the ease of drug delivery of localised treatments makes them attractive particularly in melanomas (Sloot *et al*., 2014; Agarwala, 2015). In recent years new targeted therapies have been developed that have been shown to be more effective than chemotherapy. Agents demonstrating promise include: Vemurafenib (selective BRAF inhibitor), Dabrafenib (selective BRAF inhibitor) and Trametinib (MEK inhibitor). While these novel therapies have ameliorated significantly the overall time of survival still a definite cure for melanoma is lacking. A striking feature of melanoma is also the development of resistance to therapy over time. In an effort to improve response rates and delay resistance, a possible strategy is to combine the new targeted drugs and immunetherapies with compounds that overcome the ability of melanoma cells to respond to damage and eventually modulate the apoptotic and autophagy pathways. A large variety of natural products have been isolated from natural sources, principally from plants, microorganisms and marine organisms (Khazir *et* al., 2014) and some of which are been exploited by the pharmeceutical industry. In fact, to date, approximately 80% of anticancer drugs approved by the FDA are natural products, natural products derived or synthetic molecules inspired to natural compounds. Recent studies have revealed that the protozoan ciliates, common

almost everywhere there is water where they play a key role in microbial food web, are able to synthesize secondary metabolites and for this properties they may considered as a source of biological agents.

2. State of the art

2.1 Biologically active compounds from the protozoan ciliates

Natural compounds have been reported to be involved in the modulation of several cellular events, thus showing a great potential to unravel physiological process and to be translated into clinical use, as for instance cancer treatment (Nobili *et al*., 2009; Harvey *et al*., 2015). Given this context, we proposes to explore eukaryotic microbes (protists), essentially ciliates, as source of natural products. Ciliophora, also called ciliates, is a group of protists within the superphylum Alveolata, that are characterised by the presence on their cell surface of hair-like organelles called cilia, and are equipped with two kind of nuclei, a diploid micronucleus and a polyploid macronucleus (Ruggiero *et al*., 2015). Free-living ciliates are common almost everywhere there is water, where they play a key role in microbial food web. There are about 8000 species of ciliates and many of them are able to synthesise cell type-specific signalling protein pheromones presiding cell–cell communication, and secondary metabolites belonging to different biogenetic classes (Guella *et al*., 2010). Among these, one class is represented by pheromone peptides and proteins, isolated from five species, *i.e*. *Blepharisma japonicum*, *Euplotes raikovi*, *Euplotes octocarinatus*, *Euplotes nobilii*, and *Euplotes crassus* (Luporini *et al*., 2006; Luporini *et al*., 2015). From a functional point of view, these class of peptides may act both via paracrine-like (or heterotypic) interactions to induce mating of cells, thus promoting the vegetative (mitotic) proliferation of the same cells from which they are released (Vallesi *et al*., 1995; Vallesi *et al*., 2005; Luporini *et al*., 2006; Luporini *et al*., 2015). Of note, *Euplotes raikovi* pheromone Er-1 is able to increases DNA synthesis, proliferation and viability of human lymphoid Jurkat T-cells, binding to IL-2 receptor and this represents a possible application in pharmacological perspective (Cervia *et al*., 2013). The acetylated sesquiterpenoid euplotin C, isolated from cultures of the marine ciliate protist *Euplotes crassus*, provides a potent mechanism for reducing populations of potential competitors via its cytotoxic properties (Guella *et al*., 1994). At molecular level, euplotin C decreases mitochondrial function and activates a caspase-dependent type of apoptosis in *Euplotes vannus*, that does not produce euplotin C, without affecting the generation of reactive oxygen species (ROS) (Trielli *et al*., 2008; Cervia *et al*., 2009). Recently, it has also been shown that euplotin C is a powerful cytotoxic and pro-apoptotic agent in tumour cell lines, including different human melanoma cell lines (Cervia *et al*., 2007; Guella *et al*., 2018). Another class of products from ciliates is depicted by pigments. The blue-green pigment stentorian and blepharismin produced by Stentor coeruleus and Blepharisma japonicum respectively (Lobban *et al*., 2007; Pant *et al*., 1997; Matsuoka *et al*., 2010), which display a cytotoxic effect against

predatory protozoans (Giese, 1973; Kato and Matsouka, 1995). In addition, blepharismins were found to have a strong bactericidal effect against methicillin-resistant *Staphylococcus aureus* (MRSA), and this effect was enhanced by light irradiation (Pant, 1997). The toxins keronopsin A and B produced by *Pseudokeronopsis rubra*, are able to crippling or killing the predators (Höfle *et al*.,1994).

The advantage of using ciliates, as source of new drugs, relies on the sustainability of the natural resource practically with no environmental impact. In fact, the ciliates can be easily collected from practically everywhere there is availability of liquid water without affecting biodiversity. Although a vast and representative number of species is already in collection only a small number of different ciliate species is cultivated in the laboratories, implying that the vast biodiversity of eukaryotic microbial natural products remains underappreciated. Single-celled eukaryotes can be well adapted to captivity, cheap to cultivate under laboratory conditions, perpetuated even into large-scale cultures at reduced costs and with no legal restrictions, and simple to manage for the production of candidate drugs with practically no waste.

Thus, the huge, untapped, ecological biodiversity of ciliates and their molecules holds great promise for the discovery of novel natural products and deserve to be investigated in drug development.

2.2 Climacostol

This PhD thesis is focused on recent data on the biological activities of climacostol (Masaki *et al*., 1999), a defensive secretion produced by the freshwater ciliated protozoan *Climacostomum virens* for chemical defense against natural predators. This colourless toxin is located in membrane-bond organelles, that ciliates evolved in association with their cortex, called exstrusomes in relation to their unique capacity of discharging after mechanical or chemical stimuli. The molecular structure of climacostol was established as 1,3-Dihydroxy-5-[(Z)-2'-nonenyl]benzene and confirmed by the total synthesis (Muto *et al*., 2011; Masaky *et al*., 1999). On the basis of this, climacostol is classified as a resorcinolic lipid, which is one of the most investigated classes of phenolic lipids for their abundance in nature, structure and potent biological activities. In fact, they are secondary metabolites synthesized largely by 11 families of the higher plants, 5 lower plant families (algae, mosses and fungi), several bacterial family, in one animal species, a marine sponge, and in a ciliated protozoan. The structural motif of resorcinolic lipids is the resorcinol unit as the core (1,3-dihydroxybenzene), linked to an odd-numbered carbon chain substituent, with various degrees of unsaturation. Hence, climacostol has a dual hydrophilic and hydrophobic character as well as all resorcinolic lipids. In particular, climacostol is resorcinol with an alkenyl chain at 5-position of the

aromatic ring, which have in turn a Z-configured carbon–carbon double bond at the 2-position (Fiorini *et al*., 20009). The prevention of isomerization of the Z-configuration is notable to maintain climacostol biological activities and to gain this purpouse, various methodologies have been suggested. However, to date, the strategy introduced by Fiorini *et al*. (2010) resulted more useful than the previously reported for providing exclusively the desired Z-isomer.

2.2.1 Biological effects of Climacostol

It has been proved that climacostol exerts a potent antimicrobial activity against eight different Gram-positive bacteria, such as *Staphylcoccus aureus*, *Staphylcoccus epidermidis*, *Staphylcoccus pneumonia* and *Enterococcus faecalis*, and a fungicidal activity against *Candida albicans*. Conversely, climacostol is no active against Gram-negative species, such as *Eschierichia coli* and *Pseudomonas aeruginosa*. The scarce activity of climacostol can be explained by the peculiar structure of the Gram-negative bacteria cell wall, that represents a selective barrier to the penetration of the compound (Petrelli, 2012). Buonanno and Ortenzi investigated the cytotoxic activity of climacostol and its derivatives on *C. virens* and nine other common species of free-living freshwater ciliates. Their results show that all compounds studied exerted a considerable cytotoxic effect on all the species examined in a concentration and exposure time-dependent manner. Interestingly, the cytotoxic potential of the compounds appeared inversely correlated to their unsaturation level of the aliphatic side chains and the potency of theirs action was also related to the target organism. Of interest, some alkylresorcinol molecules are able to interact with double helix of DNA, this interaction is realized across the incorporation by intercalation of chains into the helix interior. It was also demonstrated that other alkylresorcionol exhibit the ability for mediating Cu^{2+}-dependent DNA cleavage associated with the generation of reactive oxygen species and apoptosis induction. Quassinti and collegues (Quassinti *et al*., 2013) demonstrated that climacostol induces strand breakage of plasmid pBR322 DNA and also the double strand of calf thymus DNA in presence of Cu^{2+} ions. In fact, it has been observed that the DNA cleavage mediated by climacostol occurs following initial hydroxylation of the benzene nucleus, a process that is facilitated in presence of Cu^{2+} and O_2. The mechanism of climacostol pro-oxidant effect involves reduction of Cu^{2+} by the benzene moiety, with the subsequent generation of diffusible oxygen radicals that, in turn, induce oxidative DNA damage. The ability of superoxide dismutase (SOD), catalase and neucuproine, that are radical scavengers and a Cu^{+}-specific sequestering agent respectively, to suppress DNA breakage is consistent with the intermediacy of reactive oxygen species and Cu^{+} ions in climacostol DNA damage (Quassinti *et al*., 2013). Recently, climacostol was found to induces morphological changes in rat liver mitochondria and specifically inhibits the electron transport at complex I (NADH ubiquinone oxidoreductase

complex) of their respiratory chain (Muto *et al*., 2011). Among the consequences deriving from impairment of the respiratory chain complex I there is an increase of reactive oxygen species (ROS) formation, leading to activation of the mitochondrial dependent cell death signaling pathways. The generation of ROS in mitochondria might be implicated in the process of climacostol action. In this regard, it has been shown that climacostol is able to exerts a significant apoptotic effects in human pro-myelocytic leukemia HL60 cells and this fact is effectively preceded by the intracellular ROS generation, membrane potential dissipation and caspase-9/-3 activation (Buonanno *et al*., 2008). To further investigate the involvement of ROS in climacostol-induced cytotoxicity, Buonanno et al. (2009) examined the antioxidant effects of N-acetylcysteine (NAC) on caspases activation. In fact, NAC has been widely used as a research tool in the field of apoptosis research. As expected, the citotoxicity of climacostol in HL60 cells appears to be appreciably inhibited by the action of Nac, that neutralizes ROS generation and limits caspases activation. Taken together, these preliminary data suggest that climacostol might be used for cancer chemoprevention or therapy.

In this study, using well-established mouse models of melanoma, we characterized at pre-clinical level the anti-tumor properties of climacostol and its newly synthesized derivatives in order to evaluate their therapeutic potential.

3. Materials and Methods

3.1 Climacostol and its analogues

Chemically synthesised climacostol ($C_{15}H_{22}O_2$, alkenyl resorcinol) was obtained as previously described (Fiorini *et al*., 2010). The configuration of the double bond was assigned as (*Z*)-based. The NMR spectroscopy of the climacostol obtained by our procedure allowed to determine that the content of (*Z*)-diastereomer (the active molecule) was major than 99%, without contamination with the (*E*)-diastereomer (less active molecule). Synthetic climacostol was then dissolved in absolute ethanol at 10 mg/ml stock, and stored in the dark at - 20 °C until use. The stock solution of climacostol was diluted in phosphate buffered saline (PBS) (Euroclone, Pero, Italy) or in culture medium for *in vivo* injections and *in vitro* experiments, respectively. Buonanno *et al*. (2018) have synthetized two synthetic new analogs of climacostol, *i.e*. the 1,3-dihydroxy-2-methyl-5-[(Z)-non-2'-enyl]benzene (AN1) and the 1,3-dihydroxy-2-methyl-5-[(Z)-non-2'-enyl]benzene (AN2), carrying an additional OH- group and an CH3- group, respectively, in the aromatic ring. Also the climacostol analogues AN1 and AN2 were dissolved in ethanol (1 mg/ml) and stored in the dark at –20°C. The solutions were diluted with the appropriate medium at the time of the experiment.

3.2. Animals and cell cultures

Female C57BL/6 mice (8-12 weeks old) were purchased from Charles River Laboratories (Calco, Italy), housed in a regulated environment (23 ± 1°C, 50 ± 5% humidity) with a 12 h light/dark cycle (lights on at 08.00 a.m.), and provided with food and water ad libitum. All studies were conducted in accordance with the Italian law on animal care N°116/1992 and the European Communities Council Directive EEC/609/86. All efforts were made to reduce both animal suffering and the number of animals used.

Hela, PC12, AtT-20, NIH/3T3, B16-F1025–32, P3X and TM3 (American Type Culture Collection) cell lines were cultured at 37°C, 5% CO_2 in an humidified atmosphere. Cells were maintained in the presence of 10% fetal bovine serum-cointainig medium and in logarithimic growth phase. Murine melanoma B16-F10, murine glioma GL261, human glioblastoma U87MG (Bizzozzero *et al*., 2014; Assi *et al*., 2015; Cervia *et al*., 2016; Perrotta *et al*., 2016; Perrotta *et al*., 2018), human melanoma A375 and SK-MEL-5 (obtained by the American Type Culture Collection) cell lines were cultured in Iscove's supplemented with 10% heat inactivated foetal bovine serum, glutamine (200 mM),

penicillin/streptavidin (100 U/ml), 1% Hepes 1 M (Euroclone), pH 7.4, and grown at 37°C in a humidified atmosphere containing 5% CO2 (logarithmic growth phase, routine passages every 3 days). To create GFP-expressing B16-F10 cells (B16-GFP), cells were transfected with lentivirus pLVX-Puro (Takara Bio USA, Mountain View, CA, USA) encoding for EGFP, produced upon transfection of HEK-293T packaging cells with the lentiviral vector. After two cycles of infection cells were selected with puromycine (1 μg/ml) for 2 weeks in order to obtain a stable GFP-expressing cell line.

3.2.1 RNA interference

Gene silencing of p53 and AMPKα in B16-F10 cells was performed as previously published (Chen *et al*., 2011; Perrotta *et al*., 2016). Briefly, according to the manufacturer's protocol, iBONI siRNA Pool (Riboxx, Radebeul, Germany) targeting mouse p53 (trp53) and AMPKα1/2 (Santa Cruz Biotecnology, Dallas, Tx, USA) were mixed to Lipofectamine RNAiMax transfection reagent (Life Technologies, Monza, Italy). iBONI siRNA Pool negative control (Riboxx) and control siRNA-A (Santa Cruz Biotecnology) (non-targeting siRNAs) were also used. The mix was added to cultured B16-F10 cells at a siRNA concentration of 10-50 nM. for 48 h.

3.2.2 Animal handling and allograft tumour models

Using published protocols (Perrota *et al*., 2007; Bizzozzero *et al*. 2014; Cervia *et al*., 2013; Cazzato *et al*., 2014; Catalani *et al*., 2016;), mice (weighting 18–21 g) received subcutaneous injections of 5×10^4 cells B16-F10 in the lower-right flank. When the syngeneic implantation was established (usually 10 days after tumour cells inoculation) and the tumour was palpable (volume range between 15–30 mm^3), mice were randomly assigned to one of the two experimental groups. In particular, transplanted mice received 100 μl intra-tumour injections of vehicle or climacostol (600 μg/ml, equivalent to ca. 3 mg/kg dose, respectively) every 3–4 days. Mice were then photographed and tumour growth was monitored twice a week by means of external calliper measurements and volume calculation (length × width2/2) until mice reached IACUC euthanasia criteria, as for instance clinical signs of tumour or when tumour size exceeded 10% of body weight (tumour volume ca. 1500 mm^3). The mice were also observed to determine the duration of survival for each group using the Kaplan-Meier estimator (median survival). At day 16 mice were sacrificed, tumours removed and processed for PCR, immunostaining and western blot. In testing the toxicity of intraperitoneal injection of climacostol, mice were administered with dissolved drug (at 2 and 4 mg/kg) every 3-4 days. A single cell suspension from tumours was also obtained by collagenase IV (0.2 mg/ml), dispase (2 mg/ml) and DNase I (0.1 mg/ml) treatment in Iscove's modified Dulbecco's

medium. Cell viability was measured after 0.2% Trypan Blue staining by counting trypan blue-excluding cells with a TC20 Automated Cell Counter (Bio-Rad, Hercules, CA, USA). In another set of experiments, mice received 1×10^5 B16-F10 cells into tail vein (Bizzozzero *et al*., 2014). The week after, climacostol was intraperitoneally injected every 4-3 days at 4 mg/kg. Two weeks after climacostol treatments mice were sacrificed and the diaphragm skeletal muscle tissue removed for immunofluorescence evaluation.

3.3 MTT and Trypan blue viability assay

Cell viability on human or murine cancer cell lines was determined by MTT assay using published protocols (Cervia *et al*., 2006; Armani *et al*., 2007; Cervia *et al*., 2007; Di Giuseppe *et al*., 2011; Cervia *et al*., 2013; Bizzozzero *et al*., 2014; Perrotta *et al*. 2014). MTT absorbance was quantified spectrophotometrically using a Glomax Multi Detection System microplate reader (Promega, Milano, Italy). B16-F10 cells were also stained with trypan blue (Bio-Rad) and the amount of living cells was determined using a Bio-Rad TC10 Automat Cell Counter. Cells were visualized sing a Leica DMI4000 B automated inverted microscope equipped with a DCF310 digital camera.

3.3.1 Proliferation assay

B16-F10 cell proliferation was assessed by measuring the serial halving of cell fluorescence intensity via flow cytometry (Cervia *et al*., 2013). The CytoTrack Cell Proliferation Assays (CytoTrack Green; Bio-Rad, Hercules, CA, USA) was used, according to the manufacturer's protocol. CytoTrack Assay dye is evenly distributed in the cytoplasm and stoichiometrically distributed to daughter cells during cell division. The fluorescence was analysed by Gallios Flow Cytometer (Beckman-Coulter, Brea, CA, USA) and the software FCS Express 4 (De Novo System, Portland, OR, USA). The proliferation index, defined as the average number of cells that an initial cell became, was calculated using FCS Express software.

3.3.2 Annexin V-FITC/PI staining and mitochondrial membrane potential

B16-F10 cells were incubated with 5 µg/ml Annexin V-FITC to assess the phosphatidylserine exposure on the outer leaflet of the plasma membrane, and 5 µg/ml PI (DNA-binding probe) to exclude necrotic cells in binding buffer (10 mM HEPES, 140 mM NaCl, 2.5 mM CaCl2). Mitochondrial potential was measured by cell staining with 500 nM of sensitive fluorescent dye, TMRM (Sigma-Aldrich, Saint Louis, MO, USA), according to the manufacturer's protocol. Cell staining was acquired by flow cytometry.

3.3.3 Immunofluorescence microscopy

In vivo resected B16-F10 tumours were immersion-fixed in 4% paraformaldehyde in 0.1 M phosphate buffer (PB), pH 7.4, for 3 h, as previously published (Cervia *et al*., 2003; Catalani *et al*., 2016; Cervia *et a*l., 2016; Perrotta *et al*., 2016). The fixed tissue was transferred to 25% sucrose in PB. Tumour sections were cut at 10 μm with a cryostat, mounted onto positively charged slides and stored at -20°C. For Caspase 3 staining, sections were pre-incubated for 15 min with 5% BSA and 10% of normal goat serum (Life Technologies, Monza, Italy) in 0.1 M phosphate buffer (pH 7.4) containing 0.5% Triton X-100. Pre-treated sections were incubated overnight with the rabbit polyclonal anti-cleaved Caspase 3 primary antibody (Cell Signaling Technology, Danvers, MA, USA). For fluorescence detection, sections were stained with the appropriate Alexa Fluor secondary antibody (Life Technologies, Monza, Italy) and cover slipped with a phosphate buffer-glycerin mixture containing DAPI. Incubation in secondary antibody alone was performed as negative control. Images were acquired by a Zeiss Axioskop 2 plus microscope equipped with the Axiocam MRC photocamera and the Axiovision software (Carl Zeiss, Oberkochen, Germany). Dissected diaphragm tissues (De Palma *et al*., 2014; Pambianco *et al*., 2016) were rapidly frozen and then cut at 10 μm with a cryostat, mounted onto positively charged slides and stored at -20°C until use. Slides were then immersion-fixed in 4% paraformaldehyde in PB, pH 7.4, for 10 minutes. Sections were treated for 30 min at room temperature with 5% bovine serum albumine and 10% of normal goat serum (Life Technologies) in PB containing 0.5% Triton X-100. Overnight incubation was performed with one of the following rabbit primary antibodies: anti-LC3, anti-p62/SQSTM1 and anti-laminin A (Sigma-Aldrich), anti-melan-A (GeneTex, Irvine, CA, USA), anti-cleaved-caspase 3 (Cell Signaling Technology, Danvers, MA, USA) (Amato *et al*., 2017; Cammalleri *et al*., 2017), in PB containing 0.5% Triton X-100. For fluorescence detection, sections were stained with the appropriate Alexa Fluor secondary antibody (Life Technologies) in PB containing 0.5% Triton X-100 for 1.5 h and cover-slipped with Fluoroshield Mounting Medium containing DAPI (nuclei detection) (Abcam, Cambridge, UK). Incubation in secondary antibody alone was performed as a negative control. Images of resected tumours were acquired by a Zeiss Axioskop 2 plus microscope equipped with the Axiocam MRC photocamera and the Axiovision software (Carl Zeiss, Oberkochen, Germany). Images of diaphragm tissue were acquired by a Zeiss LSM 710 inverted confocal microscope. B16-F10 cells cultured in 120-mm coverslips were visualised by phase-contrast microscopy. Mitochondria were stained using MitoTracker Green FM (ThermoFisher Scientific, Waltham, MA, USA), according to the manufacturer's protocol. Cells were fixed in 4% paraformaldehyde and stained with the rabbit polyclonal anti-cleaved Caspase 3, anti-cleaved Caspase 9, anti-Bax, or the mouse monoclonal anti-Cytochrome c (Cell Signaling Technology,

Danvers, MA, USA), anti-phospho-histone H2A.X (ser139) (Merck Millipore, Darmstadt, Germany), anti-LC3, anti-p62/SQSTM1, anti-phospho-p53 (Ser15), and anti-p53 (Cell Signaling Technology, Danvers, MA, USA) primary antibodies. For fluorescence detection, cells were also stained with the appropriate Alexa Fluor secondary antibodies in PB containing 0.5% Triton X-100 for 1 h and cover-slipped in a ProLong Gold Antifade Mountant (Life Technologies, Monza, Italy), stained with DAPI (Sigma-Aldrich) and fluorescein phalloidin (cytoskeleton detection) (Life Technologies). Slides were analysed using a DMI4000B automated inverted microscope equipped with a DCF310 digital camera (Leica Microsystems, Wetzlar, Germany). Confocal imaging was performed with Leica TCS SP5 AOBS microscope system. Image acquisitions were controlled by the Leica LAS AF software.

3.3.4 Western blot analysis

Using published protocols (Pezzetti *et al*., 2009; Bizzozzero *et al*., 2014; Perrotta *et al*., 2015; Catalani *et al*., 2016; Cervia *et al*., 2016; Perrotta *et al*., 2016), *in vivo* resected B16-F10 tumours and human or murine cancer cell lines were homogenized in RIPA lysis buffer, supplemented with a mix of protease and phosphatese inhibitors (cOmplete and PhosSTOP; Roche Diagnostic, Milano, Italia). After removal cell debris by centrifugation (15,000 g x 30 min at 4°C), the proteins were estimated. Equal amounts of proteins were separated by 4-20% SDS-polyacrylamide gel electrophoresis (Criterion TGX Stain-free precast gels and Criterion Cell System) and transferred onto nitrocellulose membrane using a Bio-Rad Trans-Blot Turbo System. The membranes were blocked with 5% nonfat dry milk and incubated with mouse monoclonal anti-p53, the rabbit anti-LC3 and anti-p62/SQSTM1, anti-cleaved-caspase 3, anti-phospho-Akt (Ser473), anti-phospho-S6 (Ser240/244), and anti-phospho-AMPKα (Thr172) and mouse anti-p53 (Cell Signaling Technology, Danvers, MA, USA) (Amato *et al*., 2017; Cammalleri *et al*., 2017) primary antibodies. After the incubation with the appropriate horseradish-peroxidase-conjugated secondary antibody (Cell Signaling Technology, Danvers, MA, USA), bands were visualised using the Clarity Western ECL substrate with ChemiDoc MP imaging system (Bio-Rad). To monitor for potential artefacts in loading and transfer among samples in different lanes, the blots were routinely treated with the Restore Western Blot Stripping Buffer (ThermoFisher Scientific, Waltham, MA, USA) and re-probed with the mouse anti-vinculin (Sigma-Aldrich) or goat anti-HSP60 or anti-LDH-A and rabbit polyclonal anti-GAPDH (Santa Cruz Biotechnology, Dallas, TX, USA). Primary antibodies, *i.e.* rabbit anti-Akt and anti-AMPKα, and mouse anti-S6 (Cell Signaling Technology), that recognize the protein independently of its phosphorylation state, were also used in reprobing experiment for

normalization purposes. Then, immunoreactive bands were quantified for densitometry using the Bio-Rad Image Lab software.

3.3.5 Real-time PCR

The analysis of mRNA expression was performed as previously described (Cervia *et al*., 2013; Bizzozero *et al*., 2014; Cazzato *et al*., 2014; Catalani *et al*., 2016; Perrotta *et al*., 2016). Briefly, total RNA from *in vitro* B16-F10 cells and *in vivo* resected B16-F10 tumours was extracted with the High Pure RNA Isolation Kit and the High Pure RNA Tissue Kit, respectively (Roche Applied Science, Mannheim, Germany), according to the manufacturer's protocol. First-strand cDNA was generated from 1 µg of total RNA using iScript Reverse Transcription Supermix (Bio-Rad, Hercules, CA, USA). A set of primer pairs (Eurofins Genomics, Milano, Italy) was designed to hybridize to unique regions of the appropriate gene sequence (Table 2). PCR was performed using SsoAdvanced Universal SYBR Green Supermix and the CFX96 Touch Real-Time PCR Detection System (Bio-Rad, Hercules, CA, USA). The fold change was determined relative to the control after normalizing to Rpl32 (internal standard) through the use of the formula $2^{-\Delta\Delta CT}$.

Name	Gene	Primer sequence
p53	*trp53*	F: 5'-CACGTACTCTCCTCCCCTCAAT-3' R: 5'-AACTGCACAGGGCACGTCTT-3'
p21	*cdkn1a*	F: 5'-GGCCCGGAACATCTCAGG-3' R: 5'-AAATCTGTCAGGCTGGTCTGC-3'
Noxa	*noxa1*	F: 5'-ACGCGAAGACTGGGACTCT-3' R: 5'-AGCCCCTGTTAAAGTACATCCTA-3'
Puma	*bbc3*	F: 5'-GCTGAAGGACTCATGGTGAC-3' R: 5'-CAAAGTGAAGGCGCACTG-3'
LC3b	*map1lc3b*	F: 5'-CACTGCTCTGTCTTGTGTAGGTTG-3' R: 5'-TCGTTGTGCCTTTATTAGTGCATC-3'
p62	*sqstm1*	F: 5'-GAAGCTGCCCTCTACCCACA-3' R: 5'-AGAAACCCATGGACAGCATC-3'
beclin1	*becn1*	F: 5'-TGAATGAGGATGACAGTGAGCA-3' R: 5'-CACCTGGTTCTCCACACTCTTG-3'
bnip3	*bnip3*	F: 5'-TTCCACTAGCACCTTCTGATGA-3' R: 5'-GAACACGCATTTACAGAACAA-3'
bnip3L	*bnip3l*	F: 5'-TTGGGGCATTTTACTAACCTTG-3' R: 5'-TGCAGGTGACTGGTGGTACTAA-3'
atg3	*atg3*	F: 5'-CGGTCCTCAAGGAATCAAAA-3' R: 5'-TAGCTTTGCAGGCTTCCACT-3'
atg4	*atg4b*	F: 5'-ATTGCTGTGGGGTTTTTCTG-3' R: 5'-AACCCCAGGATTTTCAGAGG-3'
atg5	*atg5*	F: 5'-AGCAGCTCTGGATGGGACTGC-3' R: 5'-GCCGCTCCGTCGTGGTCTGA-3'
rpl32	*rpl32*	F: 5'-TTAAGCGAAACTGGCGGAAAC-3' R: 5'-TTGTTGCTCCCATAACCGATG-3'

Table 2. Primer pairs designed for real-time PCR analysis. F: forward, R: reverse

3.3.6 mRFP-GFP-LC3 assay

B16-F10 cells were seeded on 14 mm coverslips coated with poly-D-lysine and then cultured for 24 h. Cells were then transiently transfected with mRFP-GFP-LC3 plasmid (Garcia-Prat *et al.*, 2016), kindly provided by Dr. Pura Muñoz-Cánoves (Pompeu Fabra University, Barcelona, Spain), using Lipofectamine LTX and Plus Reagent (Life Technologies). Three hours following transfection at 37°C, two-thirds of the media is replenished with fresh media. After drug treatments, cells were washed once in PBS and fixed with 4% paraformaldehyde (in PBS) for 15 min at room temperature. After washing, coverslips were mounted on glass slides with ProLong Gold Antifade Mountant with DAPI and analysed using a Carl-Zeiss LSM 710 inverted confocal microscope. The number of

autophagosomes (number of yellow puncta per cell) and autolysosomes (number of red puncta per cell) was quantificated per cell, and at least 100 cells for each experiment were included.

3.3.7 Transmission electron microscopy

The collected B16-F10 cells were stored overnight at 4°C in a fixative solution containing 2.5% (v/v) glutaraldehyde and 2% (v/v) paraformaldehyde in 0.1 M cacodylate buffer, pH 7.2. Fixed cells were washed in cacodylate buffer and post-fixed with 2% (v/v) osmium tetroxide in 0,1 M cacodylate buffer, pH 7.2 for 2 h at 4°C. Samples were washed in the same buffer and dehydrated through an ascending series of ethanol and embedded in LRWhite resin (Electron Microscopy Science, PA, USA). For ultrastructural observations at least 20 ultra-thin sections (60-90 nm) were obtained using a Reichert Ultracut ultramicrotome equipped with a Leica diamond knife (Leica Microsystems, Wetzlar, Germany). Ultra-thin sections were collected on copper grids, stained with uranyl acetate and lead citrate, and observed with a JEOL 1200 EXII electron microscope (Jeol Ltd. Tokyo, Japan). Micrographs were captured by the Olympus SIS VELETA CCD camera equipped with iTEM software (Olympus, Tokyo, Japan).

3.3.8 Statistical analysis

Statistical significance of raw data between the groups in each experiment was evaluated using unpaired Student's t-test (single comparisons) or one-way ANOVA followed by the Newman-Keuls post-test (multiple comparisons). EC50 (the concentration producing half the maximum effect) and E_{max} concentration (producing the maximum effect) were determined by non-linear regression curve analysis of the concentration-effect responses. Potency values among concentration-response curves were compared with the F test. Kaplan-Meyer data were analysed with the multiple comparison survival curve method using the Log-rank (Mantel-Cox) test. Tumour growth was analysed using two-way ANOVA, followed by the Bonferroni post-test. Data belonging from different experiments were represented and averaged in the same graph. The GraphPad Prism software package (GraphPad Software, San Diego, CA, USA) was used. The results were expressed as means ± SEM of the indicated n values.

4. Results and discussion

4.1 Climacostol inhibits tumour cell growth

To investigate the cytotoxic properties of climacostol (Fig. 3a) , we used a panel of additional cells of tumour and non-tumour origin confirming the pharmacological properties and efficacy of this drug. Cells were analysed by Lactate dehydrogenase (LDH) activity and 3-(4,5-dimethylthiazol-2-yl)-2,5-diphenyltetrazolium bromide (MTT) assay. As shown in Table 1, the treatment of Hela, P3X, PC12, and AtT-20 cells for 24 h with increasing concentrations of climacostol inhibited viability in a dose-dependent manner, with an EC_{50} ranging from 0.60 to 6.23 μg/ml; instead, the EC_{50} values obtained analysing TM3 and NIH/3T3 cell viability were more than 11.30 μg/ml. These comparative data indicated that viability of tumour cells is negatively affected by climacostol with higher potency when compared to non-tumour cells. However, the possibility that climacostol preferentially affects cancerous *vs* normal cells deserves to be further investigated.

Cell line	Origin	Species	EC_{50}	Assay
HeLa	cervix carcinoma	human	0.605	MTT
A431	squamous carcinoma	human	~2.0	MTT/LDH
HL60	pro-myelocytic leukemia	human	~2.0	MTT/LDH
PC-3	prostatic adenocarcinoma	human	2.685	MTT
T98G	glioblastoma	human	3.545	MTT
U87MG	glioblastoma	human	4.627	MTT
P3X	myeloma	mouse	5.665	MTT
PC12	pheochromocytoma	rat	5.702	MTT
atT-20	pituitary adenoma	mouse	6.232	MTT
TM3	Leydig cells	mouse	11.30	LDH
NIH/3T3	fibroblasts	mouse	12.16	MTT
EA.hy926	endothelial cells	human	>50	MTT/LDH

Table 1. Parameters of climacostol-induced inhibition of cell viability: tumourigenic and nontumourigenic cell lines. EC_{50} (μg /ml) = concentration required to produce 50% of the effects. MTT or LDH assays were performed treating cells for 24 h in the absence (vehicle) or in the presence of increasing concentrations of climacostol.

4.2 Climacostol inhibits viability and proliferation of melanoma cells

The cytotoxic properties of climacostol were examined on the highly tumourigenic B16 mouse melanoma cells, which is a common model in melanoma research (Bizzozero *et al*., 2014; Assi *et al.*, 2015; Cervia *et al*., 2016). In line with the results obtained in other tumour cells, the treatment

of B16-F10 cell for 24 hours with climacostol caused a concentration-dependent reduction of MTT absorbance with an EC_{50} of 6.23 µg / ml and a concentration value E_{max} of 30 µg / ml (Fig 3b). The E_{max} concentration of climacostol decreased cell viability by nearly 90%. Then, to evaluate whether the climacostol-induced inhibition of cell viability affects melanoma proliferation rate, B16-F10 cells were analysed by flow cytometry at a single-cell level. As shown in Fig. 3c, cell proliferation was clearly inhibited during 24 h of climacostol (30 µg/ml) exposure while no difference was observed at 8 h. In particular, the cell proliferation index in the presence of climacostol significantly decreased by 57% when compared to control (2.21 ± 0.04 *vs* 5.08 ± 0.67 in vehicle-treated cells) (Fig. 3d). These data suggest the potent and effective cytotoxic and anti-proliferative role of climacostol in mouse melanoma cells.

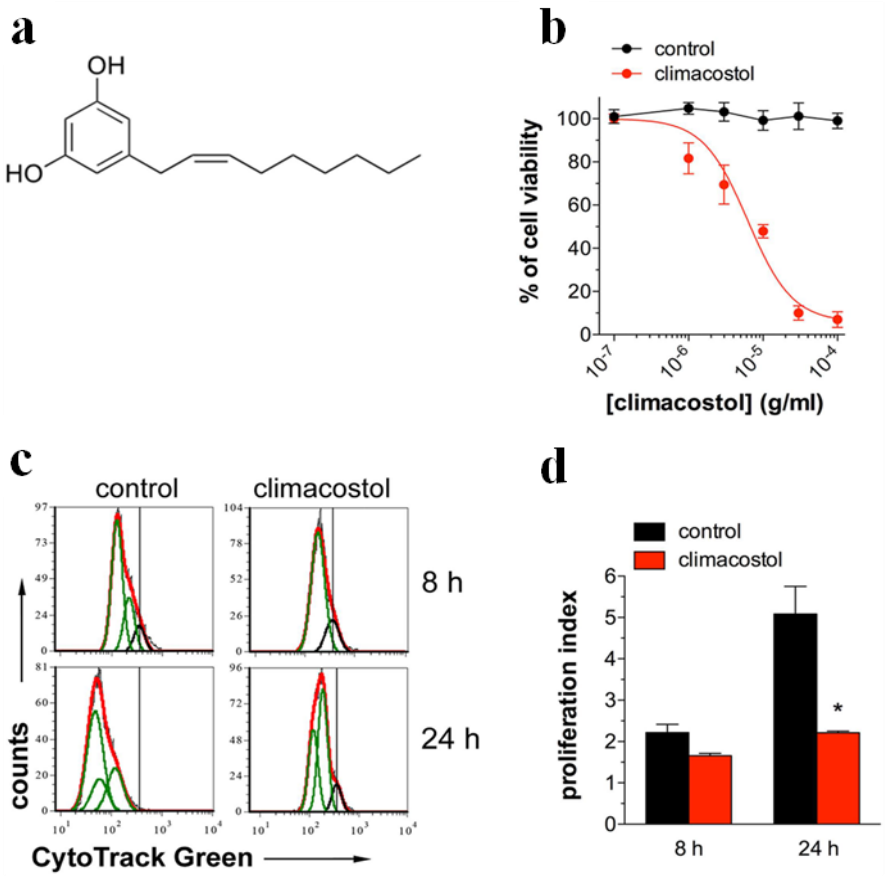

Figure 3. Cytotoxic and anti-proliferative properties of climacostol in melanoma cells. (**a**) The chemical structure of climacostol. (**b**) B16-F10 cells were treated with increasing concentrations of climacostol for 24 h before the MTT assay. Serial dilutions of vehicle (control) were also used. Data are expressed by setting the absorbance of the reduced MTT in the absence of climacostol as 100%. The data points represent the results obtained from 4 independent experiments. (**c**) Flow cytometry analysis of B16-F10 proliferation at 8 and 24 h after cell treatment with climacostol (30 µg/ml) or vehicle (control). The vertical black line represents the undivided cell peak used as point of reference for the CytoTrack Green profile. The data are representative of 3 independent experiments. (**d**) Proliferation index for experiments shown in (**c**). * $p < 0.001$ *vs* the respective control.

4.3. Climacostol induces a fast DNA damage in melanoma cells

DNA-damaging agents have a long history of use in cancer chemotherapy and many used anti-tumoural drugs, as for instance platinum agents, act by inducing DNA damage (Siddik *et al*., 2003; Basu *et al*., 2010; Nikolaou *et al*., 2012). The formation of double-strand breaks (DSBs) triggers phosphorylation of the histone H2AX at Ser139; phosphorylated H2AX is called gamma-H2AX (γH2AX). Confocal immunostaining experiments for phospho-H2AX indicate that a short treatment (1 h and 6 h) with 30 µg/ml climacostol caused a remarkable phosphorylation of H2AX in B16-F10 cells (Fig. 4a). This further demonstrates that climacostol is a compound that are capable of interacting with the DNA double helix, forms covalent drug–DNA adducts and leading to DNA damage and cell death (Quassinti *et al*., 2013). There is ample clinical precedent for drug combinations that include a DNA-targeting drug with other chemotherapeutic agents. Therefore, cell viability was then assessed using the MTT assay in B16-F10 cells treated for 24 h with the chemotherapeutic compound cisplatin or climacostol at increasing concentrations (equals or below their EC_{50}), or combinations of the two. As shown in Fig. 4b, cisplatin and climacostol did not show an additive action since melanoma cell viability in response to their combination was comparable to the viability achieved in the presence of the most effective single drug. In fact, combinations of these drugs have shown response rates only slightly higher than those achieved with single drug administration suggesting that the sensitivity of melanoma cells in response to platinum chemotherapy remains unchanged in the presence of climacostol.

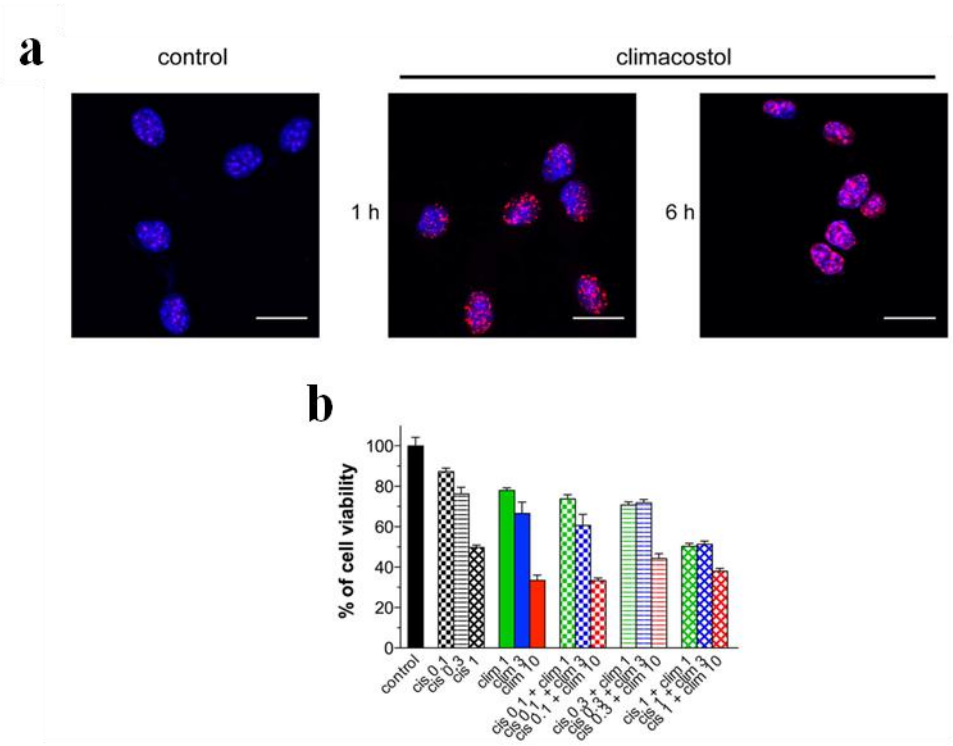

Figure 4. DNA damaging effects of climacostol in melanoma cells and absence of additive effects with DNA binding agents. (**a**) Confocal immunofluorescence imaging of phospho-histone H2A.X in B16-F10 cells cultured in the presence of 30 µg/ml climacostol or vehicle (control) for 1 or 6h. DAPI (blue) was used for nuclei detection. The images are representative of 4 independent experiments. Scale bar: 20 µm. (**b**) MTT assay of B16-F10 cells treated for 24h in the absence (control) or in the presence of increasing concentrations of cisplatin (0.1, 0.3, and 1 µg/ml) and climacostol (1, 3, and 10 µg/ml). Compounds were administered alone or in combination. Data are expressed by setting the absorbance of the reduced MTT in control samples as 100%. Each histogram represent the results obtained from 4–8 independent experiments.

4.4 Climacostol-induced apoptosis in melanoma cells

Cells in phase-contrast images normally appear as dark regions surrounded by brighter halo artefacts, except for apoptotic cells, which are smaller, rounder and have very bright appearance. As shown in Fig. 5a phase-contrast microscopy revealed that melanoma B16-F10 cells at 24 h, but not at 8 h, after exposure to 30 µg/ml climacostol became round, presented a shrunken cytoplasm and the formation of apoptotic bodies. Morphological modifications were also observed in the most of cells exposed to climacostol for 48 h. Under physiological conditions, choline phospholipids are exposed on the external leaflet while aminophospholipids, such as phosphatidylserine, are located on the cytoplasmic surface of the lipid bilayer. However, during apoptosis lipid asymmetry is lost and phosphatidylserine becomes exposed on the outside leaflet of the membrane. The Annexin V/ PI protocol is a commonly used approach for studying apoptotic cells: fluorescently labeled Annexin V, a 36-kDa calcium-binding protein, can be used to detect phosphatidylserine that is exposed on the outside of apoptotic cells. Annexin V can also stain necrotic cells due to the ruptured membranes that allow Annexin V to access the entire plasma membrane. However,

apoptotic cells can be distinguished from necrotic cells by co-staining with propidium iodide (PI), because PI enters in late apoptotic and necrotic cells, but it does not stain live or early apoptotic cells. The flow cytometry analysis of PS exposure on the outer leaflet of the plasma membrane revealed that 30 µg/ml climacostol treatment for 24 and 48 h, but not 8 h, induced a significant increase in the Annexin V^+/PI^- B16-F10 fraction (regarded as early apoptotic stage) and Annexin V^+/PI^+ B16-F10 fraction (regarded as late apoptotic/end-stage) (Fig. 5b,c). Overall apoptotic cells in the presence of climacostol at 24 and 48 h were ca. 35 and 75% of total cells, respectively. As expected, apoptosis in vehicle-treated cells (control) was almost undetectable. In addition, immunostaining with a fluorescently labelled antibody that binds specifically to cleaved (active) Caspase 3 revealed that B16-F10 cells expressed high levels of Caspase 3 activity at 24 h after 30 µg/ml climacostol treatment while no specific stain was observed in control cells (Fig. 5d). Caspase 3 is responsible for the majority proteolysis during apoptosis and detection of cleaved Caspase 3 is therefore considered an hallmark of apoptosis. In agreement with previous study (Buonanno *et al*., 2008), our results demonstrate that climacostol promotes apoptosis in mouse melanoma cells, triggering a Caspase 3-dependent apoptotic programme with enzymatic degradation of DNA.

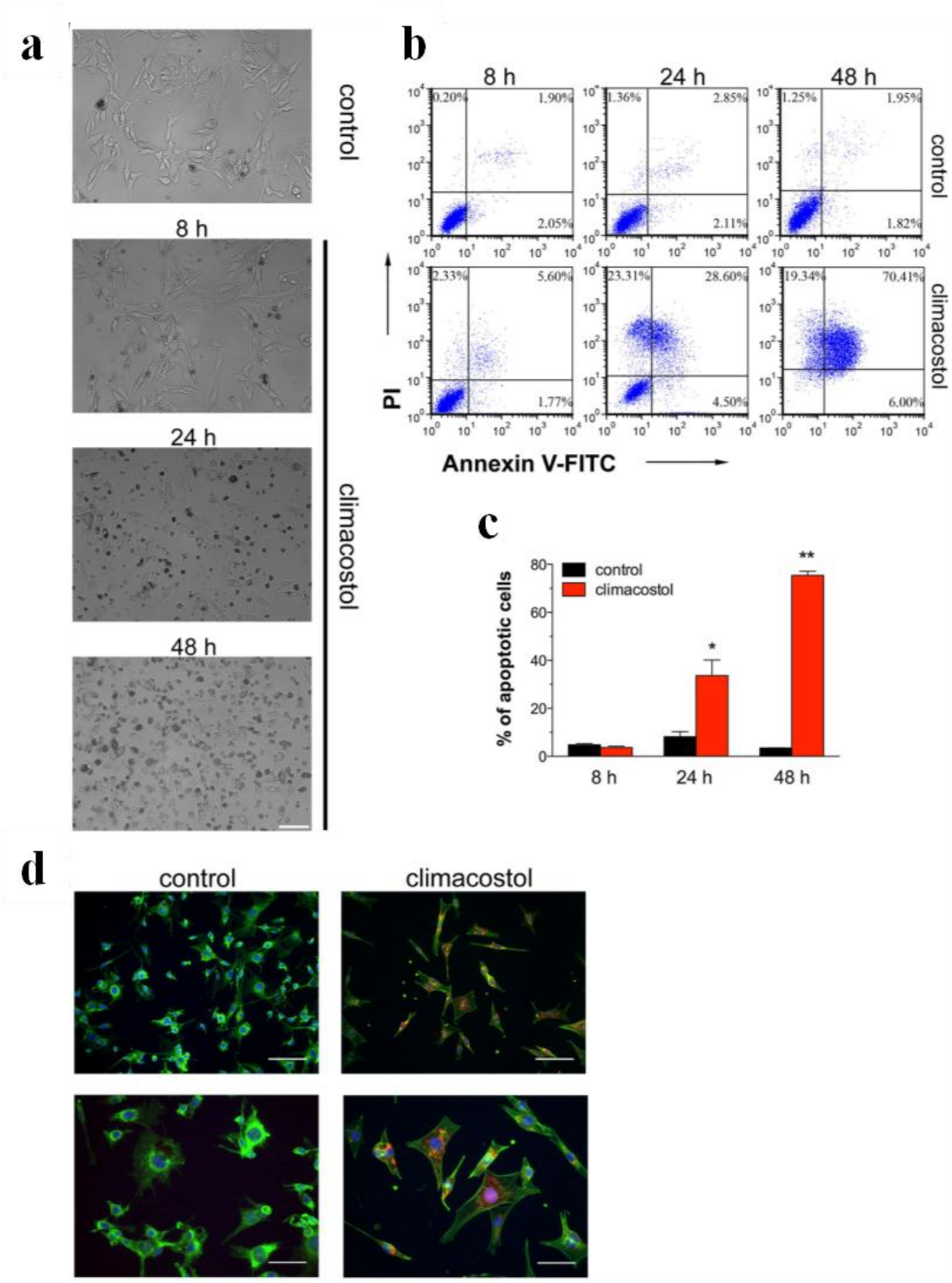

Figure 5. Apoptosis in melanoma cells treated with climacostol. (**a**–**c**) B16-F10 cells were cultured in the presence of 30µg/ml climacostol or vehicle (control) for 8, 24 or 48h. (**a**) Phase-contrast microscopy. The images are representative of 3 independent experiments. Scale bar: 50µm. (**b**) Evaluation by flow cytometry of Annexin V/PI staining. Quadrants are drawn, and relative proportion of dying cells is indicated. The events shown in the lower left-hand quadrant are unlabeled cells. (**c**) Percentage of apoptotic cells (Annexin V^+/PI^- + Annexin V^+/PI^+ fraction; theAnnexin V^-/PI^+ fraction, regarded as necrotic stage, was excluded) for experiments shown in (**b**). * $p < 0.001$ and ** $p < 0.0001$ *vs* the respective control. (**d**) Immunofluorescence imaging of cleaved Caspase 3 (punctate red pattern) in B16-F10 cells cultured in the presence of 30µg/ml climacostol or vehicle (control) for 24h. DAPI (blue) and phalloidin (green) were used for nuclei and cytoskeleton detection, respectively. The images are representative of 3 independent experiments. Upper panels: 100µm scale bar; lower panels: 50µm scale bar.

4.5 Climacostol-induced activation of the mitochondrial-caspase-dependent apoptotic pathway in melanoma cells

As mentioned before, climacostol was suggested to induce cell death by activating the intrinsic apoptotic programme in human pro-myelocytic leukemia HL60 cells, but not in squamous carcinoma cells (Buonanno *et al*., 2008). Herein, we aim to demonstrate and further characterise this mechanism in melanoma. The disruption of normal mitochondrial function is a distinctive feature of apoptosis, especially changes that affect the mitochondrial membrane potential (ΔΨm). To further investigate the role of mitochondria in climacostol-induced apoptotic cell death, we analyzed the mitochondrial membrane potential using flow cytometry analysis of tetramethylrhodamine methyl ester (TMRM) staining. TMRM is cationic (positively-charged) fluorescent dye that accumulate in the negatively-charged mitochondrial matrix in inverse proportion to ΔΨm (*i.e.* the more negative the ΔΨm, the more dye accumulates). Depolarized or inactive mitochondria have decreased membrane potential and fail to sequester TMRM, thus an healthy cell will contain more dye than an apoptotic cell. In particular, we found that about 70% of B16-F10 cells treated for 24 h with 30 μg/ml climacostol displayed depolarised mitochondria (Fig. 6a,b). During apoptosis, Bax translocates from the cytosol to the mitochondrial outer membrane and stimulates Cytochrome c release and Caspase 9-dependent proteolytic cleavage of Caspase 3. To identify the subcellular distribution of Bax and Cytochrome c was utilised confocal immunofluoresence microscopy in melanoma cells. As shown in Fig. 6c, in vehicle-treated (control) cells Bax displayed a coarse staining pattern, which did not co-localise with mitochondria as determined using a mitochondrial markers, such as MitoTracker Green. However, 30 μg/ml climacostol treatment (24 h) resulted in a punctate Bax staining pattern with evidence of mitochondrial clustering due to its extensive overlapping with MitoTracker Green. The mitochondrial clustering of Bax was associated with an alteration in the Cytochrome c staining pattern from mitochondrial (co-localization with MitoTracker Green), to a more cytosolic distribution (presence of many clusters which did not overlap with MitoTracker Green), indicating a release of Cytochrome c from the mitochondria (Fig. 6d). In addition, exposure of B16-F10 cells to climacostol (24 h, 30 μg/ml) induced the expression of high levels of cleaved (active) Caspase 9 while no specific immunofluorescence stain was observed in control cells (Fig. 6e). Considering this mechanistic insight in melanoma cells, our data are consistent with the induction of an intrinsic apoptotic pathway, characterised by the central role of the mitochondria dysfunction in the initiation of the pro-apoptotic effects of climacostol. Of interest, melanoma drug resistance is often attributed to defect in the intrinsic apoptosis pathway. Targeting regulators of mitochondria-mediated

apoptosis is thus considered a promising approach to sensitising melanomas to treatment (Mohana-Kumaran *et al*., 2014).

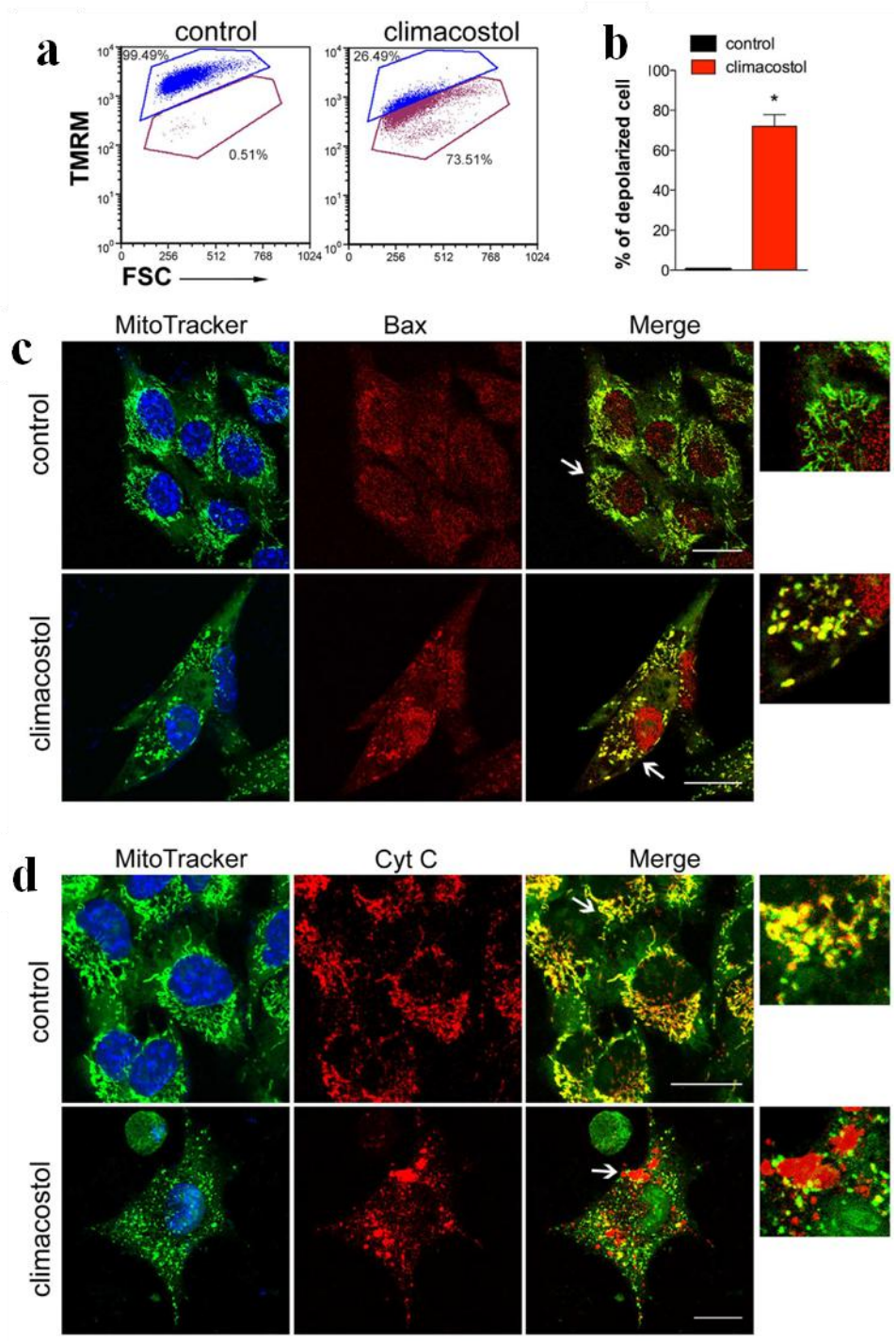

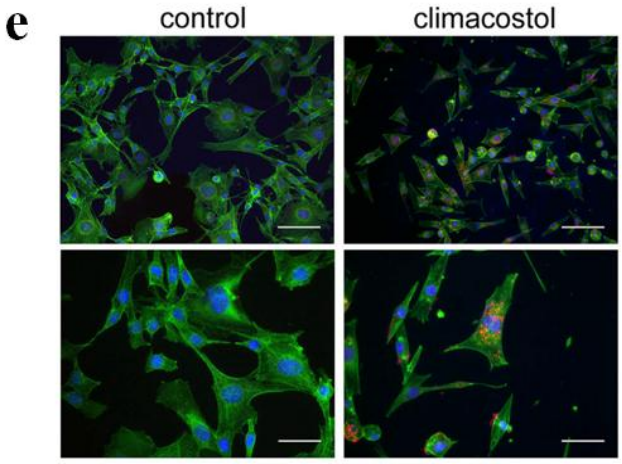

Figure 6. Climacostol activates mitochondrial-dependent apoptosis in melanoma cells. B16-F10 cells were cultured in the presence of 30µg/ml climacostol or vehicle (control) for 24h. (**a**) Evaluation by flow cytometry of mitochondrial potential, using TMRM staining. The percentage number of cells with intact mitochondrial potential (TMRM fluorescence in top gate) and percentage number of cells with reduced mitochondrial potential (depolarised cells; TMRM fluorescence in bottom gate). FSC: forward scatter. Images and data are representative of 3 independent experiments. (**b**) Percentage of depolarised cells for experiments shown in (**a**). * $p < 0.0001$ *vs* control. (**c**,**d**) Confocal microscopy for co-localization of Bax and Cytochrome c with mitochondria. Cells were stained for Bax or Cytochrome c (red) and the fluorescent mitochondrial dye MitoTracker Green. DAPI (blue) was used for nuclei detection. The images are representative of 3 independent experiments. Scale bar: 20 µm. Panels on the right represent enlarged image details marked by the white arrows. (**e**) Immunofluorescence imaging of cleaved Caspase 9 (punctate red pattern). DAPI (blue) and phalloidin (green) were used for nuclei and cytoskeleton detection, respectively. The images are representative of 3 independent experiments. Upper panels: 100 µm scale bar; lower panels: 50 µm scale bar.

4.6 Climacostol induces p53-dependent apoptosis in melanoma cells

As shown Fig. 7a, B16-F10 cells treated with 30 µg/ml climacostol for 24 h displayed a significant increase of p53 protein levels when compared to vehicle-treated (control) cells. In addition, the mRNA expression of Noxa and Puma, but not p21, also known as cyclin-dependent kinase inhibitor 1, was found to be significantly up-regulated by climacostol (Fig. 7b). By using siRNA, we then determined whether the pro-apoptotic effect of climacostol involved p53 signalling. In order to achieve this end, B16-F10 cells were transiently transfected for 48 h with a p53-specific or a non-targeting siRNA, followed by climacostol treatment (24 h, 30 µg/ml). Vehicle was also used as control. As expected, we found that climacostol significantly increased p53 levels in cells transfected with non-targeting siRNA, while its effect was completely inhibited after p53 siRNA transfection (Fig. 7c). Of interest, the analysis of Annexin V^+/PI^- and Annexin V^+/PI^+ B16-F10 populations, early and late apoptotic cells rispectively, revealed that p53 silencing abolished the apoptotic effects of climacostol (Fig. 7d) thus indicating that the mechanism by which climacostol is able to induce apoptosis in B16-F10 melanoma cells is mainly, if not completely, dependent on p53 activity. Therefore, climacostol effects are in line with the role of anticancer agents, including

cisplatin, leading to melanoma cell death with changes in the expression of p53 and its signaling pathway (Siddik, 2003; Basu and Krishnamurthy, 2010).

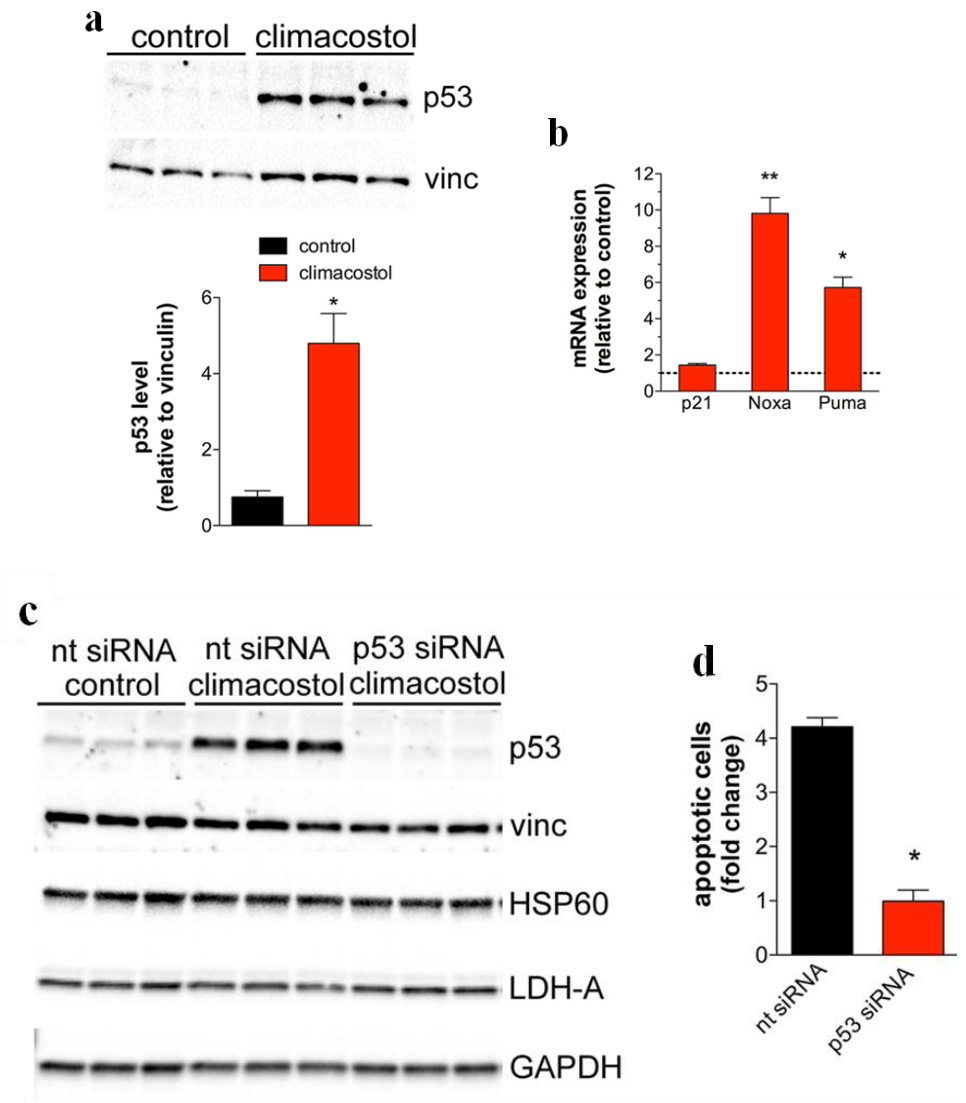

Figure 7. Pro-apoptotic effects of climacostol in melanoma cells depend on p53 activity. (**a**) Western blot analysis of p53 expression. Vinculin was used as the internal standard; Lower panel: densitometry analysis of p53 expression (n = 3) * $p < 0.001$ *vs* control. (**b**) mRNA levels of p53 target genes p21, Noxa and Puma, as measured by real-time PCR. Each histogram represent the results obtained from 3 independent experiments. Data are expressed as the fold change over control (set as 1). * $p < 0.001$ and ** $p < 0.0001$ *vs* the respective control. (**c**) Western blot analysis of p53 expression. Vinculin, HSP60, LDH-A, and GAPDH were used as internal standards and to test possible off-target effects of siRNA transfection (n = 3). (**d**) Evaluation by flow cytometry of Annexin V/PI staining (Annexin V^+/PI^- + Annexin V^+/PI^+ fraction; the Annexin V^-/PI^+ fraction, regarded as necrotic stage, was excluded). Data are expressed as fold change over the respective control. Each histogram represent the results obtained from 3 independent experiments. * $p < 0.001$ *vs* nt siRNA.

4.7 Climacostol inhibits melanoma allografts growth in vivo, increases animal survival and apoptosis, and induces p53 network

The efficacy of climacostol was tested *in vivo*. Consequently, B16-F10 melanoma cells were injected subcutaneously into flanks of mice; when the syngeneic implantation was established, mice were intra-tumour injected with vehicle (control) or climacostol at 600 μg/ml, in total volume of 100 μl, every 3–4 days for 3 weeks. Local administration of climacostol decreased tumour volumes throughout the entire study period, as illustrated in Fig. 8a. In particular, as is clear from the melanoma volume analysis (Fig. 8b), in vehicle-treated animals (control) the tumour growth rate increased steadily while in the case of transplantes treated with climacostol we noted a persistent inhibition of tumour load. In agreement with these results, the Kaplan-Meier analysis of Fig. 8c revealed that climacostol significantly improved the survival of B16-F10 melanoma-injected mice (median of survival: control = 18 days, climacostol-treated group = 29 days).

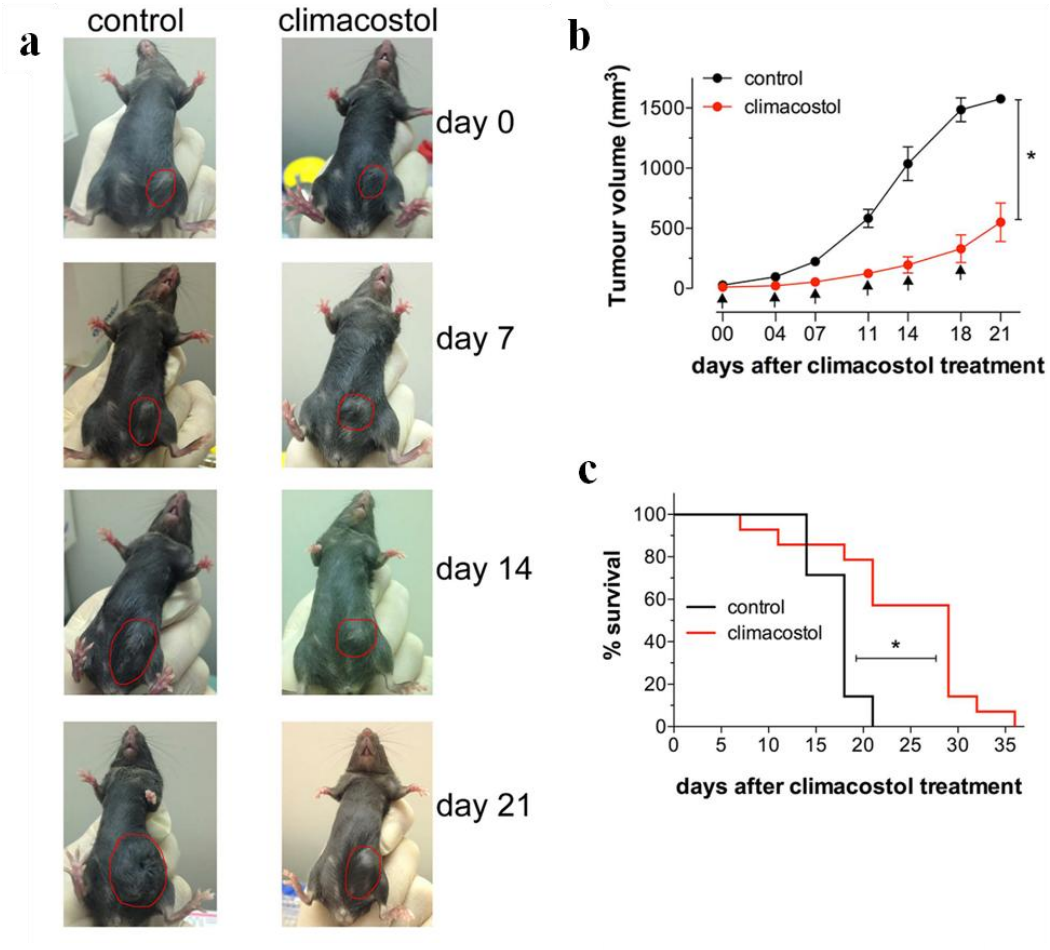

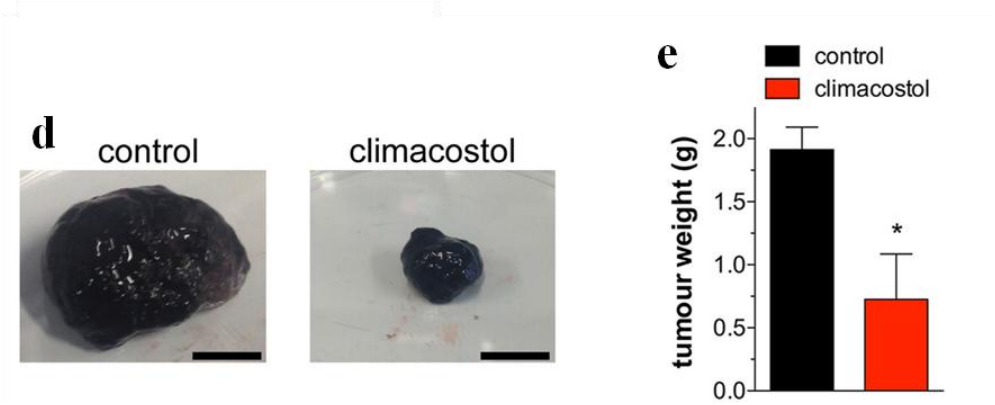

Figure 8. ***In vivo*** **anti-tumour properties of climacostol in mice bearing melanoma allografts.** (**a**) Typical photographs taken at different time-points and depicting the growth of subcutaneous melanomas, as indicated by red circles. (**b**) Tumour growth monitored by means of external caliper measurements and volume calculation. Arrows indicate the day of climacostol treatment. (**c**) Percentage survival analysed by Kaplan-Meier curve. Images and data points in (**a–c**) represent the results obtained from 7–15 animals per experimental group. (**d**) Typical photographs of subcutaneous melanoma allografts excised from mice at day 16 of treatment (from day 0 - every 3–4 days) with vehicle (control) or climacostol (600 µg/ml). Scale bar: 5 mm. (**e**) Weight of the excised tumours. Images and data in (**d**,**e**) represent the results obtained from 3 animals per experimental group. * $p < 0.001$ *vs* the respective control.

In another set of experiments, B16-F10 tumours were removed at day 16 of treatment with local administration of climacostol at 600 µg/ml. As shown in Figures 6d and 6e, it is found that climacostol significantly reduced melanoma weight by ca. 60% when compared to vehicle-treated group (control). Viability measurements with Trypan Blue staining showed that climacostol exposure induced a remarkable reduction of viable cells inside the tumour (ca. 55% reduction *vs* control), (Fig. 9a). The immunostaining experiments of the cleaved Caspase 3 revealed higher amount of clustered apoptotic cells in tumours treated with climacostol while the stain for the cleaved Caspase 3 was scarce in control tumours (Fig. 9b). These findings were also confirmed by Western blot experiments since climacostol-treated melanomas displayed an increase of active Caspase 3 when compared to control (Fig. 9c). In agreement with the *in vitro* results, the expression of p53 was also enhanced in melanomas treated with climacostol (Fig. 9d). In addition, we found a significant increase of p53, Noxa and Puma mRNAs in the climacostol-treated group, while mRNA expression of p21 was unchanged (Fig. 9e). Ultimately, our results indicate that climacostol exerts an effective inhibitory action on B16-F10 mouse melanoma progression thus increasing animal survival. After cell entry, climacostol triggers the death process of tumour cells by damaging DNA by non-covalent binding; the signalling events responsible of the climacostol-induced pro-apoptotic effects rely on the up-regulation of p53 network that, in turn, activates the intrinsic programed cell death pathway.

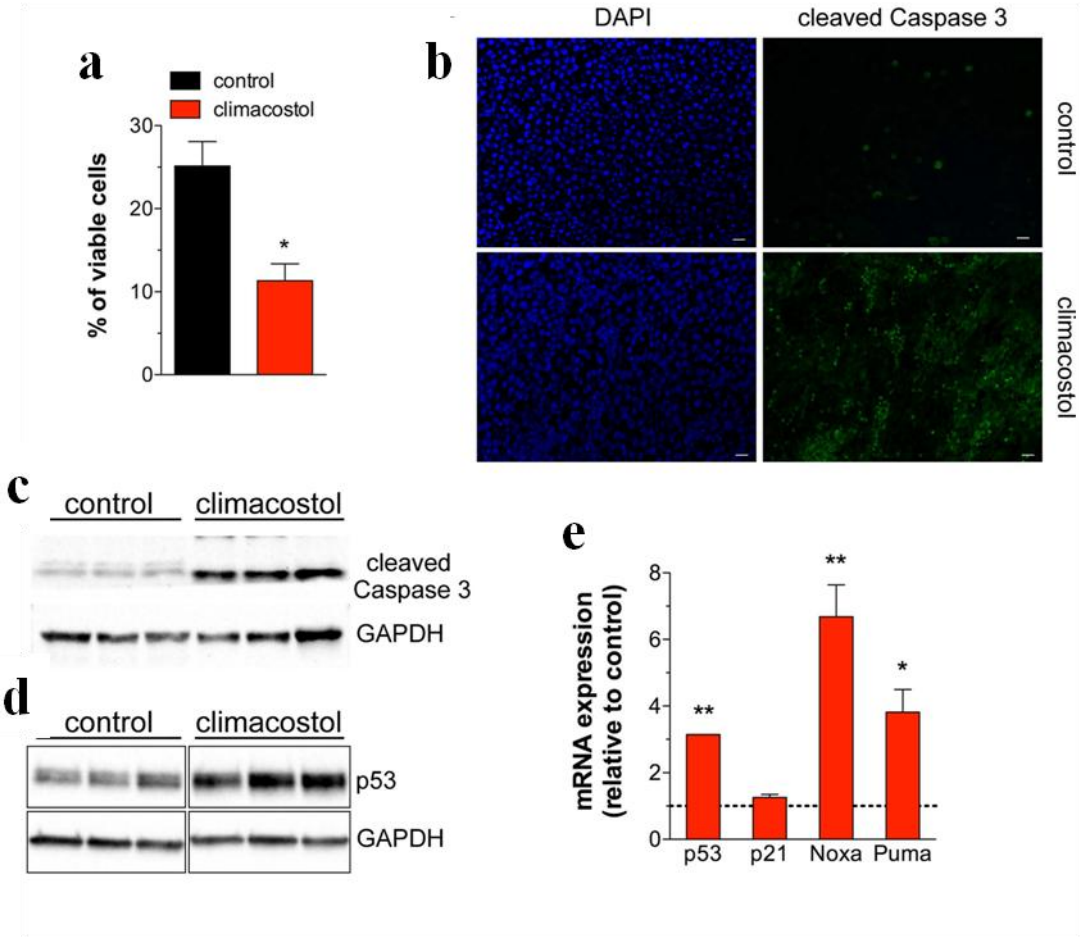

Figure 9. ***In vivo*** **pro-apoptotic properties of climacostol in mice bearing melanoma allografts.** Subcutaneous B16-F10 melanoma allografts were excised from mice at day 16 of treatment (from day 0 - every 3–4 days) with vehicle (control) or climacostol (600 µg/ml). (**a**) Percentage of viable cells inside the tumours as evaluated by Trypan Blue staining. (**b**) Representative immunofluorescence imaging of cleaved Caspase 3. DAPI (blue) was used for nuclei detection. Scale bar: 20 µm. (**c**,**d**) Western blot analysis of cleaved Caspase 3 and p53 expression, respectively. GAPDH was used as the internal standard. (**e**) mRNA levels of p53 and its target genes p21, Noxa and Puma, as measured by real-time PCR. Data are expressed as the fold change over control (set as 1). Images and data represent the results obtained from 3 animals per experimental group. * $p < 0.001$ and * * $p < 0.0001$ *vs* the respective control.

4.8 Climacostol disrupt autophagy in mouse melanomas: in vivo and in vitro evidence

Using the same experimental paradigm discussed above, we determined the autophagic status in mouse melanomas locally treated with climacostol at day 16. First, Real Time PCR was used to measure mRNA levels of autophagy mediators in resected tumours (Mizushima *et al*., 2010; Abada and Elazar, 2014; Klionsky *et al*., 2016; Antonioli *et al*., 2017; Galluzzi *et al*., 2017). The transcripts encoding LC3b, p62, beclin 1, bnip 3, bnip 3L, atg3, atg4, and atg5 autophagy genes were significantly enhanced in climacostol-treated group (Fig. 10) suggesting an important perturbation of autophagic machinery.

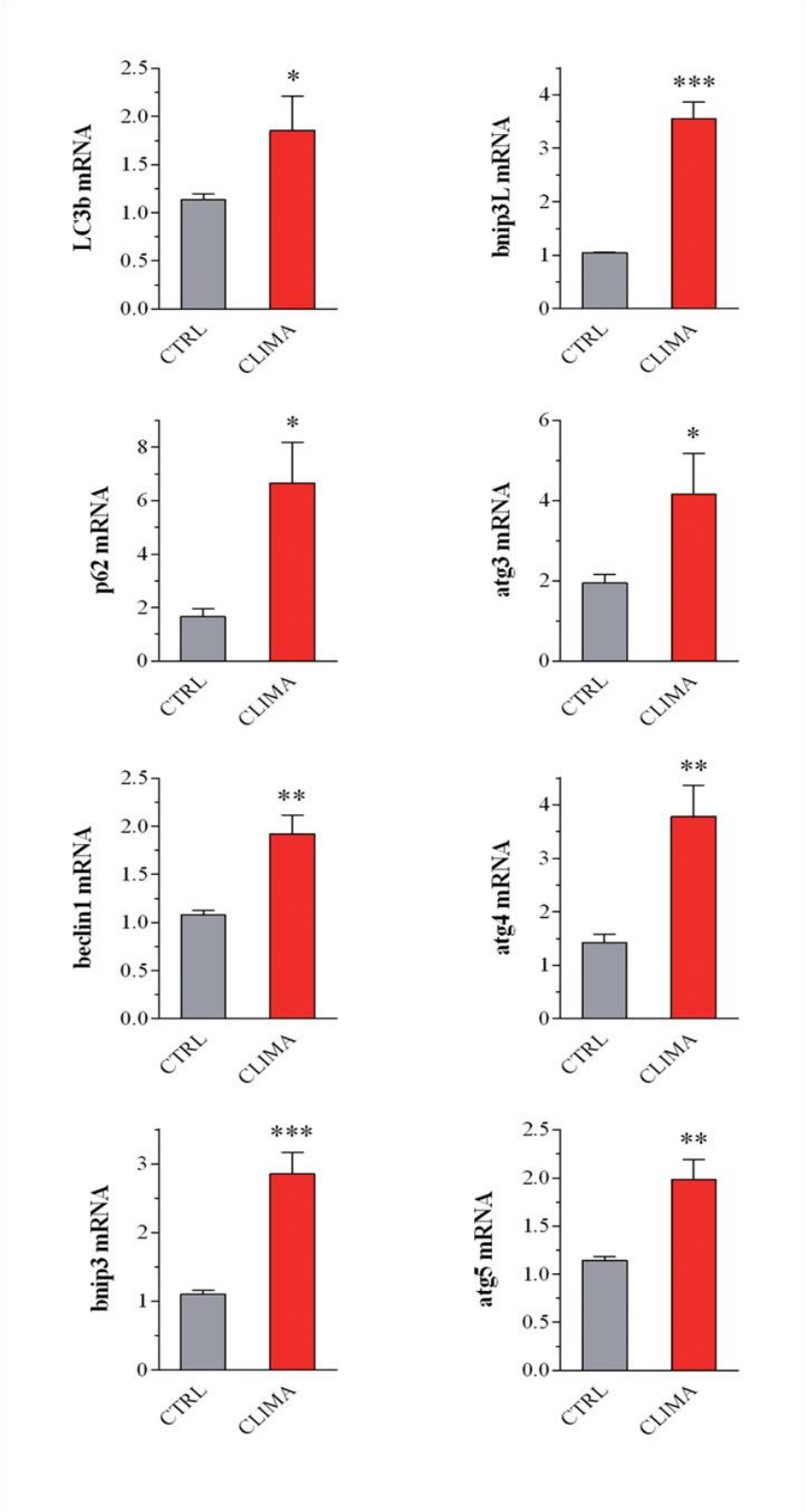

Figure 10 Climacostol affects the expression of autophagy genes in *in vivo* melanoma. Subcutaneous B16-F10 melanoma allografts were excised from mice at day 16 of treatment (from day 0 - every 3-4 days) with 100 µl climacostol (CLIMA; 600 µg/ml) or control vehicle (CTRL). mRNA levels of autophagy genes, as measured by real-time PCR. Results are expressed as fold change of CTRL. *$p < 0.05$, **$p < 0.005$ and ***$p < 0.0001$ relative to CTRL. Data represent the results obtained from 6 animals per experimental group.

To date the clustering of LC3b protein and its association with autophagosome membranes has been accepted as the gold standard for monitoring autophagy (Mizushima *et al.*, 2010; Klionsky *et al.*, 2016; Galluzzi *et al.*, 2017). Hence, we detected LC3 by fluorescence microscopy in tumour-derived slices. An increase of LC3 staining and the detection of LC3 puncta, reminiscent of formation of autophagosomes, was clearly visible by immunocytochemistry in melanoma tumours from climacostol-administered mice, while diffuse LC3 staining was visualized in control samples (Fig 11a). A quantitative analysis of LC3 imunofluorescence intensity confirmed the increase of LC3 expression caused by climacostol. Upon autophagic signal, the cytosolic form of LC3-I (18 kDa) is recruited to phagophores where LC3-II (16 kDa) is generated by proteolysis and lipidation at the C-terminus. Thus LC3-II formation positively correlates with the number of autophagosomes (Mizushima *et al.*, 2010; Klionsky *et al.*, 2016; Galluzzi *et al.*, 2017). To confirm that LC3 staining reflects an increase in the autophagosome-bound LC3-II rather than the cytosolic LC3-I, we performed immunoblotting for LC3. In B16-F10 allografts, climacostol treatment significantly increased LC3-II levels (Fig. 11b). The lipidation and clustering of LC3 may be the result of both induction and suppression of autophagosomes maturation. Measurements of the autophagy adaptor protein p62, which serves as a link between LC3 and ubiquitinated cargoes, is a useful method to distinguish whether autophagosome buildup is due to autophagy induction or rather an inhibition of autophagy steps (Mizushima *et al.*, 2010; Klionsky *et al.*, 2016; Galluzzi *et al.*, 2017). In fact, the inhibition of autophagic vacuole maturation and subsequent fusion with lysosomes correlates highly with increased levels of p62 and *viceversa*. As shown in Fig. 11c, climacostol treatment of B16-F10 allografts increased the intensity of p62 immunofluorescence in melanoma cells leading to accumulation of p62-positive aggregates when compared to control. In line with these results, western blot experiments showed a significant increase of p62 protein band in climacostol-treated tumours (Fig. 11d).

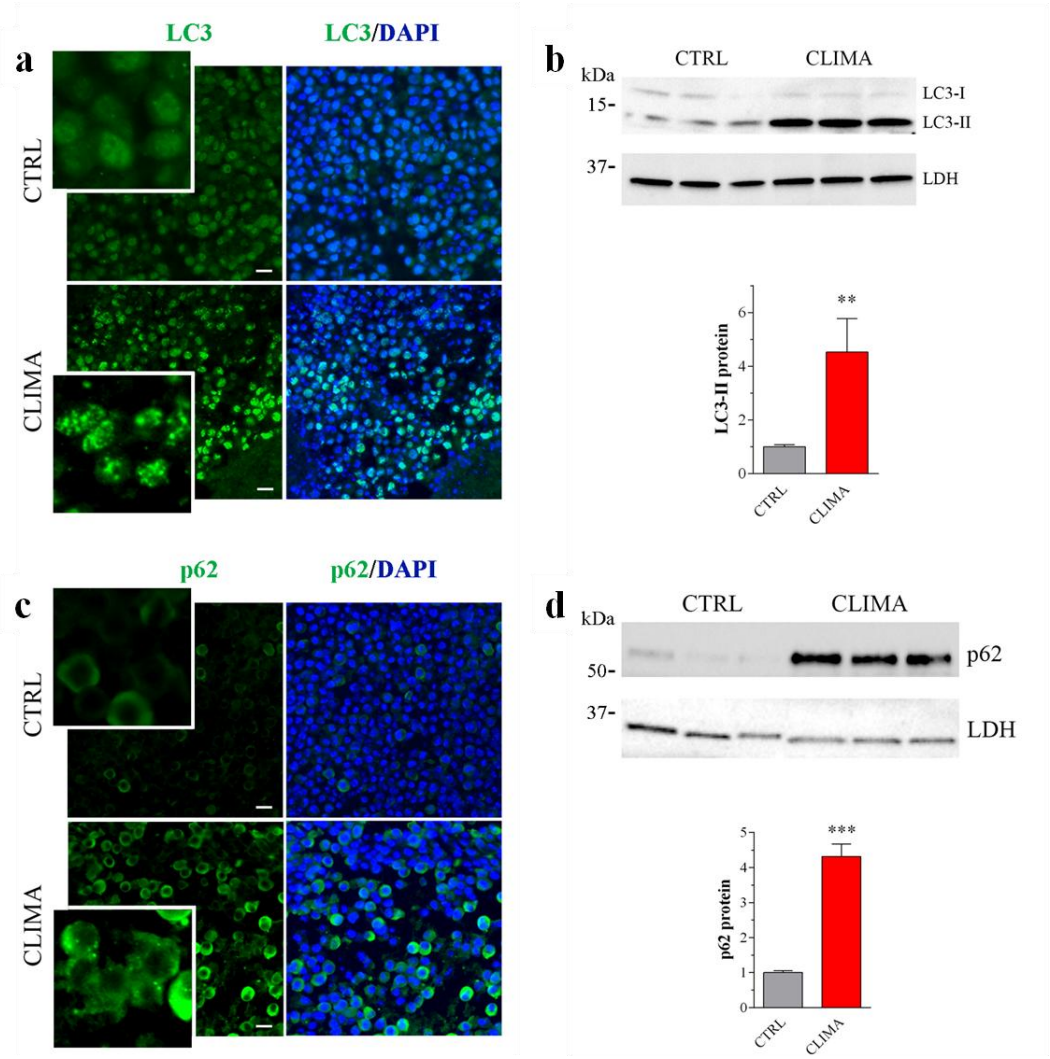

Figure 11 Climacostol impairs autophagy in in vivo melanoma. Subcutaneous B16-F10 melanoma allografts were excised from mice at day 16 of treatment (from day 0 every 3-4 days) with 100 µl climacostol (CLIMA; 600 µg/ml) or control vehicle (CTRL). **a, c** Immunofluorescence imaging of LC3 and p62. DAPI was used for nuclei detection. Scale bar: 50 µm. Inserts represent enlarged image details. **b, d** Western blotting images of LC3 and p62 in vehicle and climacostol-treated melanomas. LDH was used as internal standard. Lower panels: densitometric analysis of LC3-II and p62 relative to their respective standard. Results are expressed as fold change of CTRL. **p < 0.01 and ***p < 0.0001 relative to CTRL. Images and data represent the results obtained from 6 animals per experimental group.

To study in deep these aspects and further investigating the effects of climacostol on autophagic machinery, we treated B16-F10 cells with climacostol at its target dose for potency and efficacy (30 µg/ml), inducing cytotoxic, anti-proliferative and pro-apoptotic effects on melanoma cells (Catalani *et al.*, 2016; Perrotta *et al.*, 2016). Likewise to *in vivo* results, we found a significant increase in LC3 intensity and puncta immunofluorescence (Fig. 12a) and LC3 cleavage after 24 h climacostol treatment (Fig. 12b). In addition, we observed higher levels of aggregated p62 and a significant increase of p62 staining in climacostol-treated cells when compared to control (Fig. 12c) which paralleled with an accumulation of p62 immunoblot levels (Fig. 12d).

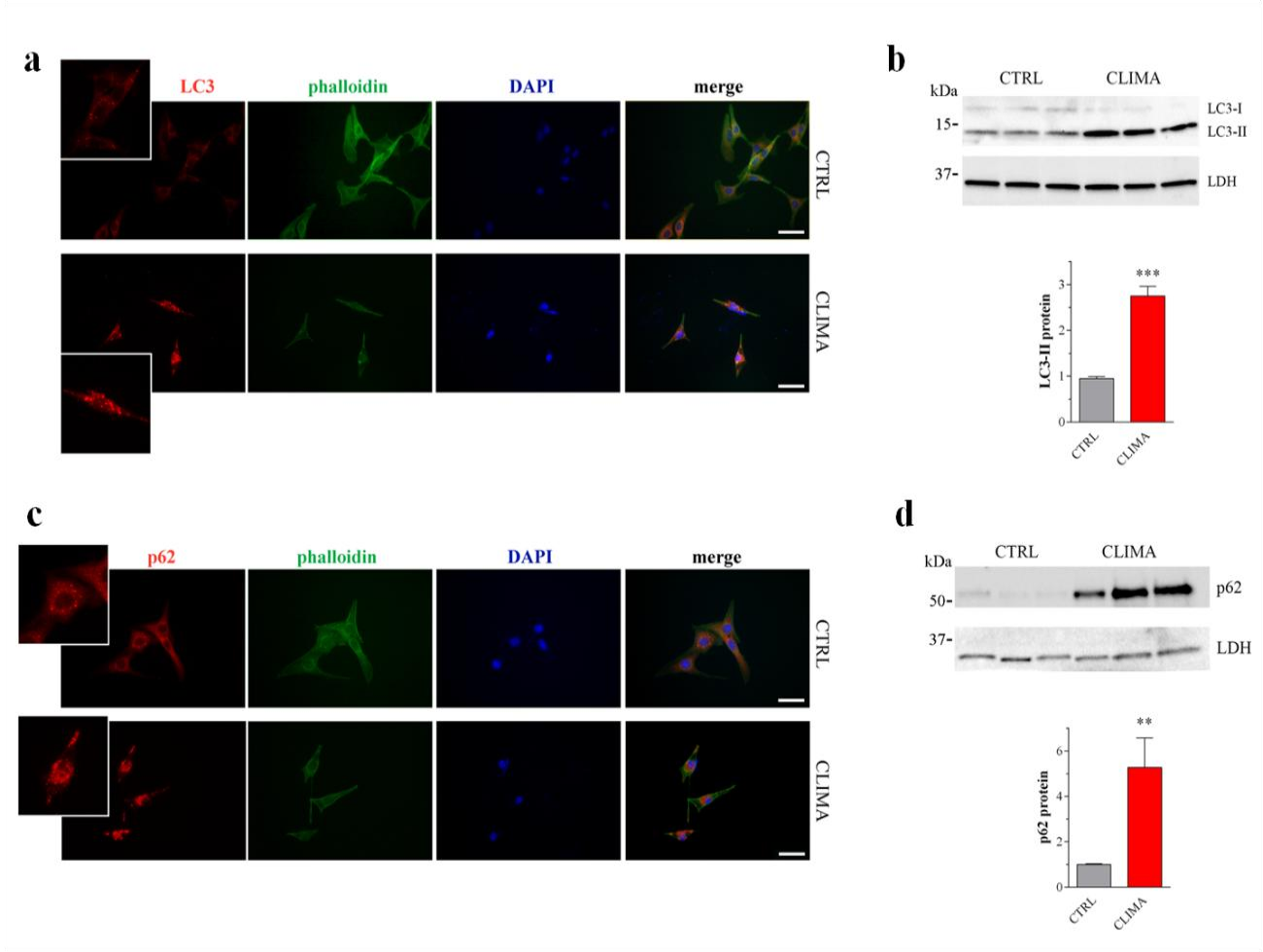

Figure 12 Climacostol impairs autophagy in melanoma cells. a, c Immunofluorescence imaging of LC3 and p62 in B16-F10 cells cultured in the presence of 30 µg/ml climacostol (CLIMA) or control vehicle (CTRL) for 24 h. Phalloidin and DAPI were used for cytoskeleton and nuclei detection, respectively. The images are representative of 6 independent experiments. Scale bar: 50 µm. Inserts represent enlarged image details. **b, d** Western blotting images of LC3 and p62 in vehicle and climacostol-treated melanoma cells. LDH was used as internal standard. Lower panels: densitometric analysis of LC3-II and p62 relative to their respective standard. Results are expressed as fold change of CTRL. **p < 0.005 and ***p < 0.0001 relative to CTRL. Images and data represent the results obtained from 11-12 independent experiments

The effect of climacostol on autophagy was then evaluated by treating cells with the well-known pharmacological inhibitor of autophagy chloroquine (CQ), which prevents the fusion of autophagosomes with lysosomes and inhibits the lysosomal degradation of proteins at the late stage of autophagy (Vakifahmetoglu-Norberg *et al*., 2015). The extent of LC3/p62 turnover in response to CQ reflects the rate of autophagic degradation (Mizushima *et al.*, 2010; Klionsky *et al.*, 2016; Galluzzi *et al*, 2017) and if a compound is an inhibitor of the autophagic flux, its combination with a saturated blocker like CQ should lead to no synergism on LC3-II and p62 levels. B16-F10 cells treated with saturated CQ (10 µM, 6 h) (Qiu *et al.*, 2014) showed an increased amount of lipidated LC3 and accumulation of p62 (Fig. 13a,b). Of notice, 24 h climacostol-induced accumulation of LC3-II and p62 was not modified in the presence of CQ. The absence of an additive effect between CQ and climacostol is consistent with the inhibition of the autophagic flux exerted by climacostol.

The autophagic response of melanoma cells was also analysed using transmission electron microscopy (TEM). As shown in Fig. 13c, B16-F10 cells treated with climacostol for 6 h showed accumulation of autophagosomes in the cytosol when compared to control cells. Autophagosomes, also referred to as initial autophagic vacuoles (AVi), have been defined as a double-membraned structure containing morphologically intact cytosol or organelles (Klionsky *et al*., 2016). The bilayers of AVi are separated by a relatively narrower or wider electron-translucent cleft, sequestering cytosol, mitochondria, or endoplasmic reticulum membranes not yet degraded. Differently, late or degradative autophagic vacuoles (AVd) (Klionsky *et al*., 2016), defined as a hybrid organelle generated by the fusion of an autophagosome and a lysosome (an endosome can also be involved) were clearly detectable in control but scarce in climacostol-administered cells (Fig. 13c). The AVd showed a single limiting membrane and contained partially degraded cytoplasmic materials that were visualized as intense, dark structures within the vacuoles (Mizushima *et al*., 2010; Klionsky *et al*., 2016). Climacostol-treated cells moreover showed disorganized structures, swollen cristae in mitochondria and accumulation of melanosomes in the cytoplasm.

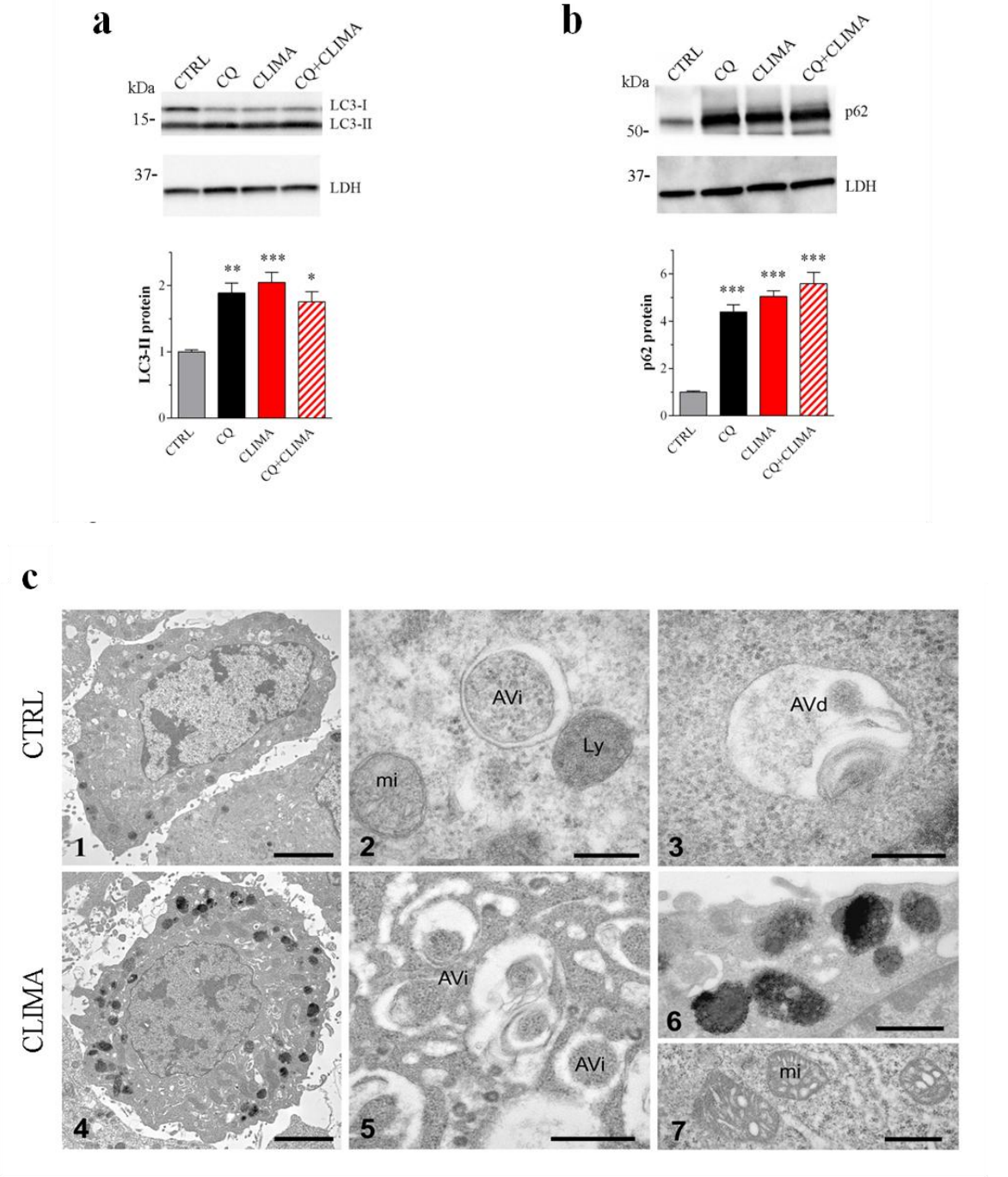

Figure 13 Climacostol impairs autophagic flux. a, b Western blotting images of LC3 and p62 in B16-F10 cells cultured with 30 μg/ml climacostol (CLIMA) or control vehicle (CTRL) for 24 h, both in the absence and presence of CQ (10 μM, 6 h). LDH was used as internal standard. Lower panels: densitometric analysis of LC3-II and p62 relative to their respective standard. Results are expressed as fold change of CTRL. *p < 0.05, **p < 0.005 and ***p < 0.0001 relative to CTRL. Images and data represent the results obtained from 3-5 independent experiments. **c** Electron microscopy images presenting ultrastructure of B16-F10 cells cultured with 30 μg/ml climacostol (CLIMA) or control vehicle (CTRL) for 6 h. The panels 1-3 depict representative control cells at increasing magnifications: (1) whole cells; (2) an early or initial autophagic vacuole (Avi), containing morphologically intact ribosomes. The electron-lucent cleft between the two limiting membranes is visible. A dense lysosome (Ly) is also found in contact with the outer limiting membrane of the autophagosome and a normal mitochondria (mi); (3) a late or degradative autophagic vacuole (Avd) containing partially degraded cytoplasmic material. The panels 4-7 depict representative climacostol-treated cells at increasing magnifications: (4) whole cells showing abundant black melanosomes; (5) note the presence of numerous autophagosome-like compartments in the cytoplasm; (6) higher magnification of melanosomes and (7) mitocondria with swollen crestae. Scale bars: 1 and 4: 2 μm; 2 and 3: 200 nm; 5, 6 and 7: 500 nm. Images represent the results obtained from 3 independent experiments.

To get further insights on the dynamics of autophagic flux we employed B16-F10 cells transiently expressing monomeric red fluorescent protein (mRFP)-green fluorescent protein (GFP)-LC3 as a dual-fluorescence pH sensor to test over time the acidification of autophagic vacuoles (autophagosome-lysosome fusion) in the live cells after climacostol treatment (Kimura *et al.*, 2007). The expression of this tandem fluorescent-tagged LC3 reporter results in both green and red fluorescence and is useful to monitor autophagosomes (pH neutral) and autophagosome-lysosome fusion (pH acid) (Kimura *et al.*, 2007; Mizushima *et al*., 2010; Klionsky *et al.*, 2016). With this construct, autophagosomes appear yellow (*i.e.*, mRFP and GFP) and autolysosomes as red vacuoles (*i.e.* mRFP only), since the low pH inside the lysosomes quenches the fluorescence signal of GFP more quickly than the fluorescence signal of mRFP. In control conditions, about half of autophagic vacuoles in melanoma cells had only red fluorescence signal while the other half had yellow signal (Fig. 14a,b). After treatment with climacostol for increasing times, yellow punctate fluorescence significantly increased whilst only-red puncta markedly decreased, indicating a time-dependent blockade of autophagosome maturation/autophagosome-lysosome fusion to form autolysosomes. The effect of climacostol was detected at 3 h (although below the statistical significance) and reached the almost maximal effect already at 6 h. Close to 90% of the autophagic vacuoles had yellow signals following treatment with climacostol for 24 h. Similar results were observed with CQ (10 μM, 6 h). The kinetics of climacostol as an inhibitor of autophagic flux in melanoma cells was further confirmed by immunoblot experiments showing evident LC3 cleavage and p62 accumulation induced by 6 h of climacostol treatment (Fig. 14c).

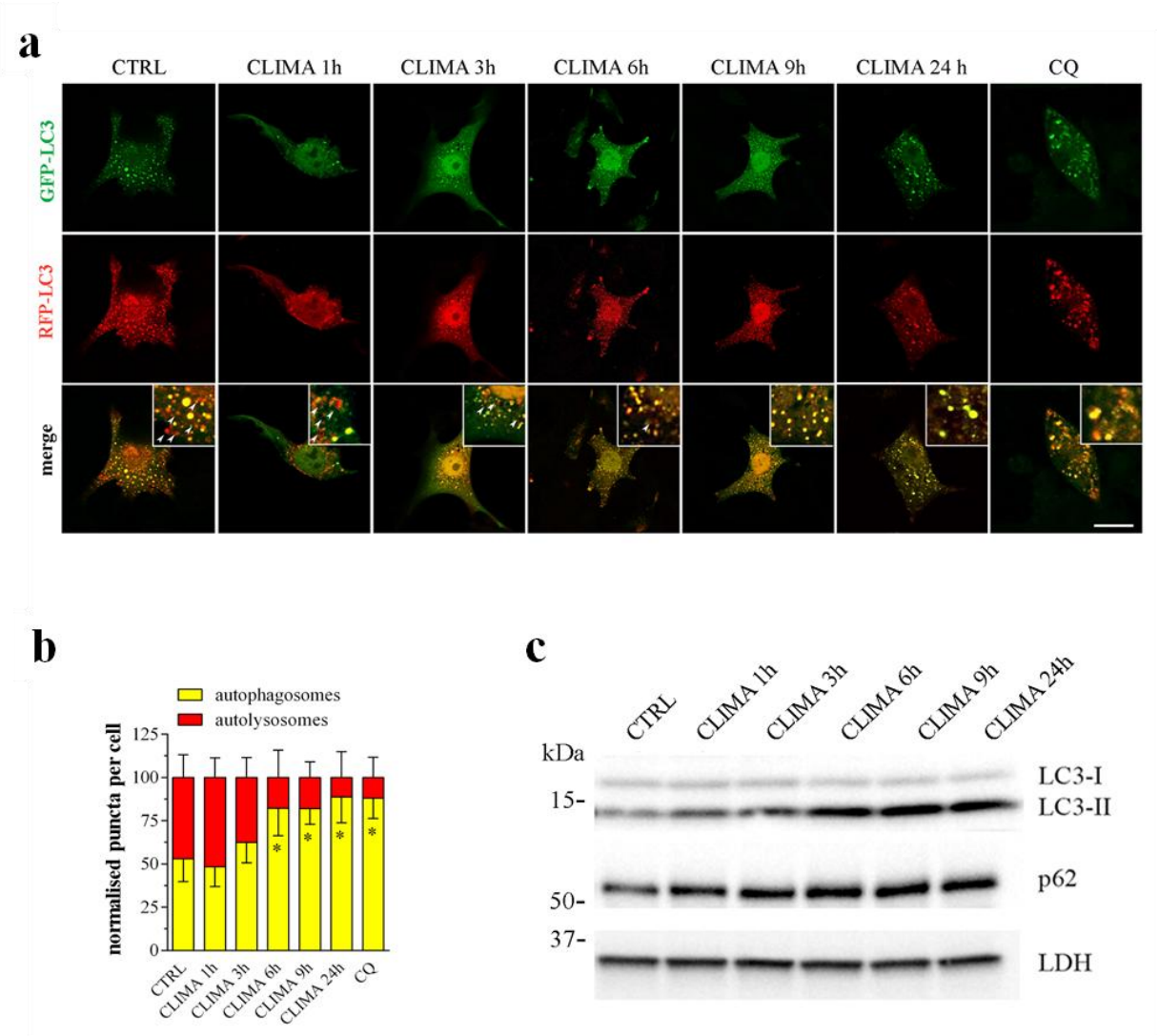

Figure 14 Climacostol impairs autophagic flux. B16-F10 cells were cultured with 30 μg/ml climacostol (CLIMA) or control vehicle (CTRL) for increasing times. Choroquine (CQ; 10 μM, 6h) was also used. **a** Confocal immunofluorescence imaging of cells transiently transfected with mRFP-GFP-LC3 plasmid. This tandem fluorescent-tagged LC3 reporter results in both green (GFP) and red (RFP) fluorescence: autophagosomes appear yellow (with green and red fluorescence) and autolysosomes as only red vacuoles. Scale bar: 30 μm. Inserts represent enlarged image details highlighting the presence of red (arrows) and yellow puncta. The number of autophagosomes and the number of autolysosomes in the merged images were counted (right panel) and the total number of puncta per cell was calculated as percentage (>30 cells per group). *$p < 0.05$ relative to CTRL. **B** Western blotting images of LC3 and p62. LDH was used as internal standard. Images and data represent the results obtained from 3 independent experiments.

4.9 Climacostol induces cell death/apoptosis and autophagy impairment in different tumour cells

In an attempt to broaden the role of climacostol to cancer cells other than murine melanomas, human melanoma A375 and SK-MEL-5, murine glioma GL261 and human glioblastoma U87MG cells were treated for 24 h with climacostol. In agreement with previous results obtained in multiple human and rodent cell lines (Buonanno *et al*., 2008; Fiorini *et a*l., 2010; Catalani *et al*., 2016; Perrotta *et al*., 2016), climacostol caused a concentration-dependent reduction of cell

viability with an E_{max} concentration value (nearly 100% inhibition) of ca. 30 μg/ml, as assessed by MTT assay (Fig. 15a-d). Data also indicated that climacostol affects the viability with a comparable potency among cells, *i.e*. EC_{50} of 5.7, 6.4, 6.7 and 5.8 μg/ml for A375, SK-MEL-5, GL261 and U87MG cells, respectively. Similar results were obtained in B16-F10 cells as a control (Perrotta *et al*., 2016). Accordingly, climacostol treatment (24 h, 30 μg / ml) induced apoptosis and impaired autophagy of A375, SK-MEL-5, GL261 and U87MG cells since it increased the expression of cleaved-(active) executioner caspase 3 and induced a robust accumulation of LC3-II and p62 levels (Fig. 15e-h).

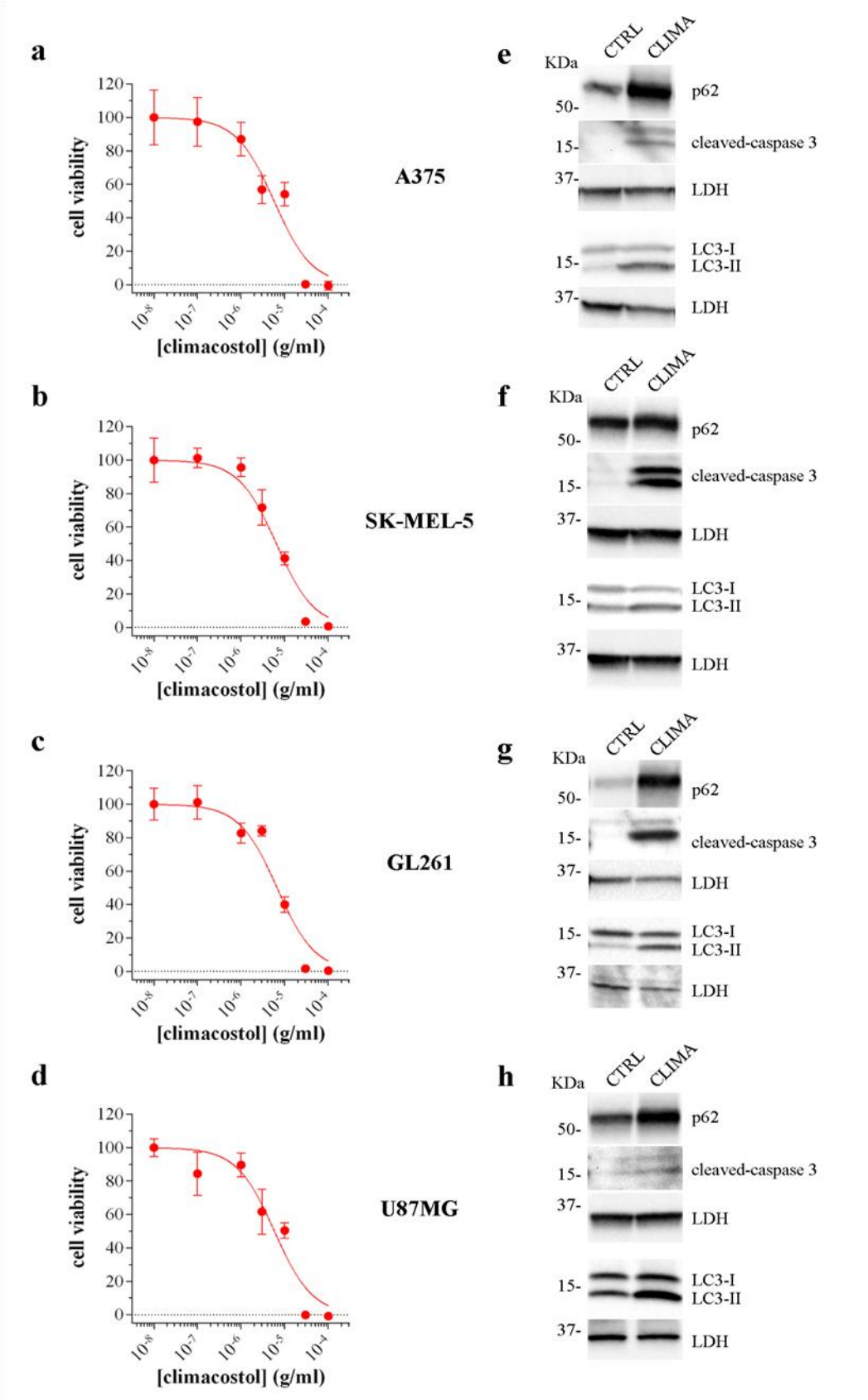

Figure 15 Climacostol effects in multiple tumour cell lines. MTT assay assessing the viability of A375 (**a**), SK-MEL-5 (**b**), GL261 (**c**), and U87MG (**d**) cells treated with increasing concentrations of climacostol for 24 h. Data are expressed by setting the absorbance of the reduced MTT in the absence of climacostol as 100%. The data points are representative of 8 independent experiments. Western blotting images of cleaved-caspase 3, LC3 and p62 expression in A375 (**e**), SK-MEL-5 (**f**), GL261 (**g**), and

U87MG (**h**) cells cultured in the presence of 30 µg/ml climacostol (CLIMA) or control vehicle (CTRL) for 24. LDH was used as internal standard. Images are representive of 3 independent experiments.

4.10 Climacostol signalling regulating autophagy: p53-dependent and independent effects

We have previously demonstrated that the signalling events responsible for the climacostol-induced pro-apoptotic effects in melanomas rely on the up-regulation of p53 and its downstream effectors Noxa and PUMA that, in turn, activates the intrinsic programed cell death pathway, including the executioner caspase 3 (Perrotta *et al*., 2016). Indeed, when the climacostol-induced increase of p53 was efficiently silenced the activation of caspase 3 by climacostol treatment was abolished (24 h, 30 µg) (Fig. 16a). Concerning p53 regulation, the mRNA levels of p53 did not change (Fig. 16b) while p53 protein expression clearly enhanced following climacostol exposure at increasing times, with a detectable effect obtained between 3 h and 6 h of treatment (Fig. 16c). Consistently, confocal immunofluorescent microscopic analysis revealed a time-dependent accumulation of p53 staining, which is almost completely localized in the nuclei of B16-F10 cells (Fig. 16d). The p53 protein phosphorylated at Ser15 site (p-p53^{Ser15}), a modification responsible of p53 stability/activation (Levine and Oren, 2009; Vousden and Prives, 2009), up-regulated as well in the presence of climacostol and p53/ p-p53^{Ser15} staining was perfectly superimposable, thus indicating a post-translational effect on p53 induced by climacostol.

We then determined whether the role of climacostol on autophagic flux involved p53 signalling. The silencing of p53 somewhat perturbed climacostol effects on autophagic flux. In particular, LC3 lipidation in response to climacostol (24 h, 30 µg) was still active (Fig.16e). In contrast, p62 levels significantly decreased in p53 siRNA cells treated with climacostol reaching values comparable to control, despite climacostol was shown to induce a sustained increase of the mRNA transcript encoding p62 in native cells (Fig. 16e). These data are consistent with a sustained autophagy turnover induced by climacostol in the absence of p53, thus suggesting that climacostol treatment simultaneously induces autophagosome formation and compromises autophagosome turnover, this latter via the up-regulation of p53.

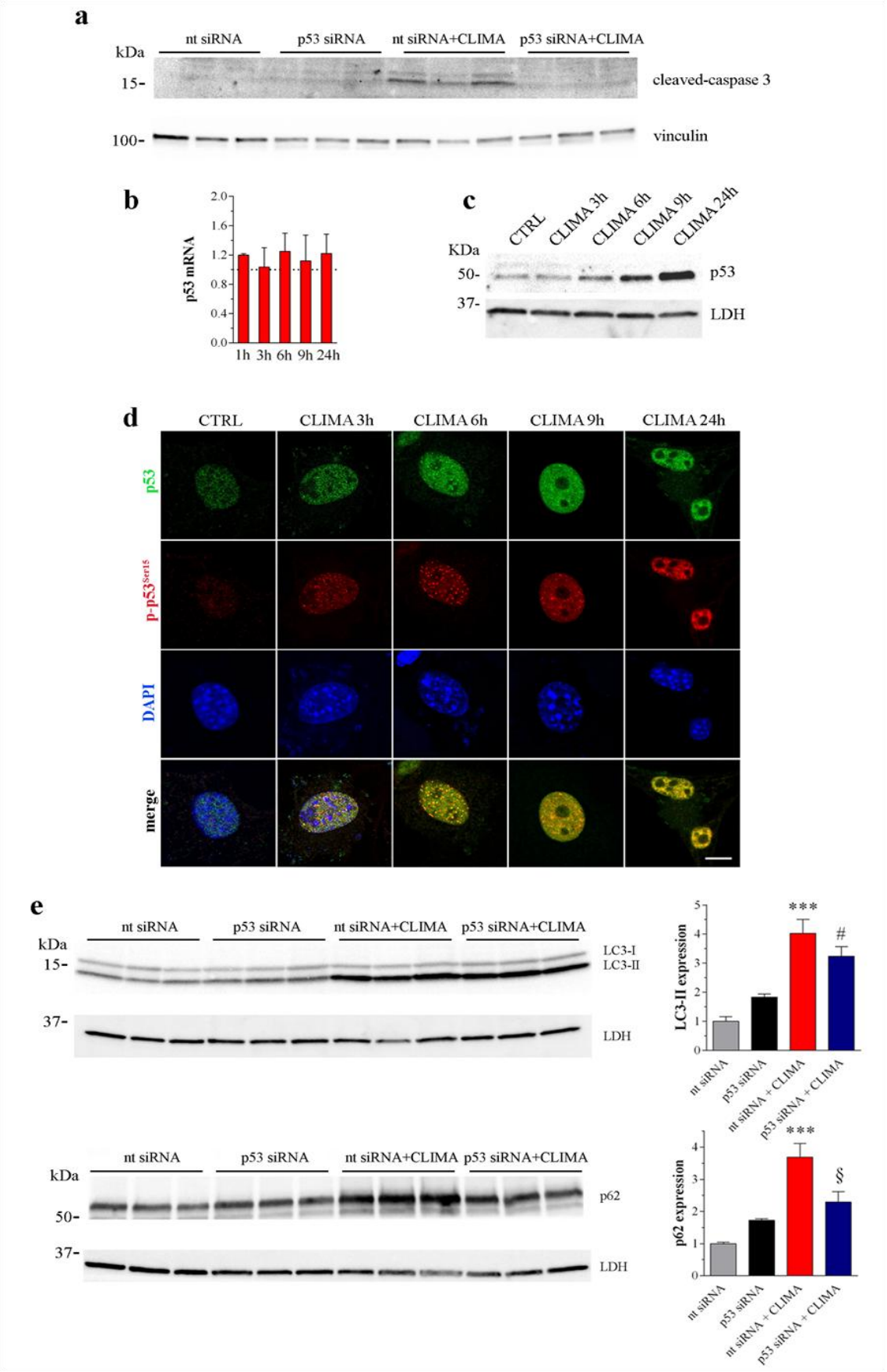

Fig. 16 p53 is involved in the climacostol regulation of autophagy. a Western blotting images of cleaved-caspase 3 expression in B16-F10 cells transfected for 48 h with a p53-specific (p53 siRNA) or a non-targeting siRNA (nt siRNA), followed by vehicle or climacostol (CLIMA) treatment (24 h, 30 μg/ml). Vinculin was used as internal standard. **b - d** B16-F10 cells were cultured with 30 μg/ml CLIMA or control vehicle (CTRL) for increasing t 912 imes. **b** mRNA levels of p53 gene, as measured by real-time PCR.

Results are expressed as fold change of control (dashed line), set as 1. **c** Western blotting images of p53 expression. LDH was used as internal standard. **d** Confocal immunofluorescence imaging of total p53 and p53 phosphorylated at Ser15 site (p-p53Ser15). Scale bar: 10 μm. DAPI was used for nuclei detection. **e** Western blotting images of LC3 and p62 expression in B16-F10 cells transfected for 48 h with a p53-specific (p53 siRNA) or a non-targeting siRNA (nt siRNA), followed by vehicle or CLIMA treatment (24 h, 30 μg/ml). LDH was used as internal standard. Right panels: densitometric analysis of LC3-II and p62 relative to their respective standard. Results are expressed as fold change of nt siRNA. ***$p < 0.0001$ relative to nt siRNA, #$p < 0.05$ relative to p53 siRNA, §$p < 0.05$ relative to nt siRNA + CLIMA. Images and data are representative of 3 independent experiments.

To deepen this aspect and to gain more mechanistic insights on climacostol effects, we evaluated different autophagy signalling molecules. Among the critical signalling connections governing autophagy, the mammalian target of rapamycin (mTOR), when is activated by protein kinase B (PKB/Akt), drives (directly and indirectly) the phosphorylation of autophagy controlling proteins including S6 (Abada and Elazar, 2014; Klionsky *et al.*, 2016; Antonioli *et al.*, 2017; Galluzzi *et al.*, 2017). The activation of this system down-regulates autophagy. The AMPK signalling can also impact on autophagy induction and autophagosomes accumulation (Kim *et al.*, 2013; Abada and Elazar, 2014; Klionsky *et al.*, 2016; Antonioli *et al.*, 2017; Galluzzi *et al.*, 2017). Within the temporal window of the climacostol-induced effects on autophagosome turnover, climacostol (30 μg) induced an early (3-6 h) decrease of Akt and S6 phosphorylation in B16-F10 cells which persisted over-time (Fig. 17a). In a sharp contrast, activated AMPKα substantially peaked at 6 h of climacostol treatment. Similar results were obtained *in vivo* analysing melanoma allografts intra-tumour injected with climacostol at 600 μg/ml or vehicle (control) every 3-4 days. The activity of S6 was lower in climacostol-injected mice (at day 16 of treatment) when compared with control while phosphorylated AMPKα levels increased (Fig. 17b), thus confirming that climacostol may inhibit and stimulate mTOR and AMPK pathways, respectively. B16-F10 were then transfected for 48 h with an AMPKα-specific or a non-targeting siRNA, followed by climacostol treatments (24 h, 30 μg/ml). When the expression of AMPKα halved, the lipidation of LC3 by climacostol increased while p62 levels significantly reduced (Fig. 17c), indicating that the accumulation of autophagosomes occur via AMPK activation. Given that climacostol rapidly modulates autophagy signalling, we next measured the phosphorylation of Akt/S6/AMPK after p53 silencing in cultured B16-F10 cells treated with 30 μg/ml climacostol for 6 h. Notably, the decrease of Akt and S6 activity induced by climacostol was unchanged in non-targeting siRNA and p53 siRNA cells (Fig. 17d). On the contrary, the ablation of p53 significantly inhibited climacostol activation of AMPKα, that therefore is partially p53-dependent. AMPK regulates p53 acetylation and phosphorylation in cancers (Liang and Mills, 2013). In B16 cells, the activation of AMPKα by the toxic natural compound vincristine is involved in p53 activation (Chen *et al.*, 2011). However, this is not a key mechanism in our system since B16-F10 cell transfection with an AMPKα-specific siRNA did not affect the time-course effects of climacostol (30 μg/ml) on p53 levels (Fig. 14e).

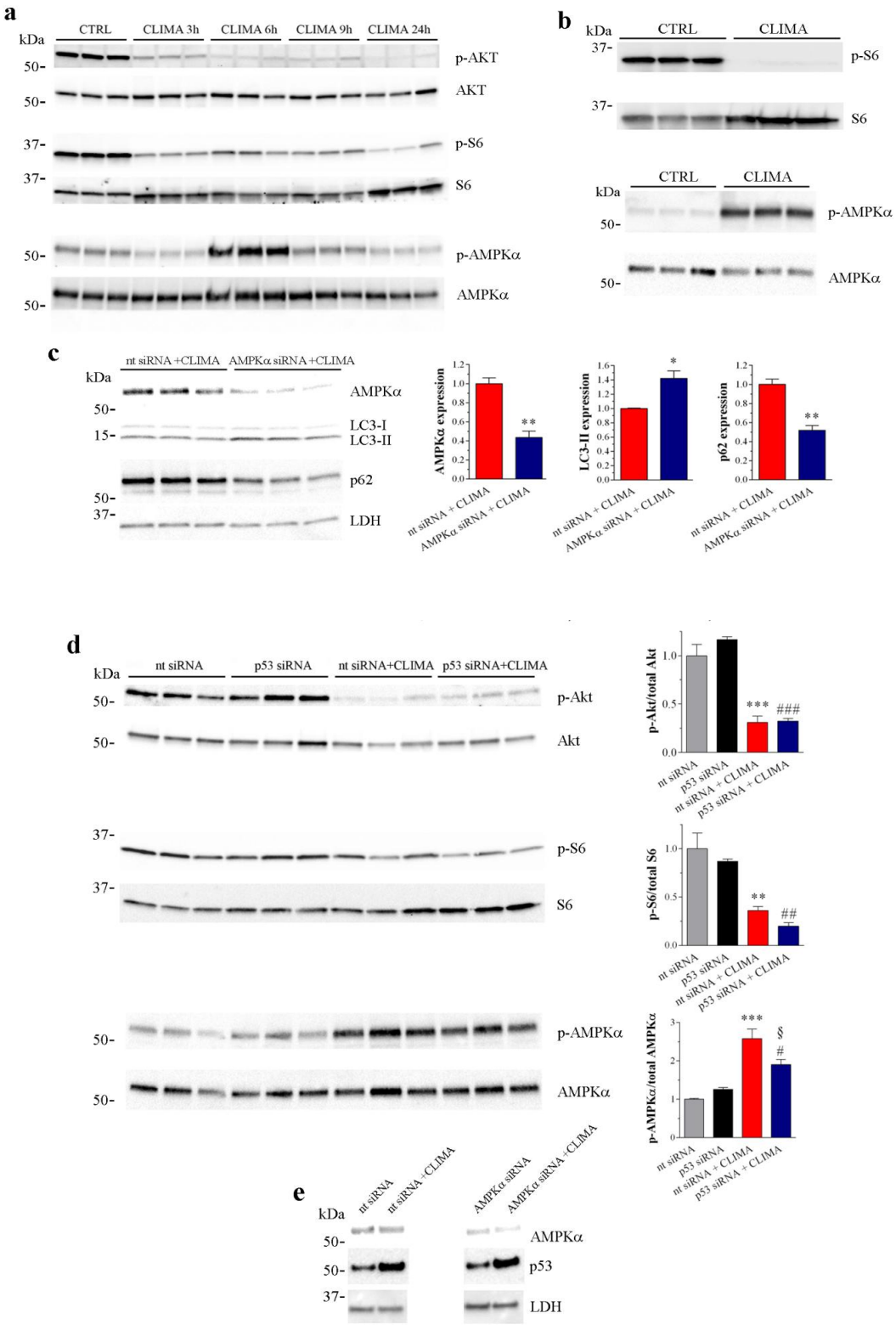

Fig. 17 Autophagy signalling molecules involved in the climacostol regulation of autophagy a B16-F10 cells were cultured with 30 μg/ml climacostol (CLIMA) or control vehicle (CTRL) for increasing times. Western blotting images of phosphorylated Akt, S6 and AMPKα. The total Akt, S6 and AMPK were used as internal standard. Images are representative of 6 independent experiments. **b** Western blotting images of phosphorylated S6 and AMPK in subcutaneous B16-F10 melanoma allografts excised from mice at day 16 of treatment (from day 0 - every 3-4 days) with 100 μl CLIMA (600 μg/ml) or CTRL. The total S6 and AMPK were used as internal standard. Images represent the results obtained from 6 animals per experimental group. **c** Western blotting images of AMPKα, LC3 and p62 expression in B16-F10 cells transfected for 48 h with an AMPKα-specific (AMPKα siRNA) or a non-targeting siRNA (nt siRNA), followed by CLIMA treatment (24h, 30 μg/ml). LDH was used as internal standard. Right panels:

densitometric analysis of AMPKα, LC3-II and p62 relative to their respective standard. Results are expressed as fold change of ntsiRNA + CLIMA. Images and data are representative of 3 independent experiments. *p < 0.05 and **p < 0.005 relative to nt siRNA + CLIMA. **d** Western blotting images of phosphorylated Akt, S6 and AMPKα in B16-F10 cell transfected for 48 h with a p53-specific (p53 siRNA) or a non targeting siRNA (nt siRNA), followed by vehicle or CLIMA treatment (6 h, 30 μg/ml). The total Akt, S6 and AMPKα were used as internal standard. Right panels: densitometric analysis of phosphorylated proteins relative to their respective standard. Results are expressed as fold change of nt siRNA. Images and data are representative of 3 independent experiments. **p < 0.005 and ***p < 0.0001 relative to nt siRNA; #p < 0.05, ##p < 0.005 and ###p < 0.0001 relative to p53 siRNA, §p < 0.05 relative to nt siRNA + CLIMA. **e** Western blotting images of AMPKα and p53 expression in B16-F10 cells transfected for 48 h with an AMPKα-specific (AMPKα siRNA) or a non-targeting siRNA (nt siRNA), followed by 946 vehicle or CLIMA treatment (24 h, 30 μg/ml). LDH was used as internal standard. Images are representative of 3 independent experiments.

4.11 Autophagy disruption and apoptotic cell death

We next assessed *in vivo* the role of climacostol-induced autophagy modulation in context with apoptosis. Climacostol at concentrations of 2 and 4 mg/kg or vehicle (control) was injected intraperitoneal in mice every 3-4 days for 4 weeks, in line with the dosage used in the intra-tumour treatments. During the test, no animal died in the experimental or the control group; all mice appeared healthy and clinically normal, with no behavioral changes, suggesting the absence of systemic toxicity over the course of the study. Accordingly, the weight of climacostol-administered animals showed a trend of increase, which was consistent with that of the control group (Tab. 2).

Week	CTRL	CLIMA	
		2 mg/kg	4 mg/kg
0	20.80 ± 0.28	20.78 ± 0.08	20.72 ± 0.23
1	22.27 ± 0.44	21.75 ± 0.52	21.39 ± 0.35
2	23.34 ± 0.58	22.79 ± 0.13	22.73 ± 0.58
3	24.29 ± 0.58	24.09 ± 0.54	24.36 ± 0.23
4	25.42 ± 0.57	25.08 ± 0.41	25.47 ± 0.48

Table 2 Body weight data: The data points are expressed in grams and have been obtained from 3 animals per experimental group. CTRL: control (vehicle); CLIMA: climacostol.

We then generated GFP expressing B16-F10 cells (B16-GFP) to clearly detect melanoma allografts by immunofluorescence. B16-GFP cells were injected into the tail vein of syngeneic mice the week before climacostol intraperitoneal treatment (4 mg/kg every 3-4 days for 2 weeks). To test the ability of climacostol to specifically affect autophagy and apoptosis in tumoural cells, diaphragm, a skeletal muscle separating the thoracic/peritoneal cavities, was analysed by confocal microscopy 3 weeks after transplantation. Tumour foci, *i.e.* GFP and melan-A-positive cells, were clearly observed in the sections of diaphgram tissue (Fig. 18a). Of interest, melanoma cells expressed robust LC3 puncta fluorescence and cleaved-caspase 3 staining (Fig. 18a) while these markers were

almost undetectable in muscular (laminin-positive) cells (Fig. 18b). Therefore, the *in vivo* experiments show that melanoma cells that have invaded the diaphragm react to climastocol by showing the same changes, increased apoptosis and disturbed autophagy, seen in B16F10 cells and in subcutaneous tumors, without any negative side effects in normal cells of diaphragm. We can hypothesize that climacostol turns out to specifically hit the tumor cells as preferential target, however our preliminary data need further and robust confirmations.

The molecular cross-talk between autophagy and apoptosis is evident and functions to dynamically maintain cellular homeostasis and respond to stress (Rubinstein and Kimchi, 2012). To test whether autophagy has a key role regulating cell fate in our system, we measured the cytotoxic effect of climacostol by exclusion dye staining with trypan blue in B16-F10 cells transfected with an AMPKα-specific or a non-targeting siRNA. As shown in Fig. 16c, cell viability of AMPKα siRNA cells remained high. Of notice, climacostol (24 h, 30 μg/ml) displayed a similar high toxicity both in the presence of AMPKα or when its expression was successfully knocked-down. Finally, we asked whether the observed effects of climacostol on autophagic flux and cell death, both via p53, could be affected by caspase blocking. To this aim, cultured B16-F10 cells were treated with climacostol (24 h, 30 μg/ml) both in the absence and in the presence of the pan-caspase inhibitor Z-VAD-(OMe)-FMK at 100 μM. As expected, western blot analysis revealed that the activation of caspase 3 induced by climacostol was indeed blunted, at least in part, by Z-VAD-(OMe)-FMK (Fig. 18d). In contrast, caspase inhibition did not affect the accumulation of LC3-II and p62 (Fig. 18e) obtained after climacostol treatment thus clearly indicating that climacostol disruption of autophagic flux is not associated with the activation of caspases. Of interest, Z-VAD-(OMe)-FMK administration was unable to rescue climacostol-induced loss of cell viability, as assessed by MTT analysis (Fig. 18f). These data argue that climacostol is able to induce a caspase-independent cell death in melanoma cells.

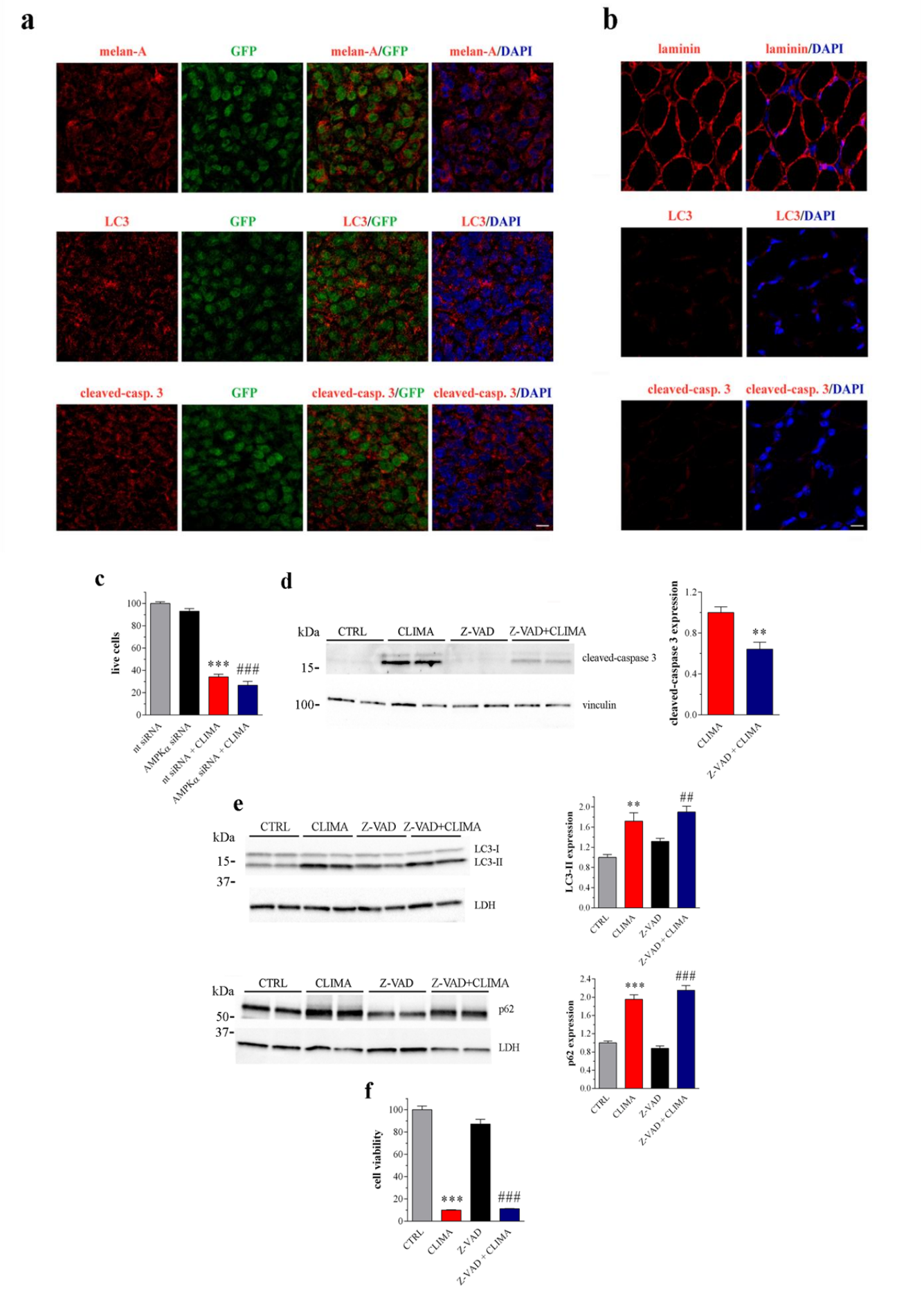
a
melan-A
GFP
melan-A/GFP
melan-A/DAPI
LC3
GFP
LC3/GFP
LC3/DAPI
cleaved-casp. 3
GFP
cleaved-casp. 3/GFP
cleaved-casp. 3/DAPI
b
laminin
laminin/DAPI
LC3
LC3/DAPI
cleaved-casp. 3
cleaved-casp. 3/DAPI
c
live cells
100
80
60
40
20
0
***
###
ni siRNA
AMPKα siRNA
ni siRNA + CLIMA
AMPKα siRNA + CLIMA
d
kDa
CTRL
CLIMA
Z-VAD
Z-VAD+CLIMA
15-
cleaved-caspase 3
100-
vinculin
cleaved-caspase 3 expression
1.2
0.8
0.4
0.0
**
CLIMA
Z-VAD + CLIMA
e
kDa
CTRL
CLIMA
Z-VAD
Z-VAD+CLIMA
15-
LC3-I
LC3-II
37-
LDH
LC3-II expression
2.0
1.6
1.2
0.8
0.4
0.0
**
##
CTRL
CLIMA
Z-VAD
Z-VAD + CLIMA
kDa
CTRL
CLIMA
Z-VAD
Z-VAD+CLIMA
50-
p62
37-
LDH
p62 expression
2.4
2.0
1.6
1.2
0.8
0.4
0.0
***
###
CTRL
CLIMA
Z-VAD
Z-VAD + CLIMA
f
cell viability
100
80
60
40
20
0
***
###
CTRL
CLIMA
Z-VAD
Z-VAD + CLIMA

Fig. 18 Autophagy/cell death events induced by climacostol. a, b GFP expressing B16-F10 cells were injected into the tail vein of syngeneic mice the week before climacostol intraperitoneal treatment (4 mg/kg every 3-4 days for 2 weeks). Diaphragm, a skeletal muscle separating the thoracic/peritoneal cavities, was analysed by confocal microscopy 3 weeks after transplantation. **a** Confocal immunofluorescence imaging of melan-A, LC3 and cleaved-caspase 3 in tumour foci observed in the sections of diaphgram tissue. The signal of GFP (tumour cells) and DAPI (nuclei) was also detected. **b** Confocal immunofluorescence imaging of laminin, LC3 and cleaved-caspase 3 in diaphgram muscle. DAPI was used for nuclei detection. Scale bar: 50 μm. Images represent the results obtained from 5 animals. **c** Exclusion dye staining with trypan blue in B16-F10 cells (> 5 x 10^5 cells per experimental condition) transfected for 48 h with an AMPKα-specific (AMPKα siRNA) or a non-targeting siRNA (nt siRNA), followed by vehicle or climacostol (CLIMA) treatment (24 h, 30 μg/ml). Data are expressed by setting the number of living cells in control samples as 100%. Data are representative of 3 independent experiments. ***p < 0.0001 relative to nt siRNA; ### p < 0.0001 relative to AMPKα siRNA. **d - f** B16-F10 cells were cultured with 30 μg/ml CLIMA or control vehicle (CTRL) for 24 h, both in the absence and presence of the pan964 caspase inhibitor Z-VAD-(OMe)-FMK (100 μM). **d** Western blotting images of cleaved-caspase 3 expression. Vinculin was used as internal standard. Right panel: densitometric analysis of cleaved caspase 3 relative to the standard. Results are expressed as fold change of CLIMA. Images and data are representative of 3 independent experiments. **p < 0.005 relative to CLIMA .**e** Western blotting images of LC3 and p62 expression. LDH was used as internal standard. Right panels: densitometric analysis of LC3-II and p62 relative to their respective standard. Results are expressed as fold change of CTRL. Images and data are representative of 3 independent experiments. **p < 0.005 and ***p < 0.0001 relative to CTRL; ##p < 0.005 and ### p < 0.0001 relative to Z-VAD. **f** MTT assay assessing cell viability. Data are expressed by setting the absorbance of the reduced MTT in control samples as 100%. Data are representative of 8 independent experiments. ***p < 0.0001 relative to CTRL; ### p < 0.0001 relative to Z-VAD.

4.12 Biological effects of climacostol analogues on mammalian cells

In order to identify the structural traits of the native molecule that could be modified to increase its bioactivity and/or stability, Buonanno *et al*. (2018) have synthetized two synthetic new analogs of climacostol, *i.e.* the 1,3-dihydroxy-2-methyl-5-[(Z)-non-2'-enyl]benzene (AN1) and the 1,3-dihydroxy-2-methyl-5-[(Z)-non-2'-enyl]benzene (AN2), carrying an additional OH- group and an CH3- group, respectively, in the aromatic ring. We examined the *in vitro* cytotoxic activities of these novel climacostol analogues on different cells of both tumor (B16-F10, GL261, SK-N-BE, and CT26 cells) and non-tumor (C2C12 cells) origin, by MTT assay. Cell treatment with AN1, AN2 and climacostol (24 h) caused a concentration-dependent reduction of MTT absorbance with an E_{max} concentration value of ca. 30 μg/ml (Fig. 19). At the E_{max} concentration compounds decreased cell viability by between 90% and 100%. Data also indicated that the viability of cells is negatively affected by AN1 and AN2 with a comparable potency, *i.e.* EC_{50} ranging from ca. 18 to 40 μg/ml (Table 3).

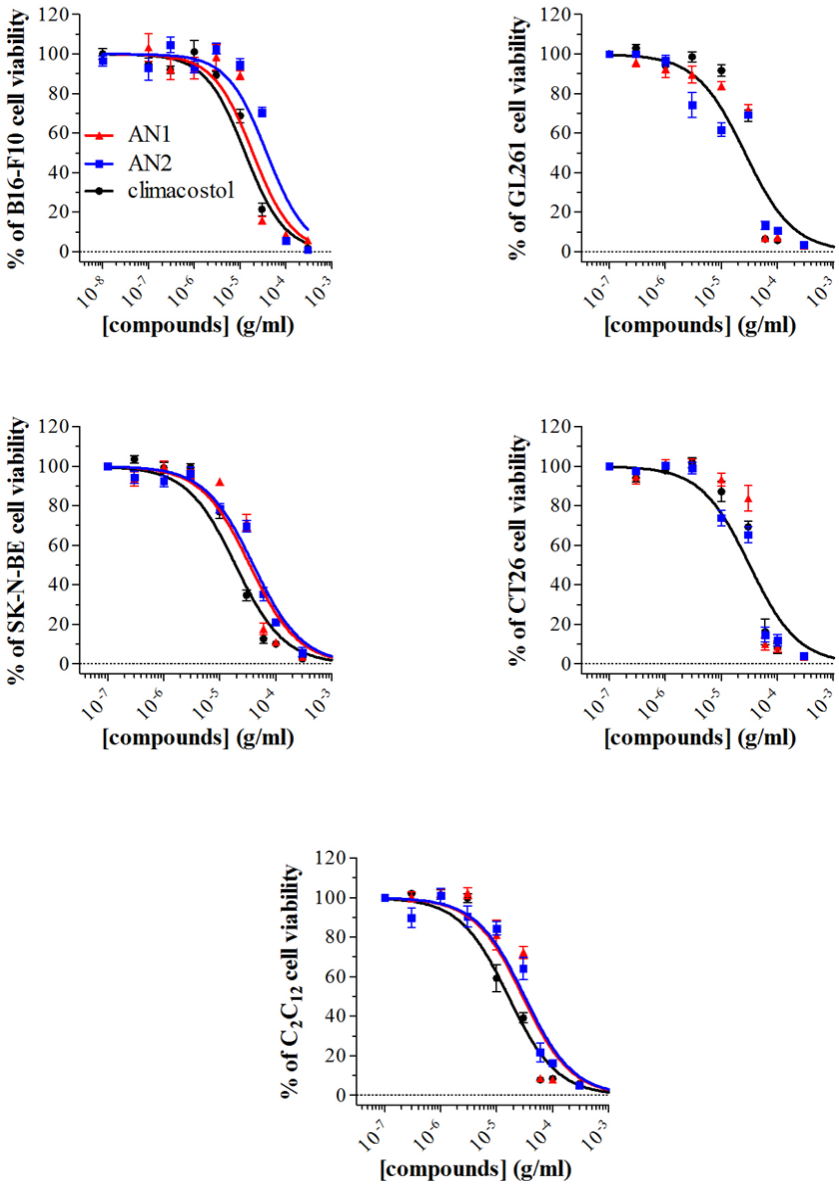

Fig. 19 Cytotoxic properties on mammalian cells. The viability of B16-F10, GL261, SK-N-BE, CT26, and C2C12 cells treated with increasing concentrations of AN1, AN2 and climacostol for 24 h was assessed by MTT assay. Data are expressed by setting the absorbance of the reduced MTT in the absence of compounds as 100%. The data points represent the mean ± SEM of results obtained from 4-6 independent experiments

cell line	origin	EC_{50}		
		climacostol	AN1	AN2
B16-F10	mouse melanoma	12.81	18.88	37.94*
GL261	mouse glioma	28.87	27.32	21.79
SK-NE-BE	human neuroblastoma	19.13	34.31*	39.84*
CT26	mouse colon cancer	31.58	36.11	27.42
C_2C_{12}	immortalized myoblasts of mouse	16.19	29.28*	31.72*

Table 3. Parameters of toxin-induced inhibition of cell viability. EC_{50} (µg/ml) = the concentration producing half the maximum effect. *: $p < 0.0001$ from climacostol value (F-test); n = 3.

Noteworthy is that both AN1 and AN2 displayed similar or even lower potencies when compared to climacostol. The concentration-dependent effects of climacostol and its analogues *in vitro* may vary among cells and this is not necessarily correlated to the nature of cells, *i.e* cancerous cells *vs* artificially immortalized cells of non-tumour origin. It should be noted that the cytotoxic activity of compounds against different tumoural cells ranged from submicromolar (below 10-6M) to micromolar (10-5M) concentrations, a quite wide window.

In agreement with our previous results, immunostaining experiments with a fluorescent labelled antibody that binds specifically to cleaved (active) caspase 3 revealed that B16-F10 melanoma cells expressed active caspase 3 at 9 h after 30 µg/ml AN1, AN2 and climacostol treatment, while no specific stain was observed in vehicle-treated (control) cells (Fig. 20).

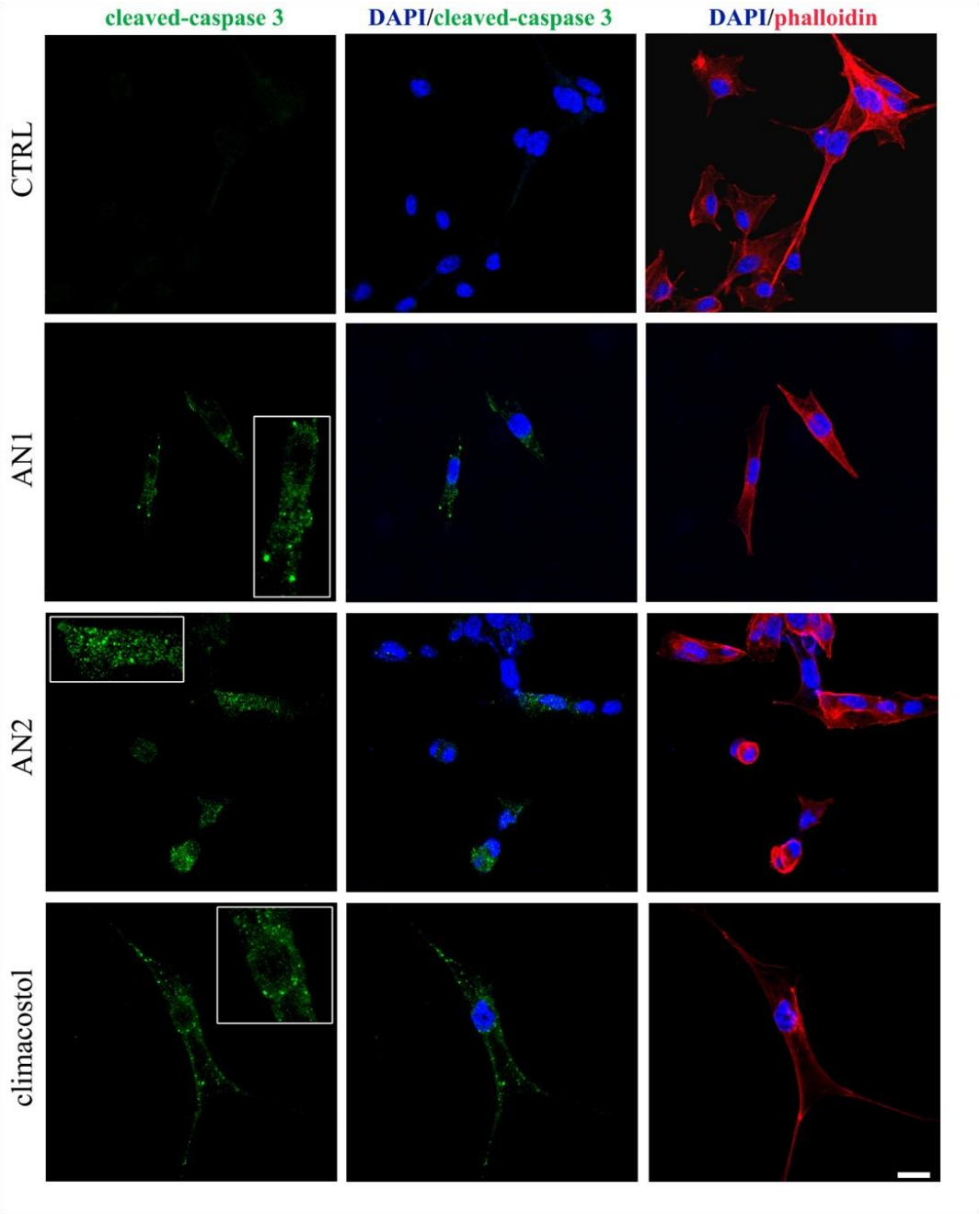

Figure 20 Apoptosis in melanoma cells. Immunofluorescence imaging of cleaved-caspase 3 (punctate green pattern) in B16-F10 cells cultured in the presence of 30 μg/ml AN1, AN2 and climacostol or vehicle (CTRL) for 9 h. DAPI (blue) and phalloidin (red) were used for nuclei and cytoskeleton detection, respectively. The images are representative of 6 independent experiments. Inserts represent enlarged image details. Scale bar = 20 μm.

5. Conclusions

Our present findings showed that one of them, *i.e.* climacostol, is a powerful and efficacious anti-cancer agent that impairs autophagy while inducing apoptosis in cancer cells, and its action may be situated at the molecular crossroads regulating both autophagic and apoptotic pathways.

Our present data provide molecular basis and confirm this hypothesis. First we demonstrated that climacostol induces apoptosis via p53 (Catalani *et al*., 2016; Perrotta *et al*., 2016). Moreover, local delivery of climacostol in melanoma transplanted mice inhibited tumour growth, tumour weight and viable cells inside the tumour thus inducing apoptosis of cancer cells and a significant improvement of animal survival (Catalani *et al*., 2016; Perrotta *et al*., 2016).

Of notice, climacostol activates p53, likely as a result of fast DNA damage and its signalling, *i.e*. Noxa and PUMA), inducing a quick and robust up-regulation of p53 protein levels in the nuclei. This is not a change in gene transcription-mechanism but largely occur through effects on p53 stability at translational level (Levine and Oren, 2009; Vousden and Prives, 2009), as for instance the phosphorylation at Ser15 site.

Then we demonstrated that climacostol, which has a chemical structure distinct from the most current blockers of autophagic flux (Vakifahmetoglu-Norberg *et al*., 2015; Wang *et al*., 2016), exerts a marked and sustained accumulation of autophagosomes in tumour cells as the result of dysfunctional autophagic degradation. Indeed, the analysis of B16-F10 allografts revealed a disruption of autophagy when melanomas were treated with intra-tumoural injections of climacostol. In addition, non-toxic doses of intraperitoneally administered climacostol reached diaphragm muscle tissue selectively targeting transplanted melanoma cells, which thus showed impaired autophagy and were committed to die by apoptosis.

As p53 is both a promoter and a suppressor of autophagy depending on the nature and extent of the inducing stress, and these effects establish a p53-dependent cell fate (Levine and Abrams, 2008; White, 2016), we examined also the role of p53 in the autophagy regulation by climacostol. The data we obtained unravelled a double-edged role played by climacostol in either promoting autophagy, independently on p53 levels, or suppressing autophagosome turnover via the up-regulation of p53. In this way, *i.e*. coordinately inducing autophagosome accumulation and inhibiting the autophagic flux, more autophagic vacuoles may be accumulated in tumour cells. Particularly, we provide evidence that the activation of autophagy by climacostol is likely due to an inhibition of mTOR signalling unrelated to p53; p53, via AMPKα activation, is however involved in the climacostol-induced impairment of autophagic process as AMPKα

phosphorylation is under its control and the knock-down of AMPKα inhibited autophagosomes accumulation by climacostol. Accordingly, the activation of p53 increased the phosphorylation of AMPK and inhibited mTOR in cancer cells in which the completion of autophagy was inhibited (Duan *et al*., 2015). A recent study in melanoma also demonstrated that the activation of AMPK induces accumulation of autophagosomes that are unable to be degraded when autophagosome clearance is inhibited (Ranieri *et al.,* 2018). Autophagy might be a protective or toxic process (Bhutia *et al*., 2013; Green and Levine, 2014; Fitzwalter and Thorburn, 2015) and AMPK may be connected with apoptosis regulation (Villanueva-Paz *et al*., 2016). The dysfunctional autophagy in climacostol-treated cells occurs prior to detectable apoptosis (Perrotta *et al*., 2016), the possibility that climacostol-induced cell death is downstream autophagy-related events is not supported by our data. Indeed, the toxicity of climacostol against melanoma cells was not affected by the inhibition of AMPKα, thus the pro-apoptotic function of climacostol could not be attributed to the block of autophagosome turnover.

In particular, climacostol disruption of autophagic flux is not necessarily associated with the activation of caspases and climacostol is able to induce a caspase-independent cell death in tumour cells. Taken together these data indicated that climacostol effects on autophagy and apoptosis are two separate events, although both reflecting the upstream activation of p53. Noteworthy, they may act independently and, likely, in a redundant manner on life/death decisions of the cell. These observations provide a platform for future studies to explore the dual targeting of autophagy and apoptosis with cytotoxic agents acting on p53 for the killing of tumours that frequently develop chemoresistance due to protective autophagy (Corazzari *et al*., 2013; Wang *et al*., 2016; Levy *et al*., 2017; Rybstein *et al*., 2018).

In essence, our study shows that climacostol potently impairs autophagy in multiple tumour cells. This suggests that the clinical potential of climacostol should be investigated further. While studying climacostol effects, we also generated valuable mechanistic insights identifying the p53-dependent increase of AMPK activity as the major responsible of autophagy disruption, although the mTOR pathway unrelated to p53-AMPK axis also plays a role. We also provide evidence that the up-regulation of p53 system is at the molecular crossroad regulating both the anti-autophagic action of climacostol and its role in the induction of apoptosis. In agreement with the promising paradigm of dual targeting of autophagy and apoptosis, different natural compounds have been shown to display anti-autophagic flux and pro-apoptotic effects in cancers (Lao *et al*., 2014; Qiu *et al*., 2014; Yuan *et al*., 2015; Zhao *et al*., 2015; Goncalves *et al*., 2016; Yan *et al*., 2016; Rigo *et al*., 2018; Zheng *et al*., 2018). In a therapeutic perspective, our findings suggest the efficacy of ciliate bioactive molecules, which have several intrinsic properties

(Cervia *et al*., 2006; Cervia *et al*., 2007; Guella *et al*., 2010; Catalani *et al*., 2016), favouring their consideration in drug discovery and development.

6. Acknowledgements

I would like to thank my supervisor Prof. Davide Cervia and co-supervisor Prof. Simona Picchietti for their help and support during the course of this project.

I am grateful to the group of Prof. Enrico Marcantoni (University of Camerino), for the contribution to the design and conception of the experimental work, synthesis of climacostol and its analogues

I wish to extend my sincere gratitude to Dr. Silvia Zecchini for her generous assistance during the course of my PhD and to Dr. Alessio Giavazzi (University of Milano, Milano, Italy) for the assistance in animal care and sample collection.

I would also like to thank Dr. Pura Muñoz-Cánoves (Pompeu Fabra University, Barcelona, Spain) for providing us with the mRFP-GFP-LC3 plasmid.

The research has been supported by grant from the Italian Ministry of Education, University and Research (PRIN2015) to Emilio Clementi and Davide Cervia, and by the Italian Ministry of Health (RC2018) to Emilio Clementi.

Last, but not least, special thanks to my family and especially my mother Rosella Cerocchi for her undying support and patience throughout the past years.

7. References

Abada A, Elazar Z (2014) Getting ready for building: signaling and autophagosome biogenesis. *EMBO Rep* **15**:839-852.

Agarwala SS (2015) Intralesional therapy for advanced melanoma: promise and limitation. *Curr Opin Oncol* **27**:151–156.

AlQathama A, Prieto JM (2015) Natural products with therapeutic potential in melanoma metastasis. *Nat Prod Rep* **32**:1170–1182

Antonioli M, Di Rienzo M, Piacentini M, Fimia GM (2017) Emerging Mechanisms in Initiating and Terminating Autophagy. *Trends Biochem Sc*i **42**:28-41.

Armani C, Catalani E, Balbarini A, Bagnoli P, Cervia D (2007) Expression, pharmacology, and functional role of somatostatin receptor subtypes 1 and 2 in human macrophages. J Leukoc Biol **81**:845–855.

Assi E et al. (2015) Modulation of Acid Sphingomyelinase in Melanoma Reprogrammes the Tumour Immune Microenvironment. *Mediators Inflamm* **2015**:370482.

Basu A, Krishnamurthy S. Cellular responses to Cisplatin-induced DNA damage. *J nucleic acids* **2010**:201367.

Bizzozero L et al. (2014) Acid sphingomyelinase determines melanoma progression and metastatic behaviour via the microphtalmia associated transcription factor signalling pathway. *Cell Death Differ* **21**:507–520.

Bizzozero L, Cazzato D, Cervia D et al. (2014) Acid sphingomyelinase determines melanoma progression and metastatic behaviour via the microphtalmia-associated transcription factor signalling pathway. *Cell Death Differ* **21**:507-520.

Buonanno F et al. (2008) The protozoan toxin climacostol inhibits growth and induces apoptosis of human tumor cell lines. *Chem Biol Interact* **176**:151–164.

Buonanno F, Harumoto T, Ortenzi C (2013) The Defensive Function of Trichocysts in *Paramecium tetraurelia* Against Metazoan Predators Compared with the Chemical Defense of Two Species of Toxin-containing Ciliates. *Zool Sci* **30**:255–261.

Buonanno F, Ortenzi C (2010) The protozoan toxin climacostol and its derivatives: Cytotoxicity studies on 10 species of free-living ciliates. *Biologia* **65**:675–680.

Buono R et al. (2012) Nitric oxide sustains long-term skeletal muscle regeneration by regulating fate of satellite cells via signaling pathways requiring Vangl2 and cyclic GMP. *Stem Cells* **30**:197–209.

Button RW, Roberts SL, Willis TL, Hanemann CO, Luo S (2017) Accumulation of autophagosomes confers cytotoxicity. *J Biol Chem* **292**:13599-13614.

Bykov VJN, Eriksson SE, Bianchi J, Wiman KG (2018) Targeting mutant p53 for efficient cancer therapy. *Nat Rev Cancer* **18**:89102.

Catalani E, Proietti Serafini F, Zecchini S et al. (2016) Natural products from aquatic eukaryotic microorganisms for cancer therapy: Perspectives on anti-tumour properties of ciliate bioactive molecules. *Pharmacol Res* **113**:409-420.

Cazzato D et al. (2014). Nitric oxide drives embryonic myogenesis in chicken through the upregulation of myogenic differentiation factors. *Exp Cell Res* **320**:269–280.

Chinembiri TN, du Plessis LH, Gerber M, Hamman JH, du Plessis J (2014) Review of natural compounds for potential skin cancer treatment. *Molecules* **19**:11679–11721.

Cervia D, Martini D, Garcia-Gil M, et al. (2006) Cytotoxic effects and apoptotic signalling mechanisms of the sesquiterpenoid euplotin C, a secondary metabolite of the marine ciliate *Euplotes crassus*, in tumour cells. *Apoptosis* **11**:829–843.

Cervia D, Garcia-Gil M, Simonetti E, et al. (2007) Molecular mechanisms of euplotin C-induced apoptosis: involvement of mitochondrial dysfunction, oxidative stress and proteases. *Apoptosis* **12**:1349–1363.

Cervia D, Catalani E, Belardinelli MC et al. (2013) The protein pheromone Er-1 of the ciliate *Euplotes raikovi* stimulates human T-cell activity: involvement of interleukin-2 system. *Exp Cell Res* **319**:56–67.

Cervia D, Assi E, De Palma C et al. (2016) Essential role for acid sphingomyelinase-inhibited autophagy in melanoma response to cisplatin. *Oncotarget* **7**:24995-25009.

Corazzari M, Fimia GM, Lovat P, Piacentini M (2013) Why is autophagy important for melanoma? Molecular mechanisms and therapeutic implications. *Semin Cancer Biol* **23**:337-343.

Damgaci, S., Ibrahim-Hashim, A., Enriquez-Navas, P.M., Pilon-Thomas, S., Guvenis, A. & Gillies, R.J. (2018) Hypoxia and acidosis: immune suppressors and therapeutic targets. Immunology, **154**, 354-362.

Dashzeveg N, Yoshida K (2015) Cell death decision by p53 via control of the mitochondrial membrane. *Cancer Lett* **367**:108–112.

De Palma C et al. (2014) Deficient nitric oxide signalling impairs skeletal muscle growth and performance: involvement of mitochondrial dysregulation. *Skelet Muscle* **4**:22.

Del Bello B, Toscano M, Moretti D, Maellaro E (2013) Cisplatin-induced apoptosis inhibits autophagy, which acts as a pro-survival mechanism in human melanoma cells. *PLoS One* **8**:e57236.

Di Giuseppe G, Cervia D, Vallesi A (2011) Divergences in the Response to Ultraviolet Radiation Between Polar and Non-Polar Ciliated Protozoa: UV Radiation Effects in Euplotes. *Microb Ecol* **6**3:334–338.

Duan L, Perez RE, Davaadelger B, Dedkova EN, Blatter LA, Maki CG (2015) p53-regulated autophagy is controlled by glycolysisand determines cell fate. *Oncotarge*t **6**:23135-23156.

Fiorini D, Giuli S, Marcantoni E et al. (2010) A Straightforward Diastereoselective Synthesis and Evaluation of Climacostol, A Natural Product with Anticancer Activities. *Synthesis* **9**:1550-1556.

Fitzwalter BE, Thorburn A (2015) Recent insights into cell death and autophagy. *FEBS J* **282**:4279-4288.

Galluzzi L, Baehrecke EH, Ballabio A et al. (2017) Molecular definitions of autophagy and related processes. *EMBO J* **36**:1811-1836.

Garcia-Prat L, Martinez-Vicente M, Perdiguero E et al. (2016) Autophagy maintains stemness by preventing senescence. *Nature* **529**:37-42.

Goncalves PR, Rocha-Brito KJ, Fernandes MR, Abrantes JL, Duran N, Ferreira-Halder CV (2016) Violacein induces death of RAS-mutated metastatic melanoma by impairing autophagy process. *Tumour Biol* **3**7:14049-14058.

Green DR, Levine B (2014) To be or not to be? How selective autophagy and cell death govern cell fate. *Cell* **157**:65-75.

Guerrier S, Plattner H, Richardson E, Dacks JB, Turkewitz AP (2017) An evolutionary balance: conservation vs innovation in ciliate membrane trafficking. *Traffic* **18**:18-28.

Hambright HG, Ghosh R (2017) Autophagy: In the cROSshairs of cancer. *Biochem Pharmacol* **126**:13-22.

Hao M. et al. (2015) Advances in targeted therapy for unresectable melanoma: new drugs and combinations. *Cancer Lett* **359**:1–8.

Harvey AL, Edrada-Ebel R, Quinn RJ (2015) The re-emergence of natural products for drug discovery in the genomics era. *Nat Rev Drug Discov* **14**:111-129.

Huber, V., Camisaschi, C., Berzi, A., Ferro, S., Lugini, L., Triulzi, T., Tuccitto, A., Tagliabue, E., Castelli, C. & Rivoltini, L. (2017) Cancer acidity: An ultimate frontier of tumor immune escape and a novel target of immunomodulation. *Semin Cancer Biol*, **43**, 74-89.

Hussein MR, Haemel AK, Wood GS (2003) Apoptosis and melanoma: molecular mechanisms. *J Pathol* **199**:275–288.

Kaur J, Debnath J (2015) Autophagy at the crossroads of catabolism and anabolism. Nat Rev Mol Cell Biol 16: 461-472.

Khazir J, Riley DL, Pilcher LA, De-Maayer P, Mir BA (2014) Anticancer agentsfrom diverse natural sources, Nat. Prod. Commun. **9** 1655–1669.

Kim J, Kim YC, Fang C et al. (2013) Differential regulation of distinct Vps34 complexes by AMPK in nutrient stress and autophagy. *Cell* **152**:290-303.

Kimura S, Noda T, Yoshimori T (2007) Dissection of the autophagosome maturation process by a novel reporter protein, tandem fluorescent-tagged LC3. *Autophagy* **3**:452-460.

Klionsky DJ, Abdelmohsen K, Abe A et al. (2016) Guidelines for the use and interpretation of assays for monitoring autophagy (3rd edition). *Autophagy* **12**:1-222.

Lambelet M, Terra LF, Fukaya M, Meyerovich K, Labriola L, Cardozo AK, Allagnat F (2018) Dysfunctional autophagy following exposure to pro-inflammatory cytokines contributes to pancreatic beta-cell apoptosis. *Cell Death Dis* **9**:96.

Lao Y, Wan G, Liu Z et al. (2014) The natural compound oblongifolin C inhibits autophagic flux and enhances antitumor efficacy of nutrient deprivation. *Autophagy* **10**:736-749.

Levine AJ, Oren M (2009) The first 30 years of p53: growing ever more complex. *Nat Rev Cancer* **9**:749-758.

Levine B, Abrams J (2008) p53: The Janus of autophagy? *Nat Cell Biol* **10**:637-639.

Levy JMM, Towers CG, Thorburn A (2017) Targeting autophagy in cancer. *Nat Rev Cancer* **17**:528-542.

Lievremont JP et al. (1999) The p75(NTR)-induced apoptotic program develops through a ceramide-caspase pathway negatively regulated by nitric oxide. *J Biol Chem* **274**:15466–15472.

Lin SR, Fu YS, Tsai MJ, Cheng H, Weng CF (2017) Natural Compounds from Herbs that can Potentially Execute as Autophagy Inducers for Cancer Therapy. *Int J Mol S*ci **18**:1412

Lindqvist LM, Simon AK, Baehrecke EH (2015) Current questions and possible controversies in autophagy. *Cell death discovery* **1**:15036.

Lippens S, Hoste E, Vandenabeele P, Agostinis P, Declercq W (2009) Cell death in the skin. *Apoptosis* **14**:549–569.

Luis A, Cruz C, Duarte AP, Domingues F (2013) An alkenylresorcinol derivative from *Hakea sericea* fruits and their antimicrobial activity. *Nat prod commun* **8**:1459–1462.

Marino ML, Fais S, Djavaheri-Mergny M et al. (2010) Proton pump inhibition induces autophagy as a survival mechanism following oxidative stress in human melanoma cells. *Cell Death Dis* **1**:e87.

Marzuka A, Huang L, Theodosakis, N, Bosenberg M (2015) Melanoma Treatments: Advances and Mechanisms. *J Cell Physiol* **230**:2626–2633

Masaki ME, Harumoto T, Terazima MN, Miyake A, Usuki Y, Iio H (1999) Climacostol, a defense toxin of the heterotrich ciliate *Climacostomum virens* against predators. *Tetrahedron Lett*. **40**:8227-8229.

Megahed AI, Koon HB (2014) What is the role of chemotherapy in the treatment of melanoma? *Curr treat option on* **15**:321–335.

Michielin O, Hoeller C (2015) Gaining momentum: New options and opportunities for the treatment of advanced melanoma. *Cancer Treat Rev* **41**:660–670.

Miyake A, Buonanno F, Saltalamacchia P, Masaki ME, Iio H (2003) Chemical defence by means of extrusive cortical granules in the heterotrich ciliate Climacostomum virens. *Eur J Protistol* **39**:25-36.

Mizushima N (2018) A brief history of autophagy from cell biology to physiology and disease. *Nat Cell Biol* **20**:521-527.

Mizushima N, Yoshimori T, Levine B (2010) Methods in mammalian autophagy research. *Cell* **140**:313-326.

Mukhopadhyay S, Panda PK, Sinha N, Das DN, Bhutia SK (2014) Autophagy and apoptosis: where do they meet? *Apoptosis* **19**:555566.

Nandy A et al. (2014) Gold (I) N-heterocyclic carbene complex inhibits mouse melanoma growth by p53 upregulation. *Mol Cancer* **13**:57.

Newman DJ, Cragg GM (2012) Natural products as sources of new drugs over the30 years from 1981 to 2010, J. Nat. Prod. **75** 311–335

Nobili S, Lippi D, Witort E, Donnini M, Bausi L, Mini E, Capaccioli S (2009) Natural compounds for cancer treatment and prevention. *Pharmacol Res* **59**:365-378.

Pambianco S, Giovarelli M, Perrotta C et al. (2016) Reversal of Defective Mitochondrial Biogenesis in Limb-Girdle Muscular Dystrophy 2D by Independent Modulation of Histone and PGC-1alpha Acetylation. *Cell Rep* **17**:3010-3023.

Paolucci C, Rovere P, De Nadai C, Manfredi AA, Clementi E (2000) Nitric oxide inhibits the tumor necrosis factor alpha –regulated endocytosis of human dendritic cells in a cyclic GMP-dependent way. *J Biol Chem* **275**:19638–19644.

Perrotta C et al. (2007) Nitric oxide boosts chemoimmunotherapy via inhibition of acid sphingomyelinase in a mouse model of melanoma. *Cancer Res* **67**:7559–7564.

Perrotta C et al. (2010) Syntaxin 4 is required for acid sphingomyelinase activity and apoptotic function. *J Biol Chem* **285**: 40240–40251.

Perrotta C, Buldorini M, Assi E, Cazzato D, De Palma C, Clementi E, Cervia D (2014) The thyroid hormone triiodothyronine controls macrophage maturation and functions: protective role during inflammation. *Am J Pathol* **184**:230-247.

Perrotta C, Buonanno F, Zecchini S et al. (2016) Climacostol reduces tumour progression in a mouse model of melanoma via the p53-dependent intrinsic apoptotic programme. *Sci Rep* **6**:27281.

Petrelli D, Buonanno F, Vitali LA, Ortenzi C (2012) Antimicrobial activity of the protozoan toxin climacostol and its derivatives. *Biologia* **67**:525–529.

Qin JZ, Xin H, Sitailo LA, Denning MF, Nickoloff BJ (2006) Enhanced killing of melanoma cells by simultaneously targeting Mcl-1 and NOXA. *Cancer Res* **66**:9636–9645.

Qiu W, Su M, Xie F et al. (2014) Tetrandrine blocks autophagic flux and induces apoptosis via energetic impairment in cancer cells. *Cell Death Dis* **5**:e1123.

Quassinti L, Ortenzi F, Marcantoni E et al. (2013) DNA binding and oxidative DNA damage induced by climacostol-copper(II) complexes: implications for anticancer properties. *Chem Biol Interact* **206**:109-116.

Ranieri R, Ciaglia E, Amodio G et al. (2018) N6-isopentenyladenosine dual targeting of AMPK and Rab7 prenylation inhibits melanoma growth through the impairment of autophagic flux. *Cell Death Differ* **25**:353-367.

Rouaud F, Boucher JL, Slama-Schwok A, Rocchi S (2016) Mechanism of melanoma cells selective apoptosis induced by a photoactive NADPH analogue. *Oncotarget* **7**:82804-82819.

Rubinstein AD, Kimchi A (2012) Life in the balance - a mechanistic view of the crosstalk between autophagy and apoptosis. *J Cell Sci* **125**:5259-5268.

Ryabaya OO, Inshakov AN, Egorova AV et al. (2017) Autophagy inhibitors chloroquine and LY294002 enhance temozolomide cytotoxicity on cutaneous melanoma cell lines in vitro. *Anticancer Drugs* **28**:307-315.

Ruggiero MA, Gordon DP, Orrell TM, Bailly N, Bourgoin T, et al. (2015) A Higher Level Classification of All Living Organisms. PLOS ONE 10(6):e0130114

Rybstein MD, Bravo-San Pedro JM, Kroemer G, Galluzzi L (2018) The autophagic network and cancer. *Nat Cell Biol* **20**:243-251.

Simabuco FM, Morale MG, Pavan ICB, Morelli AP, Silva FR, Tamura RE (2018) p53 and metabolism: from mechanism to therapeutics. *Oncotarget* **9**:23780-23823.

Sloot S, Rashid OM, Zager JS (2014) Intralesional therapy for metastatic melanoma. *Expert Opin Pharmaco* **15**:2629–2639.

Song S, Tan J, Miao Y, Li M, Zhang Q (2017) Crosstalk of autophagy and apoptosis: Involvement of the dual role of autophagy under ER stress. *J Cell Physiol* **232**:2977-2984.

Stubbs, M., McSheehy, P.M., Griffiths, J.R. & Bashford, C.L. (2000) Causes and consequences of tumour acidity and implications for treatment. *Molecular medicine today*, **6,** 15-19.

Sui X, Jin L, Huang X, Geng S, He C, Hu X (2011) p53 signaling and autophagy in cancer: a revolutionary strategy could be
developed for cancer treatment. *Autophagy* **7:**565-571.

Swietach, P., Vaughan-Jones, R.D., Harris, A.L. & Hulikova, A. (2014) The chemistry, physiology and pathology of pH in cancer. Philos Trans R Soc Lond B Biol Sci, 369, 20130099.

Tang J, Di J, Cao H, Bai J, Zheng J (2015) p53-mediated autophagic regulation: A prospective strategy for cancer therapy. *Cancer Lett* **363**:101-107.

Vakifahmetoglu-Norberg H, Xia HG, Yuan J (2015) Pharmacologic agents targeting autophagy. *J Clin Invest* **125**:5-13.

Viklund, J., Avnet, S. & De Milito, A. (2017) Pathobiology and Therapeutic Implications of Tumor Acidosis. Curr Med Chem, **24**, 2827-2845.

Vousden KH, Prives C (2009) Blinded by the Light: The Growing Complexity of p53. *Cell* **137**:413-431.

Wang C, Hu Q, Shen HM (2016) Pharmacological inhibitors of autophagy as novel cancer therapeutic agents. *Pharmacol Res* **105**:164-175.

Wang P, Zhu L, Sun D, Gan F, Gao S, Yin Y, Chen L (2017) Natural products as modulator of autophagy with potential clinical prospects. *Apoptosis* **22**:325-356.

White E (2016) Autophagy and p53. *Cold Spring Harb Perspect Med* **6**:a026120.

Yan Y, Jiang K, Liu P et al. (2016) Bafilomycin A1 induces caspase-independent cell death in hepatocellular carcinoma cells via targeting of autophagy and MAPK pathways. *Sci Rep* **6**:37052.

Yoshida K; Miki Y (2010) The cell death machinery governed by the p53 tumor suppressor in response to DNA damage. *Cancer Sci* **101**:831–835.

Yu F, Watts RN, Zhang XD, Borrow JH, Hersey P (2006) Involvement of BH3-only proapoptotic proteins in mitochondrial dependent Phenoxodiol-induced apoptosis of human melanoma cells. *Anticancer Drugs* **17**:1151–1161.

Yu KS, Lee Y, Kim CM et al. (2010) The protease inhibitor, elafin, induces p53-dependent apoptosis in human melanoma cells. *Int J Cancer* **127**:1308–1320.

Yuan N, Song L, Zhang S et al. (2015) Bafilomycin A1 targets both autophagy and apoptosis pathways in pediatric B-cell acute lymphoblastic leukemia. *Haematologica* **100**:345-356.

Zhao X, Fang Y, Yang Y et al. (2015) Elaiophylin, a novel autophagy inhibitor, exerts antitumor activity as a single agent in ovarian cancer cells. *Autophagy* **11**:1849-1863.

Zheng Y, Wang K, Wu Y, Chen Y, Chen X, Hu CW, Hu F (2018) Pinocembrin induces ER stress mediated apoptosis and suppresses autophagy in melanoma cells. *Cancer Lett* **431**:31-42.

8. List of papers

1) Perrotta C, Buonanno F, Zecchini S, Giavazzi A, **Proietti Serafini F**, Catalani E, Guerra L, Belardinalli MC, Picchietti S, Fausto AM, Giorgi S, Marcantoni E, Cementi E, Ortenzi C, Cervia D (2016) Climacostol reduces tumour progression in a mouse model of melanoma via the p53-dependent intrinsic apoptotic programme. *Sci Rep*, **6**:27281-27296.

2) Catalani E**, Proietti Serafini F**, Zecchini S, Picchietti S, Fausto AM, , Marcantoni E, Buonanno F, Ortenzi C, Perrotta C, Cervia D (2016) Natural products from aquatic eukaryotic microorganisms for cancer therapy: Perspectives on anti-tumour properties of ciliate bioactive molecules**.** *Pharmacol Res* **113**:409-420.

3) Di Renzo I, **Proietti Serafini F**, Giavazzi A, Zecchini S, Giovarelli ., Cervia D, Perrotta C, De Palma C, Clementi E (2016). The therapeutic potential of autophagy in Duchenne muscular dystrophy. *Eur. J. Neurodegen*. Dis., **5**:117-126.

4) Zecchini S, **Proietti Serafini F**, Catalani E, Giovarelli M, Di Renzo I, Coazzoli M, De Palma C, Perrotta C, Clementi E, Buonanno F, Ortenzi C, Marcantoni E, Taddei AR, Picchietti S, Fausto AM, Cervia D. (2019). Dysfunctional autophagy in melanoma cells induced by the pro-apoptotic natural compound climacostol. *Cell Death & Disease*, 10:10.

5) Buonanno F, Catalani E, Cervia D, **Proietti Serafini F**, Picchietti S, Fausto AM, Giorgi S, Lupidi G, Rossi FV, Marcantoni E, Petrelli D, Ortenzi C. (2019). Bioactivity and structural properties of novel synthetic analogues of the protozoan toxin climacostol. *Toxins*, 11:42.

The natural compound climacostol as a prodrug strategy based on pH activation for efficient delivery of cytotoxic agents. Manuscript in preparation.